DISSERTATION

DETERMINING THE CANCER RISKS PRESENTED BY SPACE RADIATION: GENOMIC MAPPING IN OUTBRED MICE REVEALS OVERLAP IN GENETIC SUSCEPTIBILITY FOR HZE ION AND γ-RAY INDUCED TUMORS

Submitted by

Elijah F. Edmondson

Department of Microbiology, Immunology, and Pathology

In partial fulfillment of the requirements

For the Degree of Doctor of Philosophy

Colorado State University

Fort Collins, Colorado

Fall 2016

Doctoral Committee:

Advisor: Sue VandeWoude
Co-Advisor: Michael Weil

Douglas Thamm
Christine Olver
Debra Kamstock

ABSTRACT

DETERMINING THE CANCER RISKS PRESENTED BY SPACE RADIATION: GENOMIC MAPPING IN OUTBRED MICE REVEALS OVERLAP IN GENETIC SUSCEPTIBILITY FOR HZE ION AND γ-RAY INDUCED TUMORS

Carcinogenesis following space radiation exposures is considered the primary impediment to human space exploration. Calculating the actual risks confronted by spaceflight crews is complicated by our limited understanding of the carcinogenic effects of high charge, high energy (HZE) ions—a radiation type for which no human exposure data exists. The current NASA model to calculate cancer risk from space radiation exposures is built largely upon epidemiological data from the survivors of the Hiroshima and Nagasaki atomic bombings, a cohort of individuals exposed predominantly to γ-rays. This dissertation examines some of the assumptions underpinning the current NASA model used to assess space radiation cancer risk.

In assessing cancer risks to astronauts, the premise that HZE ion exposures increase the risk for the same types of tumors that arise in studied human populations exposed to γ-rays is supported by the few animal studies of HZE ion carcinogenesis conducted to date. So far, these studies have found that the tumor types that arise in HZE ion irradiated animals are the same as those that occur spontaneously in these animals or following exposure to sparsely ionizing radiation. However, all of the data have been derived from either inbred mice or rats, F1 hybrid mice, or rat stocks with limited genetic heterogeneity. Experimental designs employing genetically identical animals are well suited to compare the relative effectiveness of various radiation qualities for inducing specific types of tumors. But since the tumor types that arise in

inbred animals are determined, in very large part, by their genetic background, the spectrum of tumors that might arise in a diverse population exposed to HZE ions is unknown.

With the emergence of multi-parent outbreeding strategies that produce highly recombinant mouse populations with allelic variants from multiple founder strains, it is possible to model the effects of population diversity in carcinogenesis studies by minimizing the overwhelming effects of genetic background and increasing the phenotypic repertoire available within a test population. Such populations also allow for high precision genomic mapping. Quantitative trait locus (QTL) mapping is a powerful forward-genetics approach that allows for unbiased testing of genetic variants that may influence gene-environment interactions for radiation effects. Highly recombinant populations are designed for genetic mapping; therefore, QTL can be resolved to megabase resolution and subsequently compared between exposure groups. Further, complete sequence information can be utilized on genotyped individuals by imputing the genomic resources available for the fully sequenced founder strains. Studying tumors that arise in irradiated, highly recombinant mouse populations presents a unique opportunity: the ability to determine whether the same QTL that make individuals within a population susceptible to specific γ-ray induced tumors also make them susceptible to those tumor types following HZE ion exposures. If so, extrapolation of human epidemiological data from individuals exposed to γ-rays would be a valid approach for risk calculation in the space radiation environment.

Through a genetics approach using carcinogenesis data from a mouse model of population diversity, we find that not only is the spectrum of tumors induced by accelerator produced HZE ions similar to the spectra of spontaneous and γ ray-induced tumors, but that the QTL controlling susceptibilities often overlap between groups. This overlap indicates shared

tumorigenesis mechanisms between γ-ray and HZE ion exposures and supports the use of human epidemiological data from γ-ray exposures to predict cancer risk from galactic cosmic rays.

Permissible exposure limits for astronauts are based on the risk of death from cancer rather than cancer incidence. Because the incidence to mortality conversion used in current risk calculations is based on mortality from background cancers in the U.S. population, there is an assumption that radiogenic tumors are no more lethal than spontaneous tumors. We find that malignancy, as measured by metastases endpoints, is comparable for spontaneous tumors and tumor induced following HZE ion or γ-ray exposures.

To efficiently utilize the vast genetic resources produced in this study, cataractogenesis endpoints are characterized and QTL mapping is performed. The progression of radiation-induced ocular changes is followed by dilated slit lamp biomicroscopy, with each mouse being examined up to seven times post-irradiation. Progressive, radiation-associated lens changes are noted in both HZE ion and γ-ray exposed populations. QTL controlling latencies for radiation-induced cataracts are identified and overlap in susceptibility loci are observed for mice exposed to HZE ion and γ-ray radiation.

Finally, because sufficiently powered lifetime carcinogenesis studies have not been previously undertaken in highly recombinant outbred mouse populations, many of the QTL presented here are novel. QTL are described for 11 tumor histotypes, radiation-induced cataractogenesis, and neurobehavioral endpoints. For tumor incidence, 51 QTL are presented with an average confidence interval of 3.4 megabases and effect sizes averaging 3.7% (range: 0.75 - 7.46%). Commonly for these endpoints, the genetic architecture of the phenotypic variance is complex with multiple QTL individually explaining only a small proportion of the

total variance. Although loci with moderate effects on the phenotype were most common, 11 large effect QTL are described for 7 tumor histotypes, with effect sizes greater than 5%.

Ground-based studies using accelerator produced HZE ions present the best opportunities for estimating the effects of space radiation. However, due to technical limitations, protracted exposures within particle accelerators are not feasible. This technical limitation presents a key concern for the translatability of all studies of space radiation performed on Earth. The doses studied experimentally occur over the course of minutes, while exposures in space are received continuously over the course of a mission. Although experimental studies can match the total doses received in space, estimating the effects of dose rate remain a challenge. To demonstrate that changes in radiation dose rate can produce differences in the tumors produced, we present a large-scale carcinogenesis study utilizing two inbred mouse strains exposed to fractionated or single dose γ-rays. This study demonstrates that variation in dose rate, while maintaining the total dose received, can result in distinct tumor histotypes.

The results presented in this dissertation indicate that cancer risks following space radiation exposures are largely determined by genetic background and can be calculated based on epidemiologic data from terrestrial radiation exposures. Therefore, the subpopulations at increased risk for radiation-induced tumors on Earth are likely to substantially overlap with subpopulations at increased risk in the space radiation environment. These findings support the assumptions underlying the current model used by NASA to estimate fatal cancer risks from space radiation exposures. Additionally, this work indicates that individualized cancer risk assessment may be warranted to mitigate cancer and health risks from space radiation exposures.

AKNOWLEDGMENTS

Foremost, I must acknowledge my advisor, Michael M. Weil, for providing direction and support during my time at CSU. I am fortunate to have identified Dr. Weil as a mentor, as he has simultaneously provided specific guidance for each project detailed in this dissertation and, more importantly, general direction during my scientific and professional development, for which I will be forever grateful. Dr. Weil directed me to the NASA Space Radiation Summer School in 2013 and the mouse pathology and quantitative genetics course offered by Jackson Laboratories in 2014—each of these experiences were indispensable prerequisites for the completion of this work. While at Jackson Laboratories, I was introduced to Dr. Daniel Gatti, whose patience and helpfulness during our collaboration was essential to my understanding and utilization of the programming and bioinformatics procecures presented here. I would also like to thank my doctoral committee, Drs. Sue VandeWoude, Douglass Thamm, Christine Olver, and Debra Kamstock as well as the faculty and staff of the ERHS and MIP departments and the Veterinary Diagnostic Laboratories at Colorado State University.

My wife, Renea, whose love and support is unmatched, is the center around whom all of my aspirations are focused. For her attention, patience, and faith, I am eternally beholden.

Last, I acknowledge my family, whose role in my academic development was and is tremendous. Each of my three siblings, my mother, and my father have individually contributed significantly to this culmination, perhaps more than they realize.

DEDICATION

To my father, for defining to me an ideal human;

his curiosity, selfless dedications, and quiet resolve

I always aim to replicate.

TABLE OF CONTENTS

Chapter One

Biological Threats of the Space Radiation Environment

THE SPACE RADIATION ENVIRONMENT

Radiation is energy emitted in the form of electromagnetic waves or atomic particles. Some radiation carries enough energy to fragment or destabilize atoms. Radiation that can dislodge the electrons from atoms is deemed ionizing. And when ionizing radiation dislodges the electrons from the atoms of living organisms, the radicalized molecules can disrupt biological structures and threaten the molecular organization of life. Humans became aware of these invisible forms of energy starting in the 1890's and early radiation scientists were eager to characterize the properties and sources of this mysterious physical phenomenon. Wilhelm Röntgen is credited with first producing electromagnetic radiation, now known as X-rays, at a wavelength that could penetrate material and activate film[1]. Around the same time, radioactive minerals were discovered by Henri Becquerel and his student Marie Curie[2]. The original paradigm was that radiation originated from the unstable elements of Earth. However, over the next few decades, evidence began to build corroborating the existence of extraterrestrial radiation sources[3], including the observance of higher levels of radiation atop the Eiffel Tower compared to its base[4] and increasing radiation densities in balloon flights at elevations of 3.3[5] and 5.6[6] miles above sea level. The ionization rates observed at these elevations was found to be four times higher than the levels found on Earth's surface[5]. In 1925, the term "cosmic rays" was coined to describe this high-energy form of celestial radiation[7]. Cosmic radiation has since been

well characterized and can be broadly separated into two categories according to source: solar and galactic (**Figure 1.1**)[8].

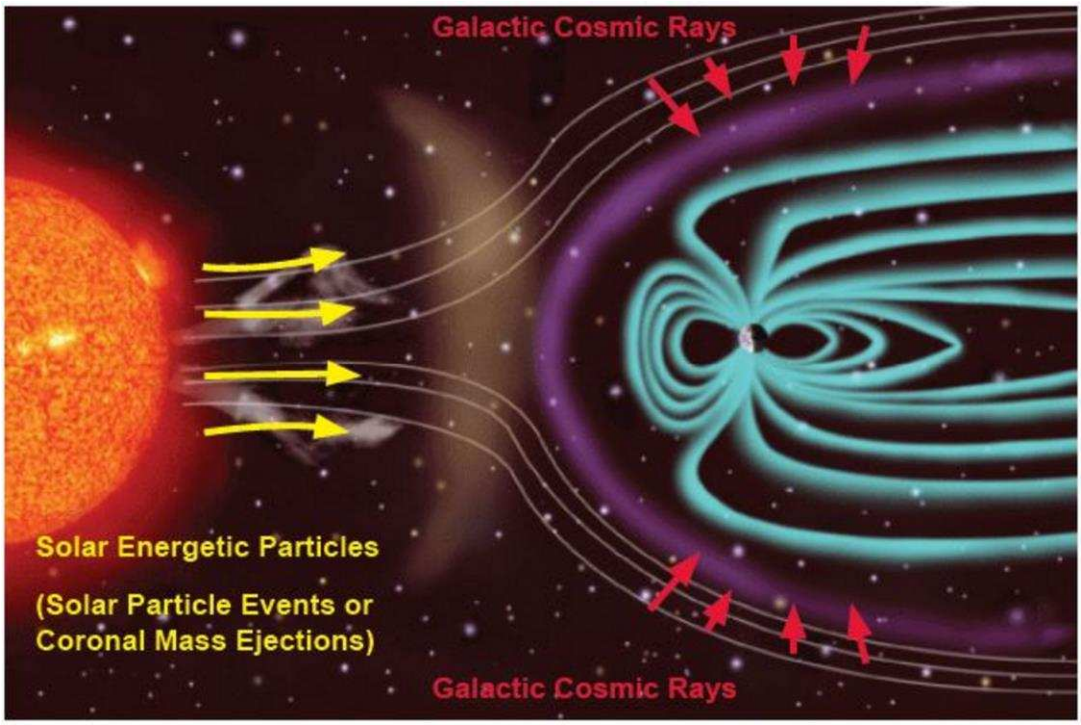

Figure 1.1: The interplanetary space radiation environment and the Earth's magnetosphere. [http://www.nasa.gov/]

Solar energetic particles (SEP) are produced at the surface of the Sun and are predominantly composed of low and medium-energy protons and electrons[9]. These SEPs are referred to as the solar wind, which is predominantly low linear energy transfer (LET) radiation. When the Sun experiences magnetic perturbations, solar particle events can occur. Solar particle events are phenomena in which dense clouds of SEP create abnormally large fluxes of radiation. Two types of solar particle events are recognized: solar flares and coronal mass ejections. Flares are local events that emit radiation across the electromagnetic spectrum, including ionizing radiation like X- and γ-rays, and non-ionizing radiation like radiowaves and white light. Solar

flares are often accompanied by coronal mass ejections. Coronal mass ejections are large coronal eruptions in which the ejected coronal material moves through the solar wind, reaching Earth within days. The radiation from these events can deform Earth's geomagnetic field, disrupt terrestrial communications, and represent a potential threat to unshielded astronauts[10]. Both the energy spectra and time profiles of solar particle events are highly variable. Events with a relatively fast onset of high-energy particles may pose potential problems for activities and can result in acute illness or death in the absence of shielding. However, SEP are relatively easy to shield with conventional spacecraft materials; a 10-15 g/cm^2 shelter is adequate for typical events[9]. Similarly, the electrons present in SEP are easily shielded. Although high energy and charge (HZE) ions can originate from the Sun during solar particle events, they are uncommon and the energies at which they occur are lower than those for HZE ions originating outside of the solar system.

Galactic cosmic radiation (GCR) originates outside of our solar system and is the component of space radiation that is of highest concern for manned missions in deep space[8]. The constituency of GCR is approximately 87% protons, 12% helium, and 1-2% heavier particles and the particle radiation exists within a wide range of energy distributions, peaking at approximately 1GeV/nucleon[8,11]. The heavier particles of GCR consist of HZE nuclei with atomic numbers ranging from Z = 3 (lithium) to Z = 28 (nickel)[12]. The relative abundance of heavier particles predominantly decreases as atomic number increases, with a notable peak Z = 26 (iron) (**Figure 1.2**)[8]. GCR nuclei travel at relativistic speeds and contain sufficient energies to penetrate spacecraft material such that no reasonable amount of shielding will prevent radiation exposures to crew members[13]. Further, secondary particles and neutrons resulting from HZE ion collisions

with shielding material can produce dramatic increases in the radiation experienced within a spacecraft.

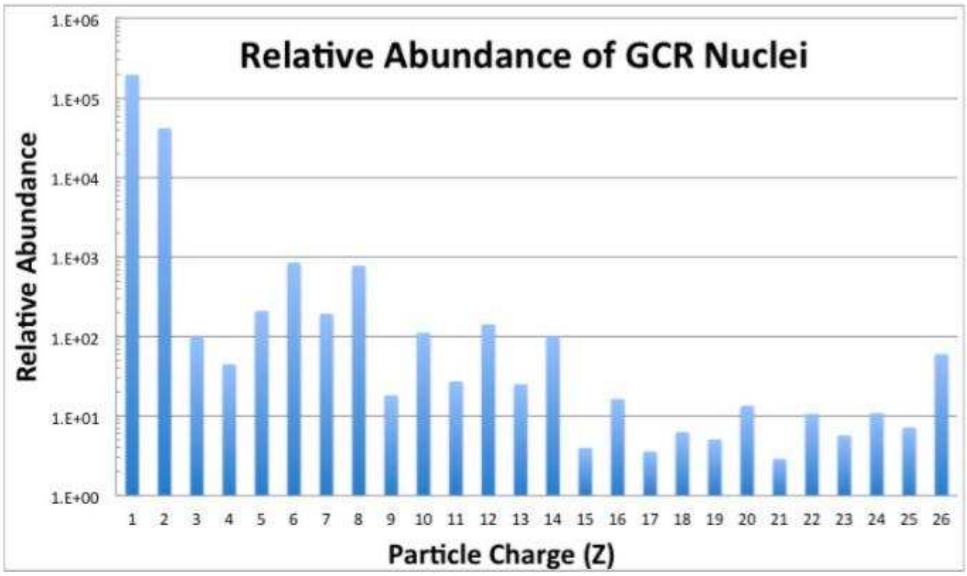

Figure 1.2: Relative abundance of GCR nuclei from hydrogen (Z = 1) to iron (Z = 26)[14].

Because of the profound effect of the solar system's magnetic environment on the fluence of both SEP and GCR, the solar cycle must be considered. The solar magnetic activity cycle—which has been recorded as far back as 1745—is defined by phases of solar maximum and solar minimum, corresponding to the maximum and minimum number of observable sunspots, respectively. The solar cycle is approximately 22 years, and involves two reversals of the Sun's magnetic field. The frequency of solar particle events is directly proportional to sunspot activity; therefore, periods of solar maximum are associated with increased energetic solar events[8]. In contrast, the fluence of HZE ions of GCR is inversely proportional to the solar cycle[8].

It is important to emphasize the distinction between deep space missions and missions in low Earth orbit (LEO), where the majority of human space activities have occurred to date. In

LEO, the Earth's magnetosphere markedly attenuates cosmic radiation. Missions into deep space not only require prolonged travel times, but also involve exposures to an environment where radiation doses are much higher than previous LEO missions. Precise GCR spectrum, fluence, and doses have been obtained for a Mars mission by the Mars Science Laboratory spacecraft during the period of December 2011 through July 2012[15]. This radiation data provides very accurate estimates for the radiation exposures astronauts on a Mars mission will receive; however, the biologic significance of these exposures remains unclear. Of all the potential health effects following space radiation, among the most concerning is the risk of carcinogenesis.

CANCER RISK ASSESSMENTS FOR SPACE RADIATION EXPOSURES

Cancer risk from exposures to cosmic radiation is considered one of the primary barriers to interplanetary travel[8,13]. Risk of cancer from space radiation exposures must be accurately estimated and, if possible, radiation countermeasures developed prior to human exploration of deep space[17]. Calculating these risks is complicated by a number of factors. First, in the absence of human data from space radiation exposures, risk must be extrapolated from epidemiological data from acute exposure to terrestrial radiation. Second, as HZE ion exposures result in unique ionization patterns for molecules, cells, and tissues[18], the effect of radiation quality on late biologic effects is unclear and the possibility for fundamental differences of carcinogenesis based on radiation quality exist. Third, radiation exposures during prolonged missions occur at low dose rates; this is in contrast to the acute doses for which increased cancer rates have been demonstrated in human populations. These key issues must be addressed in order to most accurately estimate cancer risks for interplanetary space travel.

Our understanding of the risks presented by space radiation and potential countermeasures are informed by consensus reports assembled by expert panels, including The National Council on Radiation Protection and Measurements (NCRP)[19-22] and the International Commission on Radiological Protections (ICRP)[23,24]. As an external review of these NCRP reports, the National Research Council (NRC) have also released additional consensus documents[25,26]; these documents examine all potential risks involved with deep space travel and have identified the "lack of knowledge about the biological effects of, and responses to, space radiation as the single most important factor limiting the prediction of radiation risk associated with human space exploration"[26]. The NCRP has comprehensively summarized evidence for radiation-induced health risks in a report entitled "Information Needed to Make Radiation Protection Recommendations for Space Missions Beyond Low-Earth Orbit"[27]. This report outlines recommendations for areas in which further investigation is needed, including the identification of genetic differences that result in increased susceptibility or resistance to radiation-induced cancer for an individual astronaut. These consensus documents from the NCRP, ICRP, and NRC have been implemented in the current National Aeronautics and Space Administration (NASA) radiation protection program. NASA has defined the primary categories of risk for astronauts following radiation exposures, foremost of which is carcinogenesis followed by various degenerative diseases, including pathologies of the central nervous, ocular, and cardiovascular systems[28-30]. Of these, only carcinogenesis is considered a type I risk, which is defined as a demonstrated, serious problem with no available mitigation and represents a potential "showstopper" for interplanetary spaceflight[31,32]. The NASA Space Cancer Risk Model (NSCR)[33] is the periodically revised amalgamation of estimated cancer risks from space radiation and is built on previous iterations with the goal of systematically identifying and

addressing knowledge gaps. The most current revisions are based on expert opinions in the areas of space physics, radiobiology, epidemiology, and risk assessment; these revisions were prioritized and sanctioned by the National Research Council's Space Science Board[25]. Reducing uncertainties for carcinogenesis following space radiation exposures is an essential part of moving forward with deep space exploration. Among the major uncertainties for carcinogenesis in deep space are the effects of HZE particle radiation, a form of ionizing radiation that is poorly understood in context of health risks, as well as the effects of protracted exposures at low dose rates.

NASA policy requires that, over an astronaut's career, the radiation exposures obtained are not to exceed a 3% risk of exposure-induced death (REID) from fatal cancer. Further, these REID estimates must be valid at 95% confidence[28,34]. Because human data for tumor induction following HZE particle exposure is essentially nonexistent—aside from the sparse human data for alpha particle (Z = 2) exposures—cancer risks are predominantly derived from the life span study (LSS) of Nagasaki and Hiroshima atomic bomb survivors[35,36]. This LSS follows a Japanese population of approximately 86,000 atomic bomb survivors. These individuals were exposed to acute doses of predominantly low LET radiation, although small components of neutron radiation were additionally present. This data serves as the basis for life-tables, constructed by age group and gender, which guide mortality rate estimates for specific tumor types. Scaling this human epidemiological data to spaceflight crews relies on the following assumptions:

1. That the atomic bomb survivor population is representative of the average U.S. population
2. That the acute dose-rates received by the atomic bomb survivors are applicable to the prolonged dose-rates encountered in space

3. That the low LET, photon radiation experienced by atomic bomb survivors is applicable to high LET, particle radiation in space

To account for these assumptions, the NASA model uses factors which estimate multiple parameters for the extrapolation of risks from atomic bomb survivors, including a radiation quality factor to estimate the effects of unique forms of radiation in space and factors to account for differences in total doses and dose-rate effectiveness[33]. The extrapolation parameters with the highest uncertainty levels are the radiation quality factor and the dose and dose-rate effectiveness factors (**Figure 1.3**).

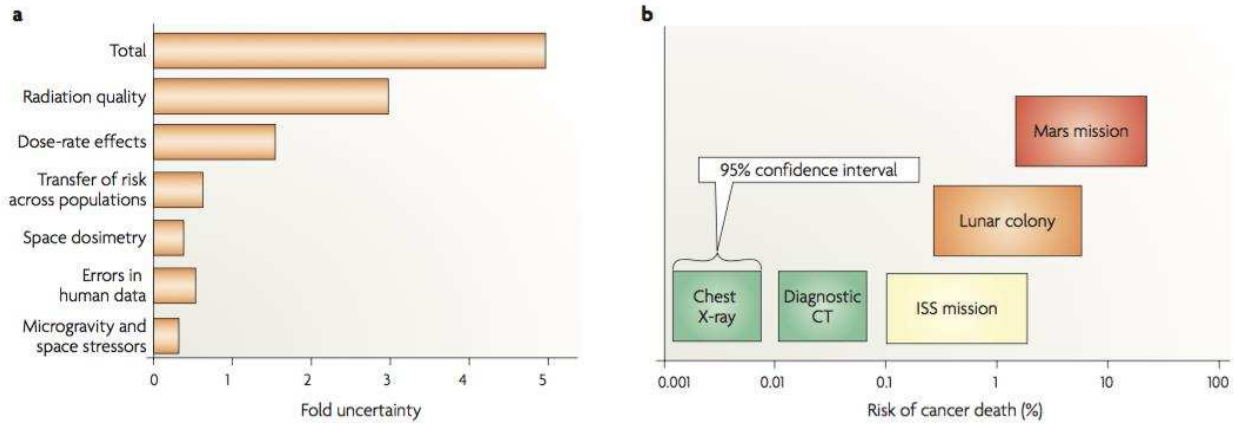

Figure 1.3: Uncertainties in space and terrestrial radiation exposures. Left: Estimate of uncertainties in projecting cancer risk for space from terrestrial exposures. Right: Current estimates of cancer risk and 95% confidence intervals for adults of age 40[17].

In addition to cancer risks, certain degenerative risks are of particular concern to NASA. Although not the focus of this dissertation, degenerative effects of the ocular system will be characterized. Cataractogenesis following exposure to radiation is a well-established phenomenon in the LSS of atomic bomb survivors, as well as radiation workers[30]. Although not fatal, the potential differences in cataractogenesis between space and terrestrial radiation

exposures could create significant life quality complications for aging astronauts. It is estimated that, in traveling to Mars, every cell nucleus in an astronauts body will be traversed by an HZE ion every few months[37].

The NASA Space Radiation Laboratory at Brookhaven National Laboratory provides a key resource for exploring the uncertainties surrounding radiation quality. The particle accelerators there allow for ground based experimentation that provide crucial tools for elucidating the effects of HZE ion exposures in model systems for cancer research[17]. Utilizing these accelerator-produced ions to determine the biologic effect of HZE ions on humans will depend predominantly on model organisms, such as the mouse. Although *in vitro*, cell based experiments can provide insight into the mechanisms of HZE ion induced cell damage, *in vivo* experiments offer many advantages for modeling of the late effects of radiation, such as cancer. Laboratory mice represent one of the best animals to model carcinogenesis.

ANIMAL MODELS

Animal Models of Radiogenic Cancer

It is estimated that most mammals, including humans and mice, descend from a common ancestor that existed approximately 80 million years ago[38-40]. The genome of this common ancestor served as the template for accumulated genetic changes that have resulted in the distinct organisms we know today. Despite the clear phenotypic differences between mice and humans, the genomes of each remain fundamentally similar (**Figure 1.4**). Each contain approximately 3 billion base pairs, about 5% of which codes for proteins, and comparison of the protein-coding sequences between the two species reveals that the DNA encoding proteins are approximately 85% identical. Of the thousands of genes that have been carefully studied, greater than 99%

contain homologs in both species. These genetic similarities (between human and mouse) are not unique—similar findings would likely be observed for the majority of mammals—but unlike other species, the mouse has several features which allow for efficient comparisons between genomes. Foremost among these advantages is that the mouse is a well-established research model, with decades of characterization and abundant shared genetic and phenotype resources. The fact that the mouse has become such a well-studied mammalian model is likely due to the following physical and behavioral characteristics: mice are relatively small, require minimal husbandry demand, have short generation times, and are easily bred in captivity.

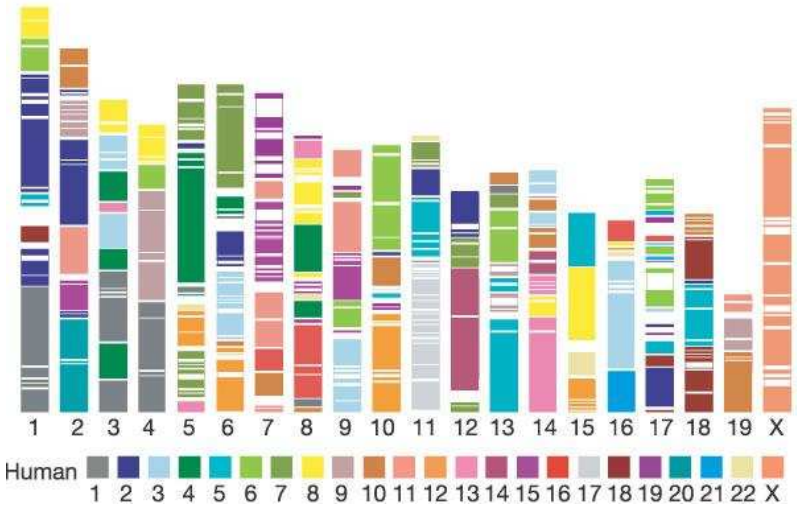

Figure 1.4: Synteny between the mouse and human genomes. The physical location of each human chromosomal segment, indicated by color, is transposed to regions of the mouse genome in which similar segments are present[39].

Animal models have been used for over a century to study radiation carcinogenesis. The results of these studies have contributed to our understanding of how radiation causes cancer, how to assess cancer risk in humans from radiation exposures, and how and why individuals differ in their susceptibilities. The preferred species have been mice and rats, as these animals provide the most realistic *in vivo* models of tumor formation that can be manipulated

experimentally. Radiation investigators have utilized a variety of inbred strains of mice to model and characterize the complex process of radiation-induced carcinogenesis. Additionally, as research techniques have advanced, the research community has taken advantage of genetically engineered mice (GEM) to focus on precise steps in the carcinogenesis process. This section will begin with a general discussion of the laboratory mouse, followed by a review of inbred strains and GEM models used in radiation research. Mouse models of genetic diversity will be covered in a dedicated section.

Inbred strains are a practical choice for examining alternative carcinogenesis mechanisms that may occur following irradiation of various doses, dose rate, or qualities. Unlike GEM models, which are predestined to follow precise carcinogenesis pathways, inbred strains allow for the holistic induction and progression of a tumor; therefore, more general conclusions can be drawn when characterizing radiation carcinogenesis. The susceptibility of certain inbred strains of *Mus musculus* to specific radiation-induced tumors has a long history[41-44]. This is not surprising considering many of the common inbred strains used today were originally developed to study the genetic basis of cancer[45]. Examples of strains selectively bred to study specific tumors histotypes include C3H/He mice (mammary tumors), BALB/c mice (multicentric lymphomas), and AKR mice (thymic lymphomas)[45]. By chance, some inbred strains that were not bred for a given tumor were incidentally discovered to be inherently prone to certain cancer histotypes, such as the DBA strain, which happen to have a high incidence of hepatocellular carcinomas. Also interesting is the unexpected susceptibility to second tumor types in strains bred for a given tumor; strain A mice were bred as a mammary tumor model and also happen to develop pulmonary adenomas at high incidences. Of the hundreds of inbred strains commercially available, relatively few have been characterized for extensive periods of time following

irradiation for tumor incidence; strains of *Mus musculus* that have been characterized include RF, CBA, C3H, BALB/c, C57BL/6, and STS. In addition, F1 crosses of C57BL/6—a relatively cancer resistant strain—with C3H or BALB/c have been observed for radiation-induced tumors. It is important to acknowledge that the tumors that are induced from radiation in a given strain often mirror those that arise spontaneously[46,47]. Among the common post-irradiation tumor types observed are lymphomas, acute myeloid leukemias, pulmonary tumors, Harderian gland tumors, ovarian tumors, and mammary gland tumors. Radiation-induced acute myeloid leukemia (rAML) is an example of what can be learned from using mouse models of radiogenic cancer.

rAML is among the first cancers to be associated with radiation. Although first suggested in 1944, as many early radiation investigators were diagnosed with this highly fatal disease[48], the link between radiation and leukemia was not widely acknowledged until further studies corroborated the first reports. Epidemiological evidence for the efficiency of radiation to induce AML was clear in studies of atomic bomb survivors[35], patients exposed to radiation for cancer treatment[49,50], and patients treated with radiation for non-malignant diseases such as fungal infections[51] and chronic inflammatory diseases[52-54]. Notably, more than a decade before published accounts of human rAML, radiation-induced leukemia was described in laboratory mice [55].

Radiation is a fundamental part of modern cancer therapy and improvements in cancer treatment have resulted in longer survival times for patients. Because of this, the risk of secondary tumors induced by therapeutic radiation are steadily increasing. Since secondary malignancies from therapeutic radiation, such as rAML, can be more consequential than the original tumors treated[49,50], survival rates for cancer patients is highly dependent on our understanding of radiation-induced tumors and development of mitigation efforts. Multiple

mouse strains, including inbred RF[56,57], SJL/J[58], CBA[59,60], and C3H/He[61], have been essential for understanding the mechanisms of radiation-induced leukemogenesis. As is desirable for a mouse model of a radiation-induced tumor, the spontaneous AML frequencies in each of these strains is relatively low. RF mice have the highest spontaneous AML rate, at 2-4% between the ages of 18-24 months[62,63]; CBA, SJL/J, and C3H/He each have an incidence of less than one percent. Despite the low spontaneous rates, a single 3 to 5 Gray dose of γ-rays produces frequencies of 25% in CBA, SJL/J, and C3H/He mice and up to 90% for RF mice. Much has been learned from these mouse models of rAML; one such example is C3H mice. Using C3H/He mice, caloric restriction has been identified as an effective method of decreasing the incidence of rAML[61,64]. Further investigation into the protective mechanisms of caloric restrictions in C3H mice suggests the suppression of insulin activated pro-growth signaling is likely involved[65].

Mouse models of rAML have also shed light on the genetic mechanisms that occur during leukemogenesis. Karyotype analysis of rAML in all of the previously mentioned strains reveals a common chromosomal lesion: the partial deletion of chromosome 2[66-68]. The deletion can be observed in susceptible cell populations as early as the first metaphase following irradiation[69], which indicates that radiation is directly responsible for the initiating events of leukemogenesis. Characterization of the common regions in which loss of heterozygosity occurs in these mouse models identifies *Sfpi1*, a gene which encodes the PU.1 transcription factor[70], as the best candidate for the deleted gene that is most significant for leukemogenesis[71,72]. PU.1 is a normal regulator of hematopoiesis, important for terminal differentiation[73,74], and lack of this transcription factor may remove important signals which limit cellular replication. The Human *SPI1* gene is present on chromosome 11[75] and the PU.1 protein is expressed in the majority of AML cases[76]. Unlike the mouse models, *SPI1* is only rarely deleted in human rAML[77,78]. This

does not exclude the possibility of epigenetic silencing of SPI1, inactivation via interaction with other proteins, such as Flt3, or decreased PU.1 expression due to aberrant miRNA expression[70,79]. The mouse models of rAML have contributed significantly to understanding of the human disease and are a powerful tool to develop potential mitigation therapies for radiation-induced tumors.

Genetically engineered mouse (GEM) models have also been used to investigate radiation tumorigenesis. GEM models represent a powerful tool to investigate precise steps in the complex carcinogenesis pathways. By investigating mice with specific genetic perturbations, the understanding of specific radiation-induced diseases, such as lung[80,81], skin[82], and colon cancer[83] have been advanced. Specific examples of genetic perturbations used for radiation research include mice with activating *K-ras* mutations, which develop lung tumors[80,81], *ApcMin/+* mice, which are susceptible to intestinal tumors[84], and *Ptch+/-* knockout mice[82], which are susceptible to basal cell carcinomas and medulloblastoma. Radiation studies using GEM models have often focused on understanding the role of radiation in inducing specific tumor types or enhancing malignancy. For example, through the use of GEM models, there is accumulating evidence that certain radiation qualities, specifically HZE ions, can produce tumors with increased malignant properties in mouse models[47,85,86].

Rodent Studies of HZE ion exposure

To assess the risk of cancer for spaceflight crews, *in vivo* models of tumor induction are essential to most closely model carcinogenesis in humans. To date, relatively few animal studies have been conducted to analyze tumor incidence following HZE ion exposures. The studies that have performed have involved either inbred mice[87,88] or rats[89], F1 hybrid mice[90-94], or rat stocks

with limited genetic heterogeneity[89,95-98]. Experimental designs employing inbred strains have shed light on the relative biologic effectiveness of various radiation qualities for inducing specific types of tumor types, including skin[46,95,96] and mammary tumors[89,97,98] in the rat and hepatocellular carcinomas[47,88], Harderian gland tumors[91,93,99], acute myeloid leukemia in the mouse[47,88]. From these studies, it appears that the tumor types that arise in HZE ion irradiated rodents are the same as those that arise spontaneously or following exposures to low LET radiation.

In one large-scale study utilizing whole-body irradiations with 1 GeV/ nucleon Fe ions, multiple tumor types were analyzed and animals were monitored for 800 days[88].
In this study, male CBA/CaJ mice exposed to 0.4 Gy HZE ions were found to have a much higher incidence of hepatocellular carcinoma, with an approximate relative biologic effectiveness of 50 compared to γ-ray exposures In the same study, Fe ions were found to be no more effective at producing AML than γ-rays.

Harderian gland tumors were the endpoint of interest for multiple early studies using B6CF1 mice and a variety of HZE ions, including helium, carbon, neon, argon, and iron[91,93]. The results of these studies serve as the foundation for understanding of the effect of LET on the efficacy of tumorigenesis. It is important to mention that these studies utilized pituitary isografts to enhance Harderian gland tumorigenesis and a relatively limited post-radiation monitoring period.

Although not typical of human exposures in space, which will be whole body exposures of low doses, one study examined the effects of local irradiation with high doses of HZE ions[87]. In this study, the hindlimbs of C3H/HeMsNrsf mice were irradiated with 5 to 65 Gy of carbon ions or 45 to 95 Gray γ-rays to detect differences in skin reactions. For carbon ions, two different

LETs were used, 290 MeV/n and 135 MeV/n. Notably, the doses analyzed in this study are much higher than previously mentioned experimental studies in this section and such high doses are not relevant for spaceflight crews. Further, as the primary goal of this study was to assess early radiation effects (skin reactions), relatively small groups of mice were used. Despite this, significant numbers of tumors were observed, most commonly sarcomas (malignant fibrous histiocytomas, fibrosarcomas, and osteosarcomas) and less frequent incidences of carcinomas. No difference in latency was observed following carbon ion and γ-ray exposures and both radiation types had linear dose responses without saturation for tumor induction.

GEM models have also been used for HZE ion exposure studies. ATM is a central protein involved in many pathways, including DNA repair, apoptosis, and cell cycle regulation. Since radiation is thought to affect carcinogenesis via damage to DNA, proteins such as ATM are theoretically important for radiation effects. Consistent with this line of thought, genetic mutations in the gene for ATM have been demonstrated to increase susceptibility to radiation carcinogenesis in humans[100]. A GEM model that recapitulates the human *ATM* 7636del9 mutation with a knock-in allele was used to study the effects of HZE ions on the genetic susceptibility to radiation[100]. Homozygous and heterozygous mice deficient in Atm activity were exposed to 1 Gy of 1 GeV/n 56Fe ions and compared to unirradiated mice. No differences were observed in tumor incidence for these mice, however, only a small number of mice were necropsied. GEM models have also been used to analyze whether HZE ions modulate the malignancy of tumors. Evidence in GEM models appears to support the notion that HZE ions produce tumors with higher malignancy. Following HZE ion exposure, transgenic models of mammary cancer develop more aggressive tumor subtypes[47,85,86]. In APCmin/+ mice, a GEM model of intestinal tumors, heavy ions increase the number of tumors as well as the invasiveness

in comparison to γ-ray irradiation mice. Also, it should be noted here that in one lifetime carcinogenesis study with C3H/HeNCrl mice, these mice appear to have higher incidences of metastatic hepatocellular carcinomas[46], although this study was not designed to quantify metastatic disease.

Adequate HZE ion carcinogenesis studies performed in mammalian models are limited and, therefore, generalizing the results of these studies must be done with caution. However, given the data from the experiments performed to date, it appears that HZE ions are highly efficient at producing certain tumor types, such as HCC, while relatively inefficient at producing others, such as AML. One key concern—that is addressable—with all previously conducted studies on HZE ion carcinogenesis is the lack of genetic diversity in the various rodent test populations. Just as GEM models focus the analysis of tumorigenesis endpoints in a way that is considered a drawback to investigating more general questions about tumor formation[62], inbred mice limit the phenotypic repertoire available to study in comparison to outbred mice. Therefore, the tumor spectrum that results in a given inbred strain is determined predominantly by the genetics of that strain, not by differences in exposure to a given carcinogen. In genetically diverse populations of mice, where there is a wide range of tumor susceptibilities, it is possible to test the effects of radiation quality on tumorigenesis. And these genetically diverse populations of mice offer a better model human genetic diversity.

Modeling Population Diversity with Highly Recombinant Mice

It is important to recall that, from a historical perspective, the goal of murine model development was to entirely remove the genetic complexity present in outbred animals. Consider the legacy of C. C. Little, a fundamental figure in the history of the laboratory mouse[101]. Little

was interested in the genetic basis of cancer. He championed the use of mice for this work and was convinced that the best method of studying genetics was by creating inbred strains[101]. Presumably, reproducing Gregor Mendel's work in a mouse model of tumorigenesis would require minimization of the independently acting Mendelian factors. Little founded Jackson Laboratories in 1929—prior to the identification of DNA as hereditary material—with the concept that cancer was a genetic disorder and with the inbred mouse as the engine of discovery. It has been stated that Little's greatest scientific accomplishment was "seeing the potential value of inbred lines for genetic and cancer research"[102]. Indeed, inbred mice have revolutionized the understanding of essentially all areas of biological research, not just cancer. Furthermore, inbred strains allow for testing the effects of an environmental variable, such as exposure to a therapeutic or radiation, and can be accomplished with relatively few animals due to the minimization of genetic and phenotypic variability. Despite the advantages to genetically identical test populations, there are also drawbacks. Strain specific responses to a given environmental agent, such as exposure to a therapeutic or radiation, may obscure the variability we might expect in a genetically diverse population. Additionally, identifying the genetic variants that contribute to a given phenotype is impossible using only a single inbred strain. Even examining panels of inbred strains, while useful to determine which genetic regions controls a given phenotype, does not allow for the segregation of genetic elements. For these reasons, crosses of mice have been utilized to dissect the genetic regions, or loci, responsible for a give quantifiable trait; mapping the location of these quantitative trait loci, referred to as QTL, has since been the goal of many scientists.

QTL mapping is a field that has benefitted tremendously from crosses of inbred mice. Much of the success in genetic mapping in mice was necessarily preceded by the extensive

phenotyping efforts of the mouse genetics community. In 1999, a meeting occurred at Jackson Laboratories to consider the value of systematically and consistently phenotyping a large number of inbred strains[103]; ten years following this consensus meeting, 178 mouse strains were evaluated in 105 phenotyping projects, yielding over 2000 unique measurements[104]. These collective results, referred to as the mouse phenome project, are publically available at (http://phenome.jax.org/) and can be utilized by the research community to determine the expected variability in a given trait. Further, the mouse phenome project allows for accurate predictions of the heritability of a given trait by calculating the ratio of the variation between strains to the total variation. Heritability provides a starting point for investigators who may be interested in genetic mapping of a given phenotype.

Initial QTL mapping studies utilized an F2 intercross approach, which involve selecting two strains on opposite ends of the phenotype spectrum and crossing them (**Figure 1.5**). The F2 progeny of such a cross are phenotyped, and the genetic markers—relatively few were needed to capture the few recombination events—that most significantly associate with the phenotype are identified. Although this method is remarkably effective and has identified thousands of QTL[105], the identified regions are broad (30 – 60 Mb) and often contain hundreds of genes. Multiple methods have been subsequently developed with the goal of narrowing the QTL window. One such method is to create congenic strains, whereby the susceptibility QTL is bred to a disease resistant background strain so that progressively smaller portions of the QTL are maintained. This congenic approach has been successfully used to isolate QTL[106-109]. However, during this backcross procedure, which is designed to narrow a given locus, it is frequently observed that a single QTL segregating in such a cross can fractionate and disappear, presumably into multiple QTL of smaller effects[110,111]. Extending the concept of the F2 cross, QTL can be further

narrowed by creating advanced intercross lines by adding additional generations of outbreeding (**Figure 1.5**), but the phenotypic variability will still be somewhat limited by the use of only two founder strains. Another approach is to create an outbred population of mice with multiple founder strains. Such populations have many benefits including increased phenotypic variability and the ability to reconstruct the genomes of individual mice into genomic blocks of known ancestry, thereby gaining haplotype information which can be used to determine which genomic blocks are most important for a given phenotype. By allowing the passage of many generations, such crosses benefit from the accumulation of meiotic recombination events, thereby reducing the size of haplotype blocks and increasing the resolution for QTL mapping. Examples of these multiparent crosses include the Heterogeneous Stock (HS) mice and, more recently, the Diversity Outbred (DO) mice (**Figure 1.5**). The primary obstacle precluding such an approach in previous decades was technological. The ability to densely genotype large numbers of mice is a product of the genomics age. In addition to the need for dense genotyping, generating information from studies with genetically diverse populations demand very large numbers of mice. Compared to an inbred strain cross, analyzing an outbred population requires an estimated 10x more animals to achieve statistical power in a population with such genetic and phenotypic diversity in addition to the 100x more markers necessary to adequately capture the genetic diversity[111]. As a result of the valiant collaborative efforts of mouse genetics community[104,112-115], populations of highly recombinant mice derived from inbred strains have been developed and maintained with the goal of finely mapping the genomic regions that effect complex diseases and traits. The most notable are the two distinct HS population and the DO, all of which are distinct multi-parent populations created with circular or randomized breeding starting with eight inbred strains[116].

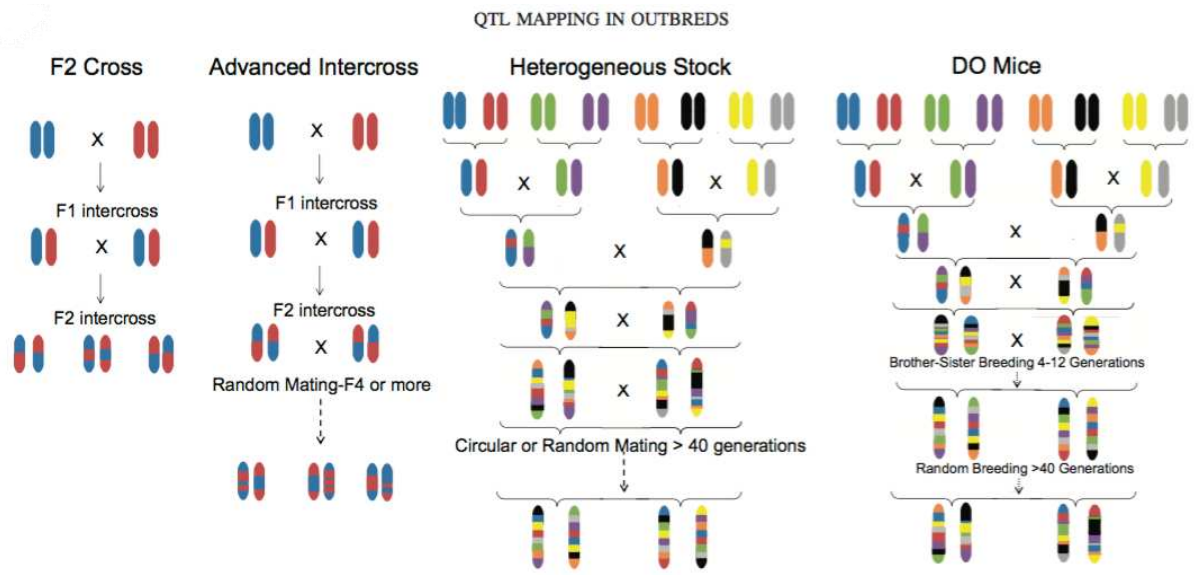

Figure 1.5: Breeding schemes to detect quantitative trait loci in mouse populations[116].

The first HS population was developed in the 1970s by McClearn[114]. The eight founder strains were C57BL/6, BALB/c, RIII, AKR, DBA/2, I, A/J and C3H. Originally, this HS was created as a source for selection studies and only decades later was utilized for QTL mapping. Because of the initial breeding designs, the resulting population was estimated to be somewhat unbalanced, meaning that the founder contributions were not equally represented on all chromosomes for all mice[116]. There was potential for complete loss of a given founder strain in particular regions of the genome. Despite the unbalanced allele frequencies in the HS, these mice demonstrated the utility of such a cross by narrowing a QTL previously identified in F2 intercross[117] to only 0.8 centimorgans[118] and paved the way for the subsequent HS.

The second HS, designated HS/Npt, was created by Hitzemann, et al. using A/J, AKR/J, BALBc/J, CBA/J, C3H/HeJ, C57BL/6J, DBA/2J and LP/J[113]. Unlike the original HS created in the 1970s, all of the progenitor strains are currently available. The HS/Npt have since been utilized in numerous high-resolution mapping studies and have helped identify hundreds of QTL

for a wide variety of phenotypes[111]. As predicted, QTL windows were much smaller than those previously identified in F2 crosses, averaging only 2.7 Mb[111]. HS/Npt mice have been used to determine the genetic contributions to a wide variety of phenotypic traits, including the susceptibility to degenerative diseases such as arthritis[119], the susceptibility to toxicity effects such as ethanol effects on motor abilities[120], and genetic effects on behavior and cognition such as fear conditioning[121]. One of the major drawbacks to the HS mouse population is that, because of the genetic diversity, for each new study involving a new test population, the entire group of animals must be fully genotyped and phenotyped. Because such large numbers of mice are needed to achieve statistical power and high-throughput SNP arrays are required, these studies can be cost-prohibitive and therefore reproducibility suffers. For carcinogenesis studies—which have not been previously attempted—the added cost of maintaining such large populations for over two years to allow for tumor development is a significant consideration. Therefore, when studying highly recombinant mouse populations, the benefit to collecting as many phenotypes as possible on the same group of mice is significant and can significantly defray the initial costs by generating information for multiple traits. Mapping in the HS can aid in discovery by revealing novel QTL containing only a small number of candidate genes. However, one drawback to the HS population as it exists today is the difficulty in performing functional follow-up studies on these identified genetic variants[116].

The Diversity Outbred (DO) population is the most recently developed stock and was created in an effort to address the previously identified shortcomings of the HS populations. First, in an attempt to further increase the phenotypic diversity, the DO is composed of representative strains from three major *Mus musculus* subspecies (M. m. musculus, M. m. domesticus, and M. m. castaneous): A/J, C57BL/6J, 129Sv/ImJ, NOD/LtJ, NZO/H1J, CAST/EiJ,

PWK/PhJ, and WSB/EiJ, the latter three being recently derived from wild mice. Second, the DO is maintained with the use of multiple funnels and 175 breeding pairs[122]; in comparison, the HS mice were developed using a single funnel (combining the founder genomes only once) and is maintained with 40 to 50 breeding pairs[123]. Third, an extensive panel of recombinant inbred (RI) lines was created from individuals of the DO population; these RI strains serve as a genetic reference population to improve the functional follow-up capabilities on candidate genes identified in DO mapping studies. These RI strains require only a single round of genotyping and, because they are a product of the same DO founders, they contain the same genetic variants that could be identified by QTL mapping in the DO. This panel of RI lines is collectively referred to as the Collaborative Cross (CC) and, in addition to improving strategies for high-resolution QTL mapping, aims to offer a unique resource to integrate phenotypic, genetic, and genomic data.

The Collaborative Cross Consortium[115] is a network of mouse geneticists with the common goal of creating a resource to support systems level genetic studies[112]. The CC is a shared resource in which RI panels from DO mice are developed and characterized at many institutions, including The Jackson Laboratories, University of North Carolina, Tel Aviv University, and Geniad in Western Australia[115]. The overarching goal of this undertaking is to characterize—and make publically available—the phenotypes, genotype, transcriptome, proteome, and metabolome for each CC strain. Currently, hundreds of genetically independent CC lines have been characterized[115]. Inbreeding of the CC lines began with DO individuals at generation 22[124]. Therefore, panels of CC lines themselves could be potentially used for mapping QTL; however, because only 22 generations of outbreeding were performed prior to inbreeding the RI panels[125], mapping with CC lines would not provide the high resolution that is achievable

with the HS or DO, in which the haplotype blocks from the founders become smaller with each generation that passes. To demonstrate the utility that the CC will possess, multiple studies have been conducted on the partially inbred, pre-CC lines; these studies have allowed for the elucidation of genetic regions controlling hematological parameters such as white blood cell count[126], the susceptibility to influenza[127], and genetic determinants of body weight[125]. As of 2012, 42 fully inbred lines were available and this number is expected to increase significantly[124].

Multiparent mouse crosses have ameliorated many of the problems that originally limited traditional genetic mapping studies: they dramatically increase mapping resolution by increasing the density of recombination events and they widen phenotypic variability by introducing allelic variants from multiple founder strains. It is important to discuss the new analytical opportunities presented by populations that result from multiparent crosses. The combination of (1) high throughput genotyping, (2) multiparent populations, and (3) fully sequenced founders can result in a population of mice that are essentially completely sequenced using only genotyping. To accomplish this, each mouse's genome must be reconstructed according to parental strain; these genome reconstructions can then serve as a scaffold for the imputation of full sequencing information. The statistical approaches used to achieve such results are discussed.

Genotyping most commonly involves determining an individual's constellation of single nucleotide polymorphisms (SNP); this is the most common form of genetic variation—a single base pair error that occurs during replication, subsequently passed along to all descendants. SNPs at any individual location are typically one of two possibilities (e.g. an "A" or a "G"). Even though it is technically possible to have a SNP region in which up to four possibilities (e.g. A, G, T, or C), this is statistically unlikely as this would mean that the same exact base pair—out of the

3.1 billion in a mouse or human—was involved in more than one replication error. Therefore, fewer SNP possibilities—two—are quantified than haplotypes—eight—for HS or DO mice. However, the eight haplotype states can be calculated from dense SNP arrays by matching the linear SNP information present along a chromosome with that of the founder strains. For multiparent highly recombinant mice, the heterozygous and mosaic haplotypes that make up an individual's genome can be calculated using a hidden Markov model to uncover the probability of hidden states[128]. There are a total of 36 possible diplotypes, including 8 homozygous and 28 heterozygous haplotype combinations. A hidden Markov model consisting of a Markov chain with 36 states can be utilized to define the probability of transitioning from one state to another[128-130]. In this case, the estimated transition represents a meiotic recombination event. By reconstructing the genomes of each mouse of known parentage, the information from SNP genotyping increases from two allelic possibilities to eight haplotype possibilities.

Many complex diseases have been successfully mapped using mouse models of population diversity, however there is one notable exception: carcinogenesis. This may be surprising as the laboratory mouse was initially championed as a model to study genetics of cancer[102]. A likely reason for the absence of carcinogenesis endpoints in the HS or DO mice, to date, is the abundant added cost of such a lengthy study. Mouse carcinogenesis studies require prolonged tumor development periods and thereby demand sizeable housing costs in addition to the need for close monitoring. If each mouse is not monitored closely for the entire duration of the study, death may go unnoticed and the resultant autolysis may rapidly obscure the detection of any potential disease process that may have occurred. Because such large numbers of outbred mice are needed to sufficiently power a QTL mapping study[116], these housing and observation costs are magnified. Additionally, carcinogenesis is a binomially distributed trait and there is the

potential of low cancer incidence, which can compromise the statistical power needed to perform association studies. Although carcinogenesis has not been previously analyzed in highly recombinant mice to date, the high heritability rate for cancer incidence among inbred strains suggests that mapping in such populations will be fruitful. This is especially true for the HS/Npt population, which is derived from founder stains with high spontaneous rates of cancer. For the DO, which is composed partially of cancer resistant wild derived strains, lifetime carcinogenesis studies may present the additional challenge of requiring a higher number of mice to achieve tumor incidence rates that provide adequate power to detect QTL. Utilizing carcinogens, such as radiation exposures, would theoretically improve QTL mapping for a variety of reasons discussed in the following section.

MAPPING GENETIC SUSCEPTIBILITY TO RADIOGENIC CANCER

Genome wide association studies (GWAS) utilizing tumor endpoints can be complicated by the (1) inherent stochastic nature of tumorigenesis, (2) confounding causes of death, and (3) incomplete penetrance of a potential susceptibility allele. Furthermore, (4) tumorigenesis can occur by a variety of molecular mechanisms, each of which may be controlled by a unique set of genetic pathways, even in tumors that appear identical histologically and originate from the same population of cells. In other words, two tumors that are classified identically based on histology may indeed be the result of two distinct molecular pathways. Although all of the tumor entities that are grouped under a single diagnosis may indeed share common susceptibility alleles in tumorigenesis pathways, ideally, each entity would be carefully defined and mapped as a separate disease. Tumorigenesis is complex and typically involves the combination of numerous pathways, each of which may be affected by numerous potential candidate gene variants. These

observations may explain why GWAS of spontaneous cancers often yield modest results. Although, to some degree, these challenges are inherent to cancer GWAS, focusing on radiation induced cancers may mitigate some of these effects for multiple reasons[131]. First, QTL mapping is improved when the phenotype is more rigorously defined. Radiation exposures, whether intentional or not, improve the definition of a tumor phenotype in that tumors that arise following radiation exposures are thought to utilize only a subset of potential oncogenic pathways. Therefore, radiogenic tumors should provide increased statistical associations with genetic variants in comparison to spontaneously arising cancers. Second, the effect of a single strong environmental factor (such as radiation) on a phenotype can potentially decrease the background of the myriad additional environmental factors that may act as confounders. This is supported by the observation that GWAS of adverse drug reactions often yield significant results despite having relatively few cases[132].

Identifying the specific genetic variations that underlie susceptibility to radiation-induced cancer in mice is complex. Known deficiencies in specific mouse genes (*Apc, Ptch, Trp53,* and *Pten*) have been associated with dramatic increases in susceptibility to radiation-induced cancer; however, these genetic defects are rare[133,134]. At a population level, genetic susceptibility to radiogenic cancer is likely much more complex and the result of many interacting polymorphic genes.

An advantage for using outbred mice in tumorigenesis studies is that the diversity of tumor phenotypes available to study will likely be larger than the sum of the tumor types common to the founder strains. Highly recombinant mice provide the capacity to analyze the phenotypic variability that results from the myriad genetic combinations produced in outbred mice[135]. For tumorigenesis studies, the mosaic of founder haplotypes present in each mouse

creates a wide range of susceptibilities at a population level and allows the possibility of evaluating the effect of a given carcinogen on a range of tumor types. Further, this phenotypic variability can be leveraged in carcinogenesis studies to determine whether a given carcinogen will produce the same spectrum of tumor phenotypes as second carcinogen. In other words, such a population can be utilized to determine whether tumors that occur following exposure to γ-rays also occur following HZE ion exposures. Carcinogenesis is a complex process and tumors—even those belonging to the same histotype—may arise via unique tumorigenesis events. As an example in mice, consider AML. AML is a broad diagnosis given to a group of malignancies that may arise via multiple distinct molecular aberrations[44]. Therefore, by mapping populations of outbred mice for susceptibility to distinct forms of radiation (HZE ions and γ-rays), it is possible to determine whether these unique forms of radiation induce tumors via the same oncogenic pathways.

The HS/Npt stock has several advantages for radiation carcinogenesis studies. Three of the progenitor stains, BALB/c, C3H/HeJ and C57BL/6J, have been previously characterized in radiation carcinogenesis studies. Strain specific increases in hepatocellular carcinoma, lung adenoma, AML, mammary tumors, or ovarian tumors have been documented. In contrast, the DO mice have certain limitations when considering carcinogenesis as an endpoint. Although the founder strains provide the DO with extensive genetic diversity, of these founders, only C57BL/6J has been well characterized for radiogenic cancers. And it should be mentioned that C57BL/6J is widely considered a relatively tumor resistant strain. Of the additional DO founders, A/J and 129S1/Sv have also been well characterized for spontaneous tumors, but the remaining five strains have not. Additionally, there is a possibility that this population may be genetically resistant to some tumor types. Part of this concern arises from the fact that the DO population is

created from three strains recently derived from wild mice (WSB/EiJ, CAST/EiJ and PWK/PhJ). These strains are likely to be relatively cancer-resistant and, therefore, confer some level of tumor resistance to the population at large. Indeed, two of these strains, CAST/EiJ[136] and PWK/Rbrc[137], have been used as the tumor resistant strain in mapping crosses to detect tumor QTL. Since tumor incidence in a population will dictate the total number of animals needed, and since estimates for tumor incidence for the DO are not readily available at this point, the use of DO for carcinogenesis studies presents large uncertainties. This may change over time, particularly if spontaneous tumor phenotypes are observed and characterized in the DO; however, currently these uncertainties make HS mice the most reasonable choice for cancer QTL discovery.

One feature of HS or DO mice that is also highly relevant to the deficiencies currently present in the NASA space cancer risk model is the following: highly recombinant mouse populations are uniquely suited to compare the similarity of multiple carcinogens at a genetic level. Specifically, this risk model lacks knowledge on whether γ-rays are similar to HZE ions during tumorigenesis. Comparative QTL mapping in HS mice represents an excellent approach to determining the significance of space radiation by determining if HZE ions produce the same types of tumors, molecularly and histologically, as γ-rays. Comparative QTL mapping in highly recombinant mice has not been previously reported; therefore, comparing QTL between groups presents additional analytical challenges when contrasted with the typical use of the DO or HS studies, which aim to identify the genetic basis of a given phenotype rather than potential similarities between QTL. Below, two additional statistical procedures are discussed that can be adopted to compare genome wide association data between radiation exposure groups: resample

model averaging to compare individual QTL and unsupervised hierarchical clustering to compare entire genome scans.

CO-OPTING STATISTICAL TOOLS TO COMPARE GENETIC SUSCEPTIBILITY

Resample Model Averaging for Comparative QTL Analysis

Bootstrap aggregation is a resample model averaging procedure which has been demonstrated to produce highly accurate estimates of QTL in structured populations[111,138]. The procedure is relatively simple: for a GWAS of *n* individuals, a sampling of *n* draws is obtained, with replacement, from the observed individuals to form a new data set in which some individuals are omitted and some appear multiple times. For each new data set created in this way, an estimate of the QTL location is calculated. This process is repeated many times and is the basis for determining a confidence interval for a given result. The use of bootstrap procedures is commonly utilized in this way to estimate QTL support intervals in experimental crosses [130,138-142]; however, this statistical method can potentially be applied to a variety of questions, including comparative QTL mapping.

An example of the variety of uses for resample model averaging is presented by Quarrie, et al[140]. This group suggested the use of nonparametric bootstrapping to differentiate pleiotropy from close linkage in QTL mapping[140]. When an identical QTL is observed for two distinct traits, one explanation is that a single gene is involved for two distinct biologic processes, also known as pleiotropy. This was sometimes assumed[143,144] in early mouse QTL studies that resulted in coincident loci for distinct traits. Another possibility, however, is that two distinct genetic variants are present in close proximity, each independently contributing to the two phenotypes. Because the two hypothetical genetic variants happen to be in close proximity, they

are difficult to distinguish in low resolution mapping studies[140]. Using resample model averaging in these situations was suggested to best differentiate precise locations of the QTL; if the same markers were repeatedly identified, the case for pleiotropy was strengthened.

For comparative QTL mapping in tumorigenesis studies, nonparametric resample model averaging could similarly be leveraged to identify whether the same QTL renders an individual susceptible to distinct environmental carcinogens. One significant advantage to using bootstrap procedures to detect potential coincident loci is that comparisons can be made between groups based on the identification of a highly significant QTL identified in only one exposure group (e.g. at a false positive rate of 1 per 20 scans). This QTL may be present in the alternative exposure group, but at lower confidence (e.g. at a false positive rate of 1 per 10 scans), and therefore discarded in a typical GWAS. A diagrammatic representation of the comparative QTL bootstrap procedure is presented in **Figure 1.6**. Because the resultant genetic positions derived from bootstrapping are composed of the most significant locus for each resampling regardless of the significance level for the mapping procedure, comparisons can be drawn between QTL that might have been discarded based on the stringent statistical demands of an assay involving hundreds of thousands of independent tests.

Using the comparative QTL procedure described, it can be determined whether an individual's cancer risk from one carcinogen will be predictive of that individual's cancer risk to another carcinogen. The application of this procedure is well-illustrated by the space radiation problem, where much is known about γ-ray exposures and little is known about space radiation exposures.

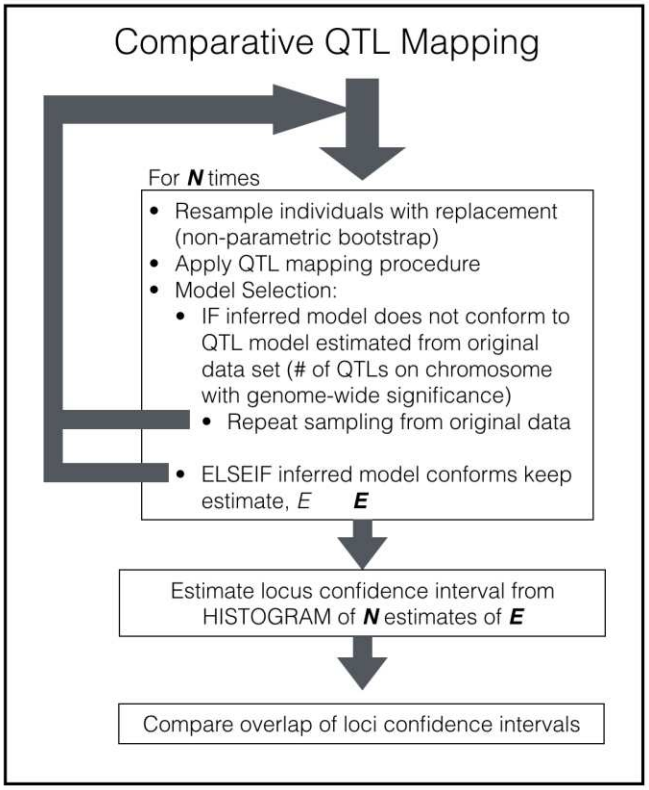

Figure 1.6: Diagram of a nonparametric resample model averaging procedure for comparative QTL mapping.

Clustering Procedures for Genome Wide Association Scans

Clustering is a common analysis procedure for high-dimensional data. It can be a useful method for identifying structure in a dataset by identifying groups based on the similarity of their components. Numerous clustering algorithms have been described and implemented over the past 50 years[145-147]. Important aspects of the clustering algorithm include the distance metric used to compare samples and the linkage criteria between sets of observations. Because any clustering procedure can be applied to any dataset, care must be taken to select the appropriate algorithm so that the information present within a given dataset is best utilized.

Clustering was widely adopted by the genetics community in an effort to interpret the dramatic increases in gene expression data that accompanied the "omics" revolution. Consensus methods were developed for algorithm selection so that the data was most appropriately utilized[148,149]. The data sets created for gene expression experiments are hundreds or thousands of measurements that are independently measured. This is in contrast to genotype data, which consists of numerous data points along a linear structure—the chromosome. These unique aspects require unique distance measures, which is the underlying comparison made during clustering. Several distance metrics are available for cluster analysis; however, these methods can be broadly separated into two families: Euclidean distances and correlations (**Figure 1.7**).

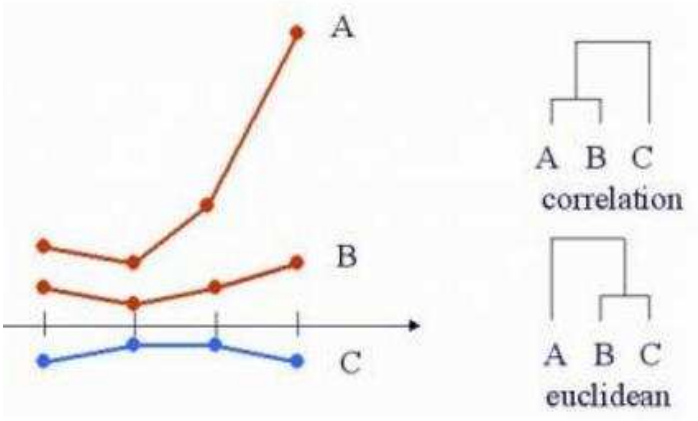

Figure 1.7: The results of clustering on a hypothetical dataset using two distinct distance metrics: correlation and Euclidean distances.

Euclidean distance calculations are based on the magnitude of difference between two samples. This distance measure is well suited to make comparisons between samples that contain large numbers of unrelated observations. Euclidean distances are the most appropriate measure for clustering gene expression data, where each value represents a single gene and no linear structure is present between given data points. However, when dealing with linearly arranged

data, such as the results of a genome scan, each successive data point is inherently associated with its neighbors. Therefore, shape should be considered during cluster analysis.

Correlation calculations are better able to detect shape or trends in a dataset. This is true, in part, because correlation measures are unit independent. If all the values of one object in a cluster analysis were scaled one hundred times, the correlation results would remain unaffected but the Euclidean distance results would be remarkably different[150]. Because of the capability for correlation analysis to capture similarities between linear trends or shapes in a dataset, this distance measure is best suited to detect similarities between genome scans.

Unlike other statistic procedures, such as regression models, clustering lacks a response variable and is not routinely performed as a formal hypothesis test. Therefore, determining the significance of a clustering result can be problematic as no consensus method exists for cluster validation[146]. Permutation analysis simply provides the distribution of clustering results that will randomly occur from a given dataset; this can then be used as a baseline from which to determine a significance level on a given dendrogram tree. While the overall validity of a given cluster can be accomplished by cluster permutation analysis, no method is identified to estimate the number of clusters that should be present in a dataset[146]. Further, methods to determine the significance of specific subset of objects clustering together do not exist; in such cases, the permutation threshold is likely overly stringent.

Project Rationale

There are a number of possibilities that could lead to the extinction of life on Earth, including asteroid collision, nuclear war, or global environmental changes that render the planet inhospitable. The future of humanity is best safeguarded from such catastrophe by establishing independence from Earth, thereby defending the future of all that has evolved terrestrially by subsidizing life on other planets. Of the many challenges associated with the pursuit of a multi-planetary existence, this dissertation addresses the interplanetary space radiation environment. Despite the growing understanding of the physical properties of the space radiation environment, the biological effects of such an environment remain unclear. These biological effects, particularly cancer risks, are considered the most significant impediment to space travel. Further, understanding the significance of space radiation is highly limited by the lack of human epidemiological data for such exposures and will continue to rely on experimental animal studies. The overarching goal of these projects is to examine some of the uncertainties surrounding the risks that face humans exposed to galactic cosmic radiation.

Cancer risk from galactic cosmic radiation exposure is considered a potential "showstopper" for a manned mission to Mars. Protected by Earth's magnetosphere, life has evolved in the absence of HZE ions, a biologically important element of the space radiation environment. In the absence of human exposures to HZE ions, risk estimates for humans are necessarily derived from a combination of the observed effects of humans exposed to γ-rays and the experimental studies analyzing the comparability of HZE ion and γ-ray exposures. In **Chapter 2 (Characterization of the Tumor Spectrum Arising in HZE ion Irradiated Outbred Mice),** we characterize the spectrum of tumors that arise in a heterogeneous stock of

mice irradiated with HZE nuclei and compare it to the spectra of tumors arising in similar populations of γ-ray irradiated or unirradiated mice. This heterogeneous stock of mice presents the best available method to study radiation effects on a genetically diverse population, such as humans, and allows the comparison of a wide variety of tumor types. These tumor types are characterized histologically by board certified veterinary pathologists and further characterized molecularly as appropriate to most rigorously define tumor entities. Lymphomas, the most common tumor observed for HS mice, are immunophenotyped using tissue microarrays and subtyped using the Bethesda protocols[27,28]. Additionally, acute myeloid leukemias are classified according to specific chromosomal deletions and hepatocellular carcinomas are classified according to the presence or absence of a known fusion gene. Tumor malignancy is also assessed in these mice. Metastasis surveillance is accomplished by histologically examining all lung lobes in mice with an observable primary tumor. Further, metastatic density is quantified to determine potential differences between exposures groups.

Genetic susceptibility to the development of radiogenic tumors is also explored to determine overlap in susceptibility for spontaneous tumors as well as tumors arising in γ-ray and HZE ion exposed mice. The capability of identifying individuals at risk for radiogenic tumors could valuably inform crew selection protocols and minimize the effects of radiation exposures on astronauts. Through a genetics approach using carcinogenesis data from a mouse model of genetic diversity, as outlined in **Chapter 3 (Genome mapping identifies overlap in susceptibility for HZE ion and γ-ray induced tumors)**, we investigate the genetic regions that are involved with susceptibility to γ-ray and HZE ion induced tumors. The combination of the methodical and balanced accumulation of genetic recombination paired with genotyping arrays that are sufficiently dense to capture these recombination events allows for gene level resolution

for QTL affecting tumor susceptibility. We identify and characterize the moderate and large effect QTL that underlie susceptibility to spontaneous, γ-ray-induced, and HZE ion-induced tumors and determine if the QTL overlap between the groups. With the current availability of novel mouse models of genetic diversity, there is abundant potential to discover mechanisms of genetic susceptibility to cancer risk. Comparative QTL analysis can also be employed for different exposures groups. In addition to cancer susceptibility, other endpoints are of concern for astronauts. The same mice from the carcinogenesis study described above are also phenotyped for cataractogenesis as described in **Chapter 4 (Overlap in genetic susceptibility to cataractogenesis following HZE ion and γ-ray exposures)**. Susceptibility to cataractogenesis, while likely not fatal, could result in significant health risks for astronauts. Further, utilizing the genetically characterized mouse resources produced in the carcinogenesis study for additional phenotypes represents a conservative strategy to maximize biologic information obtained.

One central limitation for all ground-based studies involving HZE ions produced in particle accelerators is dose rate. Chronic exposures to accelerator produced HZE ions over weeks to months is not technologically feasible; however, exposures in the space radiation environment are received over the duration of a mission at continuous low dose rates. In **Chapter 5 (Dose rate effects on carcinogenesis: differences in tumor histotype and genetic susceptibility)**, we examine whether differences in radiation dose rate, achieved via dose fractionation, can affect tumor histotype. In addition, we demonstrate that genetic background can affect an individual's response to radiation at different dose-rates by utilizing two different strains of mice. As one would expect, individuals at increased risk for tumors at acute dose rates are also at increased risk when the same total dose is delivered over a protracted time period.

This dissertation has two principal goals, each of which aim to reduce the uncertainty of carcinogenesis risk assessment from exposures to the interplanetary space radiation environment. The first is to determine whether HZE ion exposures, the most concerning constituent of the space radiation environment, produce the same types of tumors as those that occur following γ-rays exposures in a genetically diverse population. The second is to determine the genetics of tumor susceptibility for each exposure group and determine whether overlap occurs. This work is not based on an assumption that the tumors observed in HZE ion irradiated mice will likely also occur in humans. Rather, it is based on the likelihood that if mice develop the same tumors regardless of exposure to HZE ions or γ-rays, humans will as well. And if the genetic susceptibilities to tumors are the same for mice exposed to HZE ions or γ-rays, known genetic susceptibilities for humans exposed to γ-ray can be extrapolated to space radiation exposures.

References

1. Novelline, R. A., & Squire, L. F. (2004). *Squire's fundamentals of radiology*. La Editorial, UPR.
2. Malley, M. C. (2011). *Radioactivity: a history of a mysterious science*. Oxford University Press.
3. Pacini, D. (1911). *La radiazione penetrante sul mare*. G. Bertero.
4. Wulf, T. (1909). On the radiation of high penetrating power that exists in the atmosphere. *Phys. Zeit*, *1*(152-157), 124.
5. Hess, V. F. (1912). Observations in low level radiation during seven free balloon flights. *Phys. Zeit*, *13*, 1084-1091.
6. Kolhörster, W. (1914). Messungen der durchdringenden Strahlungen bis in Höhen von 9300 m. *Verh. Dtsch. Phys. Ges*, *16*, 719-721.
7. Millikan, R. A. (1925). High Frequency Rays of Cosmic Origin. *Science*,*62*(1612), 445-448.
8. Chancellor, J. C., Scott, G. B., & Sutton, J. P. (2014). Space radiation: the number one risk to astronaut health beyond low earth orbit. *Life*, *4*(3), 491-510.
9. Sihver, L., Ploc, O., Puchalska, M., Ambrožová, I., Kubančák, J., Kyselová, D., & Shurshakov, V. (2015). Radiation environment at aviation altitudes and in space. *Radiation protection dosimetry*, ncv330.
10. Hu, S., Kim, M. H. Y., McClellan, G. E., & Cucinotta, F. A. (2009). Modeling the acute health effects of astronauts from exposure to large solar particle events. *Health Physics*, *96*(4), 465-476.
11. Guo, J., Zeitlin, C., Wimmer-Schweingruber, R. F., Hassler, D. M., Ehresmann, B., Köhler, J., ... & Cucinotta, F. (2015). MSL-RAD radiation environment measurements. *Radiation protection dosimetry*, *166*(1-4), 290-294.
12. Badhwar, G. D., & O'Neill, P. M. (1994). Long-term modulation of galactic cosmic radiation and its model for space exploration. *Advances in Space Research*, *14*(10), 749-757.
13. Cucinotta, F. A., Kim, M. H. Y., & Ren, L. (2006). Evaluating shielding effectiveness for reducing space radiation cancer risks. *Radiation Measurements*, *41*(9), 1173-1185.
14. Simpson, J. A. (1983). Elemental and isotopic composition of the galactic cosmic rays. *Annual Review of Nuclear and Particle Science*, *33*(1), 323-382.
15. Zeitlin, C., Hassler, D. M., Cucinotta, F. A., Ehresmann, B., Wimmer-Schweingruber, R. F., Brinza, D. E., ... & Burmeister, S. (2013). Measurements of energetic particle radiation in transit to Mars on the Mars Science Laboratory. *Science*, *340*(6136), 1080-1084.
16. Cucinotta, F. A., Alp, M., Rowedder, B., & Kim, M. H. Y. (2015). Safe days in space with acceptable uncertainty from space radiation exposure. *Life sciences in space research*, *5*, 31-38.
17. Durante, M., & Cucinotta, F. A. (2008). Heavy ion carcinogenesis and human space exploration. *Nature Reviews Cancer*, *8*(6), 465-472.
18. Sridharan, D. M., Asaithamby, A., Bailey, S. M., Costes, S. V., Doetsch, P. W., Dynan, W. S., ... & Werner, E. (2015). Understanding cancer development processes after HZE-

particle exposure: roles of ROS, DNA damage repair and inflammation. *Radiation research*, *183*(1), 1-26.
19. Schauer, D. A., & Linton, O. W. (2009). National Council on Radiation Protection and Measurements Report Shows Substantial Medical Exposure Increase 1. *Radiology*, *253*(2), 293-296.
20. Venneri, L., Rossi, F., Botto, N., Andreassi, M. G., Salcone, N., Emad, A., ... & Picano, E. (2009). Cancer risk from professional exposure in staff working in cardiac catheterization laboratory: insights from the National Research Council's Biological Effects of Ionizing Radiation VII Report. *American heart journal*, *157*(1), 118-124.
21. Schimmerling, W., Cucinotta, F. A., & Wilson, J. W. (2003). Radiation risk and human space exploration. *Advances in Space Research*, *31*(1), 27-34.
22. Durante, M., & Cucinotta, F. A. (2011). Physical basis of radiation protection in space travel. *Reviews of Modern Physics*, *83*(4), 1245.
23. Dietze, G., Bartlett, D. T., Cool, D. A., Cucinotta, F. A., Jia, X., McAulay, I. R., ... & Sato, T. (2013). ICRP Publication 123: Assessment of Radiation Exposure of Astronauts in Space. *Annals of the ICRP*, *42*(4), 1-339.
24. Sievert, R. M., & Failla, G. (1959). recommendations of the International Commission on Radiological Protection. *Health Physics (England)*, *2*.
25. Board, S. S. (2012). *Technical Evaluation of the NASA Model for Cancer Risk to Astronauts Due to Space Radiation*. National Academies Press.
26. National Research Council (US). Committee on the Evaluation of Radiation Shielding for Space Exploration. *Managing Space Radiation Risk in the New Era of Space Exploration*. National Academies Press, 2008.
27. National Council on Radiation Protection and Measurements. "Information Needed to Make Radiation Protection Recommendations for Space Missions Beyond Low-earth Orbit: Recommendations of the National Council on Radiation Protection and Measurements." National Council on Radiation Protection and Measurements, 2006.
28. Huff, J., Carnell, L., Blattnig, S., Chappell, L., Kerry, G., Lumpkins, S., ... & Werneth, C. (2016). Evidence Report: Risk of Radiation Carcinogenesis.
29. Nelson, G. A., Simonsen, L., & Huff, J. L. (2016). Evidence Report: Risk of Acute and Late Central Nervous System Effects from Radiation Exposure.
30. Huff, J., & Cucinotta, F. A. (2009). Risk of degenerative tissue or other health effects from radiation exposure. *Human Health and performance risks of space exploration missions National Aeronautics and Space Administration, NASA SP-2009-3405, Houston, TX*, 213-35.
31. Board, Space Studies. *A risk reduction strategy for human exploration of space: a review of NASA's Bioastronautics Roadmap*. National Academies Press, 2006.
32. Hurlbert, K., Bagdigian, B., Carroll, C., Jeevarajan, A., Kliss, M., & Singh, B. (2012). Human Health, Life Support and Habitation Systems.
33. Cucinotta, F. A., Kim, M. H. Y., & Chappell, L. J. (2011). Space radiation cancer risk projections and uncertainties-2010.
34. McPhee, J. C., & Charles, J. B. (Eds.). (2009). *Human health and performance risks of space exploration missions: evidence reviewed by the NASA human research program* (Vol. 3405). Government Printing Office.
35. Preston, D. L., Kusumi, S., Tomonaga, M., Izumi, S., Ron, E., Kuramoto, A., ... & Thompson, D. E. (1994). Cancer incidence in atomic bomb survivors. Part III:

Leukemia, lymphoma and multiple myeloma, 1950-1987. *Radiation research*, *137*(2s), S68-S97.
36. Carnes, B. A., Grahn, D., & Hoel, D. (2003). Mortality of atomic bomb survivors predicted from laboratory animals. *Radiation research*, *160*(2), 159-167.
37. Cucinotta, F. A., Katz, R., & Wilson, J. W. (1998). Radial distribution of electron spectra from high-energy ions. *Radiation and environmental biophysics*, *37*(4), 259-265.
38. Madsen, O., Scally, M., Douady, C. J., Kao, D. J., DeBry, R. W., Adkins, R., ... & Springer, M. S. (2001). Parallel adaptive radiations in two major clades of placental mammals. *Nature*, *409*(6820), 610-614.
39. Chinwalla, A. T., Cook, L. L., Delehaunty, K. D., Fewell, G. A., Fulton, L. A., Fulton, R. S., ... & Miner, T. L. (2002). Initial sequencing and comparative analysis of the mouse genome. *Nature*, *420*(6915), 520-562.
40. Emes, R. D., Goodstadt, L., Winter, E. E., & Ponting, C. P. (2003). Comparison of the genomes of human and mouse lays the foundation of genome zoology. *Human molecular genetics*, *12*(7), 701-709.
41. Kaplan, H. S., Hirsch, B. B., & Brown, M. B. (1956). Indirect Induction of Lymphomas in Irradiated Mice IV. Genetic Evidence of the Origin of the Tumor Cells from the Thymic Grafts. *Cancer Research*, *16*(5), 434-436.
42. Mole, R. H., Papworth, D. G., & Corp, M. J. (1983). The dose-response for x-ray induction of myeloid leukaemia in male CBA/H mice. *British Journal of Cancer*, *47*(2), 285.
43. Storer, J. B., Mitchell, T. J., & Fry, R. J. M. (1988). Extrapolation of the relative risk of radiogenic neoplasms across mouse strains and to man. *Radiation research*, *114*(2), 331-353.
44. Szymanska, H., Sitarz, M., Krysiak, E., Piskorowska, J., Czarnomska, A., Skurzak, H., ... & Demant, P. (1999). Genetics of susceptibility to radiation- induced lymphomas, leukemias and lung tumors studied in recombinant congenic strains. *International journal of cancer*, *83*(5), 674-678.
45. Barthold, Stephen W., Stephen M. Griffey, and Dean H. Percy. *Pathology of laboratory rodents and rabbits*. John Wiley & Sons, 2016.
46. Bielefeldt-Ohmann, H., Genik, P. C., Fallgren, C. M., Ullrich, R. L., & Weil, M. M. (2012). Animal studies of charged particle-induced carcinogenesis. *Health physics*, *103*(5), 568-576.
47. Weil, M. M., Ray, F. A., Genik, P. C., Yu, Y., McCarthy, M., Fallgren, C. M., & Ullrich, R. L. (2014). Effects of 28 Si ions, 56 Fe ions, and protons on the induction of murine acute myeloid leukemia and hepatocellular carcinoma.*PloS one*, *9*(8), e104819.
48. March, H. C. (1944). Leukemia in radiologists. *Radiology*, *43*(3), 275-278.
49. Hall, E. J., & Giaccia, A. J. (2006). *Radiobiology for the Radiologist*. Lippincott Williams & Wilkins.
50. Boice Jr, J. D., Engholm, G., Kleinerman, R. A., Blettner, M., Stovall, M., Lisco, H., ... & Krementz, E. T. (1988). Radiation dose and second cancer risk in patients treated for cancer of the cervix. *Radiation research*, *116*(1), 3-55.
51. Shore, R. E., Moseson, M., Harley, N., & Pasternack, B. S. (2003). Tumors and other diseases following childhood x-ray treatment for ringworm of the scalp (Tinea capitis). *Health physics*, *85*(4), 404-408.
52. Little, M. P., Weiss, H. A., Boice Jr, J. D., Darby, S. C., Day, N. E., & Muirhead, C. R.

(1999). Risks of leukemia in Japanese atomic bomb survivors, in women treated for cervical cancer, and in patients treated for ankylosing spondylitis. *Radiation research*, *152*(3), 280-292.

53. Weiss, H. A., Darby, S. C., & Doll, R. (1994). Cancer mortality following X- ray treatment for ankylosing spondylitis. *International Journal of Cancer*, *59*(3), 327-338.
54. Weiss, H. A., Darby, S. C., Fearn, T., & Doll, R. (1995). Leukemia mortality after X-ray treatment for ankylosing spondylitis. *Radiation research*, *142*(1), 1-11.
55. Krebs, C., Rask-Nielsen, H. C., & Wagner, A. (1930). The origin of Lymphosarcomatosis and its relation to other forms of Leucosis in white mice Lymphomatosis infiltrans leucemica et aleucemica. *Acta radiologica*, (10 suppl), 1-72.
56. Upton, A. C., Wolff, F. F., Furth, J., & Kimball, A. W. (1958). A comparison of the induction of myeloid and lymphoid leukemias in X-radiated RF mice.*Cancer Research*, *18*(7), 842-848.
57. Wolman, S. R., McMorrow, L. E., & Cohen, M. W. (1982). Animal model of human disease: myelogenous leukemia in the RF mouse. *The American journal of pathology*, *107*(2), 280.
58. Resnitzky, P., Estrov, Z., & Haran-Ghera, N. (1985). High incidence of acute myeloid leukemia in SJL/J mice after X-irradiation and corticosteroids.*Leukemia research*, *9*(12), 1519-1528.
59. Major, I., & Mole, R. H. (1978). Myeloid leukaemia in X-ray irradiated CBA mice.
60. Major, I. R. (1979). Induction of myeloid leukaemia by whole-body single exposure of CBA male mice to x-rays. *British journal of cancer*, *40*(6), 903.
61. Seki, M., Yoshida, K., Nishimura, M., & Nemoto, K. (1991). Radiation-induced myeloid leukemia in C3H/He mice and the effect of prednisolone acetate on leukemogenesis. *Radiation research*, *127*(2), 146-149.
62. Rivina, L., Davoren, M. J., & Schiestl, R. H. (2016). Mouse models for radiation-induced cancers. *Mutagenesis*, gew019.
63. Rivina, L., Davoren, M., & Schiestl, R. H. (2014). Radiation-induced myeloid leukemia in murine models. *Human genomics*, *8*(1), 1.
64. Yoshida, K., Inoue, T., Nojima, K., Hirabayashi, Y., & Sado, T. (1997). Calorie restriction reduces the incidence of myeloid leukemia induced by a single whole-body radiation in C3H/He mice. *Proceedings of the National Academy of Sciences*, *94*(6), 2615-2619.
65. Yoshida, K., Hirabayashi, Y., Watanabe, F., Sado, T., & Inoue, T. (2006). Caloric restriction prevents radiation-induced myeloid leukemia in C3H/HeMs mice and inversely increases incidence of tumor-free death: implications in changes in number of hemopoietic progenitor cells. *Experimental hematology*, *34*(3), 274-283.
66. Hayata, I., Ishihara, T., Hirashima, K., Sado, T., & Yamagiwa, J. (1979). Partial deletion of chromosome# 2 in myelocytic leukemias of irradiated C3H/He and RFM mice. *Journal of the National Cancer Institute*, *63*(3), 843-848.
67. Genik, P. C., Vyazunova, I., Steffen, L. S., Bacher, J. W., Bielefeldt-Ohmann, H., McKercher, S., ... & Ray, F. A. (2014). Leukemogenesis in heterozygous PU. 1 knockout mice. *Radiation research*, *182*(3), 310-315.
68. Azumi, J. I., & Sachs, L. (1977). Chromosome mapping of the genes that control differentiation and malignancy in myeloid leukemic cells. *Proceedings of the National Academy of Sciences*, *74*(1), 253-257.

69. Ban, N., Kai, M., & Kusama, T. (1997). Chromosome Aberrations in Bone Marrow Cells of C3/He Mice at an Early Stage after Whole-Body Irradiation. *Journal of radiation research*, *38*(4), 219-231.
70. Cook, W. D., McCaw, B. J., Herring, C., John, D. L., Foote, S. J., Nutt, S. L., & Adams, J. M. (2004). PU. 1 is a suppressor of myeloid leukemia, inactivated in mice by gene deletion and mutation of its DNA binding domain. *Blood*, *104*(12), 3437-3444.
71. Alexander, B. J., Rasko, J. E., Morahan, G., & Cook, W. D. (1995). Gene deletion explains both in vivo and in vitro generated chromosome 2 aberrations associated with murine myeloid leukemia. *Leukemia*, *9*(12), 2009-2015.
72. Silver, A., Moody, J., Dunford, R., Clark, D., Ganz, S., Bulman, R., ... & Cox, R. (1999). Molecular mapping of chromosome 2 deletions in murine radiation- induced AML localizes a putative tumor suppressor gene to a 1.0 cM region homologous to human chromosome segment 11p11–12. *Genes, Chromosomes and Cancer*, *24*(2), 95-104.
73. Moreau-Gachelin, F., Tavitian, A., & Tambourin, P. (1988). Spi-1 is a putative oncogene in virally induced murine erythroleukaemias.
74. Scott, E. W., Simon, M. C., Anastasi, J., & Singh, H. (1994). Requirement of transcription factor PU. 1 in the development of multiple hematopoietic lineages. *Science*, *265*(5178), 1573-1577.
75. Kastner, P., & Chan, S. (2008). PU. 1: a crucial and versatile player in hematopoiesis and leukemia. *The international journal of biochemistry & cell biology*, *40*(1), 22-27.
76. Steidl, U., Rosenbauer, F., Verhaak, R. G., Gu, X., Ebralidze, A., Otu, H. H., ... & Wagner, K. (2006). Essential role of Jun family transcription factors in PU. 1 knockdown–induced leukemic stem cells. *Nature genetics*, *38*(11), 1269-1277.
77. Suraweera, N., Meijne, E., Moody, J., Carvajal-Carmona, L. G., Yoshida, K., Pollard, P., ... & Rowan, A. (2005). Mutations of the PU. 1 Ets domain are specifically associated with murine radiation-induced, but not human therapy-related, acute myeloid leukaemia. *Oncogene*, *24*(22), 3678-3683.
78. Mueller, B. U., Pabst, T., Osato, M., Asou, N., Johansen, L. M., Minden, M. D., ... & Tenen, D. G. (2002). Heterozygous PU. 1 mutations are associated with acute myeloid leukemia. *Blood*, *100*(3), 998-1007.
79. Fernando, T. R., Rodriguez-Malave, N. I., & Rao, D. S. (2012). MicroRNAs in B cell development and malignancy. *Journal of hematology & oncology*, *5*(1), 1.
80. Delgado, O., Batten, K. G., Richardson, J. A., Xie, X. J., Gazdar, A. F., Kaisani, A. A., ... & Wright, W. E. (2014). Radiation-enhanced lung cancer progression in a transgenic mouse model of lung cancer is predictive of outcomes in human lung and breast cancer. *Clinical Cancer Research*, *20*(6), 1610-1622.
81. Moding, E. J., & Kirsch, D. G. (2012). Genetically modified mouse models of lung cancer. *The Health Risks of Extraterrestrial Environments*.
82. Mancuso, M., Pasquali, E., Leonardi, S., Tanori, M., Rebessi, S., Di Majo, V., ... & Saran, A. (2008). Oncogenic bystander radiation effects in Patched heterozygous mouse cerebellum. *Proceedings of the National Academy of Sciences*, *105*(34), 12445-12450.
83. Trani, D., Nelson, S. A., Moon, B. H., Swedlow, J. J., Williams, E. M., Strawn, S. J., ... & Fornace Jr, A. J. (2014). High-energy particle-induced tumorigenesis throughout the gastrointestinal tract. *Radiation research*, *181*(2), 162-171.
84. Degg, N. L., Weil, M. M., Edwards, A., Haines, J., Coster, M., Moody, J., ... & Silver, A. (2003). Adenoma multiplicity in irradiated ApcMin mice is modified by chromosome

16 segments from Balb/c. *Cancer research*, *63*(10), 2361-2363.
85. Datta, K., Suman, S., Kallakury, B. V., & Fornace Jr, A. J. (2013). Heavy ion radiation exposure triggered higher intestinal tumor frequency and greater β-catenin activation than γ radiation in APC Min/+ mice. *PLoS One*, *8*(3), e59295.
86. Illa-Bochaca, I., Ouyang, H., Tang, J., Sebastiano, C., Mao, J. H., Costes, S. V., ... & Barcellos-Hoff, M. H. (2014). Densely ionizing radiation acts via the microenvironment to promote aggressive Trp53-null mammary carcinomas. *Cancer research*, *74*(23), 7137-7148.
87. Ando, K., Koike, S., Oohira, C., Ogiu, T., & Yatagai, F. (2005). Tumor induction in mice locally irradiated with carbon ions: a retrospective analysis. *Journal of radiation research*, *46*(2), 185-190.
88. Weil, M. M., Bedford, J. S., Bielefeldt-Ohmann, H., Ray, F. A., Genik, P. C., Ehrhart, E. J., ... & Callan, M. A. (2009). Incidence of acute myeloid leukemia and hepatocellular carcinoma in mice irradiated with 1 GeV/nucleon 56Fe ions. *Radiation research*, *172*(2), 213-219.
89. Imaoka, T., Nishimura, M., Kakinuma, S., Hatano, Y., Ohmachi, Y., Yoshinaga, S., ... & Shimada, Y. (2007). High relative biologic effectiveness of carbon ion radiation on induction of rat mammary carcinoma and its lack of H-ras and Tp53 mutations. *International Journal of Radiation Oncology* Biology* Physics*, *69*(1), 194-203.
90. Alpen, E. L., Powers-Risius, P., Curtis, S. B., & DeGuzman, R. (1993). Tumorigenic potential of high-Z, high-LET charged-particle radiations. *Radiation research*, *136*(3), 382-391.
91. Alpen, E. L., Powers-Risius, P., Curtis, S. B., DeGuzman, R., & Fry, R. J. M. (1994). Fluence-based relative biological effectiveness for charged particle carcinogenesis in mouse Harderian gland. *Advances in Space Research*, *14*(10), 573-581.
92. Fry, R. J. M., Powers-Risius, P., Alpen, E. L., & Ainsworth, E. J. (1985). High-LET radiation carcinogenesis. *Radiation Research*, *104*(2s), S188-S195.
93. Fry, R. J. M., Ullrich, R. L., Powers-Risius, P., Alpen, E. L., & Ainsworth, E. J. (1983). High-LET radiation carcinogenesis. *Advances in Space Research*, *3*(8), 241-248.
94. Hiromitsuwatanabe, T.O., Nishizaki, M., Fujimoto, N., Kido, S., Yoshimasaishimura, K. S., Kuramoto, K., ... & Katoh, O. (1998). Induction of ovarian tumors by heavy ion irradiation in B6C3F1 mice. *Oncology reports*, *5*, 1377-1380.
95. Burns, F. J., Jin, Y., Koenig, K. L., & Hosselet, S. (1993). The low carcinogenicity of electron radiation relative to argon ions in rat skin. *Radiation research*, *135*(2), 178-188.
96. Burns, F. J., Tang, M. S. E., Frenkel, K., Nádas, A., Wu, F., Uddin, A., & Zhang, R. (2007). Induction and prevention of carcinogenesis in rat skin exposed to space radiation. *Radiation and environmental biophysics*, *46*(2), 195-199.
97. Dicello, J. F., Christian, A., Cucinotta, F. A., Gridley, D. S., Kathirithamby, R., Mann, J., ... & Ricart-Arbona, R. (2004). In vivo mammary tumourigenesis in the Sprague–Dawley rat and microdosimetric correlates. *Physics in medicine and biology*, *49*(16), 3817.
98. Shellabarger, C. J., Baum, J. W., Holtzman, S., & Stone, J. P. (1985). Neon- 20 Ion- and X- Ray- Induced Mammary Carcinogenesis in Female Rats. *Annals of the New York Academy of Sciences*, *459*(1), 239-244.
99. Fry, R. J. M., Powers-Risius, P., Alpen, E. L., & Ainsworth, E. J. (1985). High-LET radiation carcinogenesis. *Radiation Research*, *104*(2s), S188-S195.

100. Yamamoto, M. L., Hafer, K., Reliene, R., Fleming, S., Kelly, O., Hacke, K., & Schiestl, R. H. (2010). Effects of 1 GeV/nucleon 56Fe particles on longevity, carcinogenesis and neuromotor ability in Atm-deficient mice. *Radiation research*, *175*(2), 231-239.
101. Holstein, J. (1979). *The first fifty years at the Jackson Laboratory*. Jackson Laboratory.
102. Crow, J. F. (2002). CC Little, cancer and inbred mice. *Genetics*, *161*(4), 1357-1361.
103. Paigen, K., & Eppig, J. T. (2000). A mouse phenome project. *Mammalian Genome*, *11*(9), 715-717.
104. Flint, J. (2011). Mapping quantitative traits and strategies to find quantitative trait genes. *Methods*, *53*(2), 163-174.
105. Flint, J., & Eskin, E. (2012). Genome-wide association studies in mice. *Nature Reviews Genetics*, *13*(11), 807-817.
106. Shirley, R. L., Walter, N. A., Reilly, M. T., Fehr, C., & Buck, K. J. (2004). Mpdz is a quantitative trait gene for drug withdrawal seizures. *Nature neuroscience*, *7*(7), 699-700.
107. Rangel-Filho, A., Sharma, M., Datta, Y. H., Moreno, C., Roman, R. J., Iwamoto, Y., ... & Jacob, H. J. (2005). RF-2 gene modulates proteinuria and albuminuria independently of changes in glomerular permeability in the fawn-hooded hypertensive rat. *Journal of the American Society of Nephrology*, *16*(4), 852-856.
108. Joe, B., Saad, Y., Lee, N. H., Frank, B. C., Achinike, O. H., Luu, T. V., ... & Manickavasagam, E. (2009). Positional identification of variants of Adamts16 linked to inherited hypertension. *Human molecular genetics*, *18*(15), 2825-2838.
109. Bhatnagar, S., Oler, A. T., Rabaglia, M. E., Stapleton, D. S., Schueler, K. L., Truchan, N. A., ... & Keller, M. P. (2011). Positional cloning of a type 2 diabetes quantitative trait locus; tomosyn-2, a negative regulator of insulin secretion. *PLoS Genet*, *7*(10), e1002323.
110. Flint, J., Valdar, W., Shifman, S., & Mott, R. (2005). Strategies for mapping and cloning quantitative trait genes in rodents. *Nature Reviews Genetics*, *6*(4), 271-286.
111. Valdar, W., Solberg, L. C., Gauguier, D., Burnett, S., Klenerman, P., Cookson, W. O., ... & Flint, J. (2006). Genome-wide genetic association of complex traits in heterogeneous stock mice. *Nature genetics*, *38*(8), 879-887.
112. Threadgill, D. W., & Churchill, G. A. (2012). Ten years of the collaborative cross. *Genetics*, *190*(2), 291-294.
113. Demarest, K., McCaughran, J., Mahjubi, E., Cipp, L., & Hitzemann, R. (1999). Identification of an acute ethanol response quantitative trait locus on mouse chromosome 2. *The Journal of neuroscience*, *19*(2), 549-561.
114. McClearn, G. E., Wilson, J. R., & Meredith, W. (1970). The use of isogenic and heterogenic mouse stocks in behavioral research. In *Contributions to behavior-genetic analysis: The mouse as a prototype* (pp. 3-22). Appleton-Century-Crofts New York.
115. Collaborative Cross Consortium. (2012). The genome architecture of the Collaborative Cross mouse genetic reference population. *Genetics*, *190*(2), 389-401.
116. Woods, L. C. S. (2014). QTL mapping in outbred populations: successes and challenges. *Physiological genomics*, *46*(3), 81-90.
117. Flint, J., Corley, R., DeFries, J. C., & Fulker, D. W. (1995). A simple genetic basis for a complex psychological trait in laboratory mice. *Science*, *269*(5229), 1432.
118. Talbot, C. J., Nicod, A., Cherny, S. S., Fulker, D. W., Collins, A. C., & Flint, J. (1999). High-resolution mapping of quantitative trait loci in outbred mice. *Nature genetics*, *21*(3), 305-308.

119. Johnsen, A. K., Valdar, W., Golden, L., Ortiz- Lopez, A., Hitzemann, R., Flint, J., ... & Benoist, C. (2011). Genome- wide and species- wide dissection of the genetics of arthritis severity in heterogeneous stock mice. *Arthritis & Rheumatism*, *63*(9), 2630-2640.
120. Demarest, K., Koyner, J., McCaughran Jr, J., Cipp, L., & Hitzemann, R. (2001). Further characterization and high-resolution mapping of quantitative trait loci for ethanol-induced locomotor activity. *Behavior genetics*, *31*(1), 79-91.
121. Talbot, C. J., Radcliffe, R. A., Fullerton, J., Hitzemann, R., Wehner, J. M., & Flint, J. (2003). Fine scale mapping of a genetic locus for conditioned fear. *Mammalian genome*, *14*(4), 223-230.
122. Svenson, K. L., Gatti, D. M., Valdar, W., Welsh, C. E., Cheng, R., Chesler, E. J., ... & Churchill, G. A. (2012). High-resolution genetic mapping using the Mouse Diversity outbred population. *Genetics*, *190*(2), 437-447.
123. Yalcin, B., & Flint, J. (2012). Association studies in outbred mice in a new era of full-genome sequencing. *Mammalian genome*, *23*(9-10), 719-726.
124. Welsh, C. E., Miller, D. R., Manly, K. F., Wang, J., McMillan, L., Morahan, G., ... & de Villena, F. P. M. (2012). Status and access to the Collaborative Cross population. *Mammalian Genome*, *23*(9-10), 706-712.
125. Aylor, D. L., Valdar, W., Foulds-Mathes, W., Buus, R. J., Verdugo, R. A., Baric, R. S., ... & Gralinski, L. E. (2011). Genetic analysis of complex traits in the emerging Collaborative Cross. *Genome research*, *21*(8), 1213-1222.
126. Kelada, S. N., Aylor, D. L., Peck, B. C., Ryan, J. F., Tavarez, U., Buus, R. J., ... & de Villena, F. P. M. (2012). Genetic analysis of hematological parameters in incipient lines of the collaborative cross. *G3: Genes| Genomes| Genetics*, *2*(2), 157-165.
127. Ferris, M. T., Aylor, D. L., Bottomly, D., Whitmore, A. C., Aicher, L. D., Bell, T. A., ... & Haagmans, B. L. (2013). Modeling host genetic regulation of influenza pathogenesis in the collaborative cross. *PLoS Pathog*, *9*(2), e1003196.
128. Gatti, D. M., Svenson, K. L., Shabalin, A., Wu, L. Y., Valdar, W., Simecek, P., ... & Chesler, E. J. (2014). Quantitative trait locus mapping methods for diversity outbred mice. *G3: Genes| Genomes| Genetics*, *4*(9), 1623-1633.
129. Broman, K. W. (2012). Haplotype probabilities in advanced intercross populations. *G3: Genes| Genomes| Genetics*, *2*(2), 199-202.
130. Cox, A., Ackert-Bicknell, C. L., Dumont, B. L., Ding, Y., Bell, J. T., Brockmann, G. A., ... & Tsaih, S. W. (2009). A new standard genetic map for the laboratory mouse. *Genetics*, *182*(4), 1335-1344.
131. Locke, P. A., & Weil, M. M. (2016). personalized Cancer risk assessments for space radiation exposures. *Frontiers in oncology*, *6*.
132. Knight, J. A., Skol, A. D., Shinde, A., Hastings, D., Walgren, R. A., Shao, J., ... & Larson, R. A. (2009). Genome-wide association study to identify novel loci associated with therapy-related myeloid leukemia susceptibility. *Blood*, *113*(22), 5575-5582.
133. Yu, Y., Okayasu, R., Weil, M. M., Silver, A., McCarthy, M., Zabriskie, R., ... & Ullrich, R. L. (2001). Elevated breast cancer risk in irradiated BALB/c mice associates with unique functional polymorphism of the Prkdc (DNA-dependent protein kinase catalytic subunit) gene. *Cancer research*, *61*(5), 1820-1824.
134. Mori, N., Matsumoto, Y., Okumoto, M., Suzuki, N., & Yamate, J. (2001). Variations in Prkdc encoding the catalytic subunit of DNA-dependent protein kinase (DNA-PKcs) and

susceptibility to radiation-induced apoptosis and lymphomagenesis. *Oncogene*, *20*(28), 3609-3619.
135. French, J. E., Gatti, D. M., Morgan, D. L., Kissling, G. E., Shockley, K. R., Knudsen, G. A., ... & Pedersen, L. C. (2015). Diversity outbred mice identify population-based exposure thresholds and genetic factors that influence benzene-induced genotoxicity. *Environmental Health Perspectives (Online)*, *123*(3), 237.
136. Dorward, A. M., Shultz, K. L., Horton, L. G., Li, R., Churchill, G. A., & Beamer, W. G. (2005). Distal Chr 4 harbors a genetic locus (Gct1) fundamental for spontaneous ovarian granulosa cell tumorigenesis in a mouse model. *Cancer research*, *65*(4), 1259-1264.
137. Fujiwara, K., Igarashi, J., Irahara, N., Kimura, M., & Nagase, H. (2007). New chemically induced skin tumour susceptibility loci identified in a mouse backcross between FVB and dominant resistant PWK. *BMC genetics*, *8*(1), 1.
138. Valdar, W., Holmes, C. C., Mott, R., & Flint, J. (2009). Mapping in structured populations by resample model averaging. *Genetics*, *182*(4), 1263-1277.
139. Visscher, P. M., Thompson, R., & Haley, C. S. (1996). Confidence intervals in QTL mapping by bootstrapping. *Genetics*, *143*(2), 1013-1020.
140. Lebreton, C. M., Visscher, P. M., Haley, C. S., Semikhodskii, A., & Quarrie, S. A. (1998). A nonparametric bootstrap method for testing close linkage vs. pleiotropy of coincident quantitative trait loci. *Genetics*, *150*(2), 931-943.
141. Mott, R., Talbot, C. J., Turri, M. G., Collins, A. C., & Flint, J. (2000). A method for fine mapping quantitative trait loci in outbred animal stocks. *Proceedings of the National Academy of Sciences*, *97*(23), 12649-12654.
142. Sequencing, R. G., & Mapping Consortium. (2013). Combined sequence-based and genetic mapping analysis of complex traits in outbred rats. *Nature genetics*, *45*(7), 767-775.
143. Ronin, Y. I., Kirzhner, V. M., & Korol, A. B. (1995). Linkage between loci of quantitative traits and marker loci: multi-trait analysis with a single marker. *Theoretical and applied genetics*, *90*(6), 776-786.
144. Korol, A. B., Ronin, Y. I., & Kirzhner, V. M. (1995). Interval mapping of quantitative trait loci employing correlated trait complexes. *Genetics*, *140*(3), 1137-1147.
145. Everitt, B. S., Landau, S. & Leese, M. *Cluster Analysis*. (Taylor & Francis, 2001).
146. Liu, Y., Hayes, D. N., Nobel, A., & Marron, J. S. (2012). Statistical significance of clustering for high-dimension, low–sample size data. *Journal of the American Statistical Association*.
147. Hartigan, J. A. (1985). Statistical theory in clustering. *Journal of classification*, *2*(1), 63-76.
148. Hayes, D. N., & Meyerson, M. (2006). Microarray Approaches to Gene Expression Analysis. In *Molecular Diagnostics* (pp. 121-148). Humana Press.
149. Weinstein, J. N. *et al.* An Information-Intensive Approach to the Molecular Pharmacology of Cancer. *Science* **275,** 343–349 (1997).
150. Hayes, D. N., & Meyerson, M. (2006). Microarray Approaches to Gene Expression Analysis. In *Molecular Diagnostics* (pp. 121-148). Humana Press.

Chapter Two

Characterization of the tumor spectrum arising in HZE ion irradiated outbred mice

SUMMARY

In the absence of human data for high charge, high energy (HZE) ion exposures, calculating the risk of carcinogenesis for the space radiation environment will continue to rely on animal studies of HZE ion exposures and human epidemiologic data for γ-ray induced tumors. If animals develop the same tumor spectra—histologically and molecularly—whether exposed to HZE ions or γ-rays, the similarities in tumorigenesis should also apply to human populations. Extrapolation of the data from human γ-ray exposures to HZE ion carcinogenesis risk is supported by a small number of experimental studies, in which HZE ions were shown to induce the same tumors in mice that arise following γ-ray exposure. However, only a small number of HZE ion carcinogenesis studies have been performed to date and all of these studies have utilized animal populations composed of genetically identical, or nearly genetically identical, individuals. Genetically homogeneous populations are predisposed to specific tumor types, regardless of carcinogen exposure, and may therefore obscure the variability that would be observed in a genetically diverse population, such as humans.

To compare the spectra of tumors that arise in a genetically diverse population, three groups of male and female HS/Npt mice, derived from the same outbreeding generation, were established. The first group (n = 622) was exposed to either a 0.4 Gy dose of 240 MeV/n ^{28}Si ions or 600 MeV/n ^{56}Fe ions; these two HZE nuclei have been demonstrated in the space radiation environment. The second group (n = 615) was exposed to a 3.0 Gy dose of ^{137}Cs γ-rays

and serve as a reference population for the HZE ion carcinogenesis data. Although at face value the doses for each group seem disparate, preliminary studies indicate that 0.4 Gy of HZE ions and 3.0 Gy of γ-rays are each maximally tumorigenic. Because this study aims to identify differences in the tumor spectra between the two radiation qualities, maximally tumorigenic doses are desirable. The third group (n = 613) was exposed to all the same conditions as the aforementioned groups, but was sham irradiated (placed in radiation chambers and facilities in the absence of radiation). This unirradiated control group also serves as reference population so that the tumor spectrum that occurs spontaneously in HS/Npt can be best differentiated from the tumor spectra induced following HZE ion and γ-ray exposures. The mice were monitored for cancer development until they reached 800 days of age or became moribund. Comprehensive necropsies were performed on each mouse and on all organ systems. Each detected macroscopic lesion was characterized histologically. Lymphomas, the most commonly diagnosed tumor for all exposure groups, were subcategorized according to immunophenotype and Bethesda protocols for lymphoid neoplasms. Acute myeloid leukemias were analyzed for the presence of characteristic, radiation-induced deletions in chromosome 2. Hepatocellular carcinomas were characterized for the presence or absence of a specific fusion gene transcript. Lung lobes were examined for the presence of metastases for mice with solid tumors and metastatic densities were quantified using whole slide imaging.

Tumors were the predominant cause of morbidity and mortality in all groups. HZE ion irradiated mice survived longer than γ-ray irradiated mice, but not as long as unirradiated controls. The reduced life spans of irradiated mice resulted partly from increased tumor incidences as well as decreased tumor latencies. γ-ray irradiated mice were at greater risk for hematological malignancies, pituitary tumors, and ovarian tumors than unirradiated mice; HZE

ion irradiated mice demonstrated an intermediate susceptibility to these histotypes. For Harderian gland tumors, thyroid tumors, hepatocellular carcinomas, and sarcomas, HZE ion and γ-ray irradiated mice were at a similarly and significantly increased risk compared to unirradiated controls. Radiation-induced acute myeloid leukemias, whether following HZE ion or γ-ray exposures, had increased incidences of a commonly deleted region in chromosome 2 compared to spontaneous myeloid leukemias. Malignancy, as defined by metastatic incidence and density, was not significantly different between unirradiated and irradiated mice. These results support the current NASA model used to predict carcinogenesis risk from space radiation exposures.

INTRODUCTION

Risk is inherent to exploration and acceptable levels of risk must be defined by a society based on the potential costs and benefits of exploration. Estimating the risks involved with space exploration is complicated by the uncertainty surrounding the biologic effects of the unique forms of radiation present only in space: high energy, high charge (HZE) ions. The HZE ions present in space can be replicated in particle accelerators and studied in attempts to predict space radiation associated risks for astronauts. For cancer, which is already the second most common cause of death for Americans, NASA defines risk as the amount of excess cancer deaths attributable to radiation exposures. This acceptable risk is established as a 3% increased risk of exposure-induced death (REID)[1]. The current NASA model to calculate cancer risk from space radiation exposures is built largely upon epidemiological data from the survivors of the Hiroshima and Nagasaki atomic bombings, a cohort of individuals exposed predominantly to γ-rays[2-4]. One key assumption in this model is that the spectra of tumor types, and their biologic behaviors, will be similar for individuals exposed to different forms of ionizing radiation.

However, notable physical differences exist between terrestrial radiation such as γ-rays—which are composed of sparsely ionizing photons—and the densely ionizing particle radiation found in space. Missions to a near Earth asteroid or Mars currently exceed NASA's 3% REID for fatal cancer[5]. Even the duration of International Space Station (ISS) missions are restricted by the risk for fatal cancer. Male astronauts are limited to 24 months on ISS by the 3% REID for radiation carcinogenesis[6]. Female astronauts achieve the same level of risk much sooner than their male crewmates, at approximately 18 months[6]. This difference is supported by physical dosimetry and epidemiological data, which indicates that women are at greater risk for radiogenic cancers than men due to their longer lifespans, smaller body size, and susceptibility to specific cancer types, such as ovarian and breast carcinomas.

As the 3% REID is derived from the upper 95% confidence interval for the risk estimate[1], decreasing the uncertainty for space radiation-induced cancers can significantly alter what missions NASA will support. The 95% confidence interval surrounding the risk estimates is primarily a reflection of the uncertainties of the biologic effects of HZE ions, a high energy radiation type not naturally found on Earth, but also includes uncertainties surrounding the effects of dose-rate and dosimetry in space, the translatability of risk between different human populations and errors in the current human data, and other concomitant space phenomena, such as the contributory effects of microgravity to biologic effects in astronauts[7,8].

In assessing cancer risks to astronauts, the premise that HZE ion exposures increase the risk for the same types of tumors that arise in human populations exposed to γ-rays is supported by the few animal studies of HZE ion carcinogenesis conducted to date. So far, these studies have found that the tumor types that arise in HZE ion irradiated animals are the same as those that occur spontaneously in these animals or following exposure to sparsely ionizing radiation[9].

However, all of the data are from either inbred mice[10,11] or rats[12], F1 hybrid mice[13-17], or rat stocks with limited genetic heterogeneity[12,18-21]. Experimental designs employing inbred strains are well suited to compare the relative effectiveness of various radiation qualities for inducing specific types of tumors. But since the tumor types that arise in inbred mice are determined, in very large part, by their genetic background, the spectrum of tumors that might arise in a genetically diverse population exposed to HZE ions is unknown.

To more closely model the genetic diversity present in human populations and to minimize the overwhelming effects of genetic background present in previous rodent HZE ion carcinogenesis studies, a mouse model of genetic diversity known as the HS/Npt is utilized. HS/Npt mice are a highly recombinant, genetically heterogeneous stock of mice derived from the systematic outbreeding of eight inbred founder strains[22]. This population is composed of genetically and phenotypically diverse mice, each of which has a unique constellation of the tumor susceptibility alleles present in the founder stains. HS/Npt mice have been utilized extensively for QTL mapping[23-26] and are derived from eight founder strains, each of which is prone to unique tumor histotypes.

To determine whether the tumor spectrum observed in γ-ray irradiated population, such as the atomic bomb survivors, can be extrapolated to similar populations exposed to HZE ions, such as astronauts, populations of HS/Npt mice are exposed to each. Although it is unlikely that the specific tumor types observed in mice will also occur in humans, if the same spectra of tumors occur following exposure to HZE ions and γ-rays in mice, this provides strong evidence that the human epidemiological data for γ-ray exposures can be extrapolated for HZE ion exposures risks in astronauts.

METHODS

Animals and radiation exposures

Male and female HS/Npt mice (n = 1850) were generated from breeding pairs obtained from Oregon Health & Sciences University (Portland, OR). These outbred mice were generated via circular outbreeding procedure involving 48 families. All the mice for this study were produced in generation 71. Founder strains for the HS/Npt include A/J, AKR/J, BALB/cJ, C3H/HeJ, C57BL/6J, CBA/J, DBA/2J, and LP/J (**Figure 2.1**)[22]. The mice were group housed (5 mice of the same sex per cage) in a climate-controlled facility with free access to food and sterile water, and a 12-hour light cycle. Mice were shipped to Brookhaven National Laboratories (Upton, NY) where they were exposed to accelerator produced HZE ions, γ-rays, or shame irradiated at the NASA Space Radiation Laboratory at 3 to 4 weeks of age. HS/Npt stock mice of both sexes were exposed to 0.4 Gy of 240 MeV/n ^{28}Si ions (n = 308) or 600 MeV/n ^{56}Fe ions (n = 314), 3 Gy of ^{137}Cs γ-rays (n = 615), or sham irradiated (n = 622). Following irradiation exposure or sham irradiation, mice were returned to Colorado State University Research Innovation Center (Fort Collins, CO) and monitored twice daily for the duration of the study. The mice were phenotyped for cataractogenesis by slit lamp biomicroscopy, cognitive deficits, and cancer development until they reached 800 days of age or became moribund. Moribund mice were euthanized with CO_2 according to the Colorado State University Animal Care and Use committee guidelines. A laboratory technician was trained to systematically evaluate all organ systems and thorough necropsy and tissue collection procedures were performed for each mouse. For cases of splenomegaly, thymic masses, mammary masses, and liver masses, fresh sections of tumor were frozen at negative 80 degrees Celsius and small sections were mixed in RNA stabilization solutions (RNAlater®). All gross lesions were formalin-fixed and paraffin

embedded for histologic evaluation. Five coronal sections were grossly evaluated on each mouse following 48 hours of cranial decalcification.

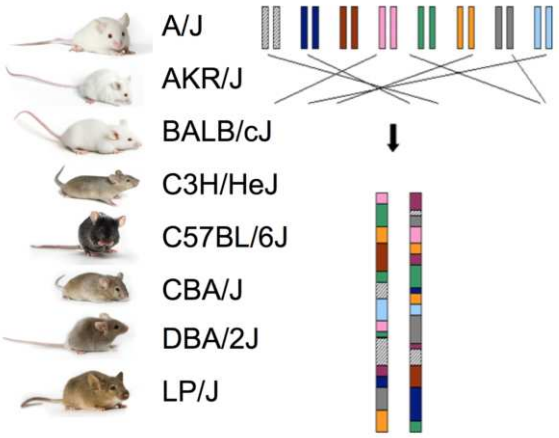

Figure 2.1: Heterogeneous stock mice founder strains and a cartoon depiction of a single chromosome following multiple generations of outbreeding. The chromosome has numerous accumulated meiotic events resulting in a mosaic of founder haplotypes and a large degree of heterozygosity.

Pathology examination for HS/Npt mice

For this lifetime carcinogenesis study, all disease-states were interpreted within the context of a systematic pathologic evaluation directed by board certified veterinary pathologists. Structured necropsy and tissue collection protocols were followed for each mouse and involved the photo-documentation of gross lesions. In order to evaluate brain tissues and bilateral Harderian glands, craniums were decalcified for 48 hours and five coronal sections of the skull were reviewed for each mouse. In the event of a solid tumor, all lung fields were examined histologically to detect the presence or absence of micro-metastases. Tumor nomenclature was based on consensus statements (https://www.toxpath.org/inhand.asp). Representative gross and microscopic pathology for select tumors are presented in **Figures 2.2, 2.3,** and **2.4**.

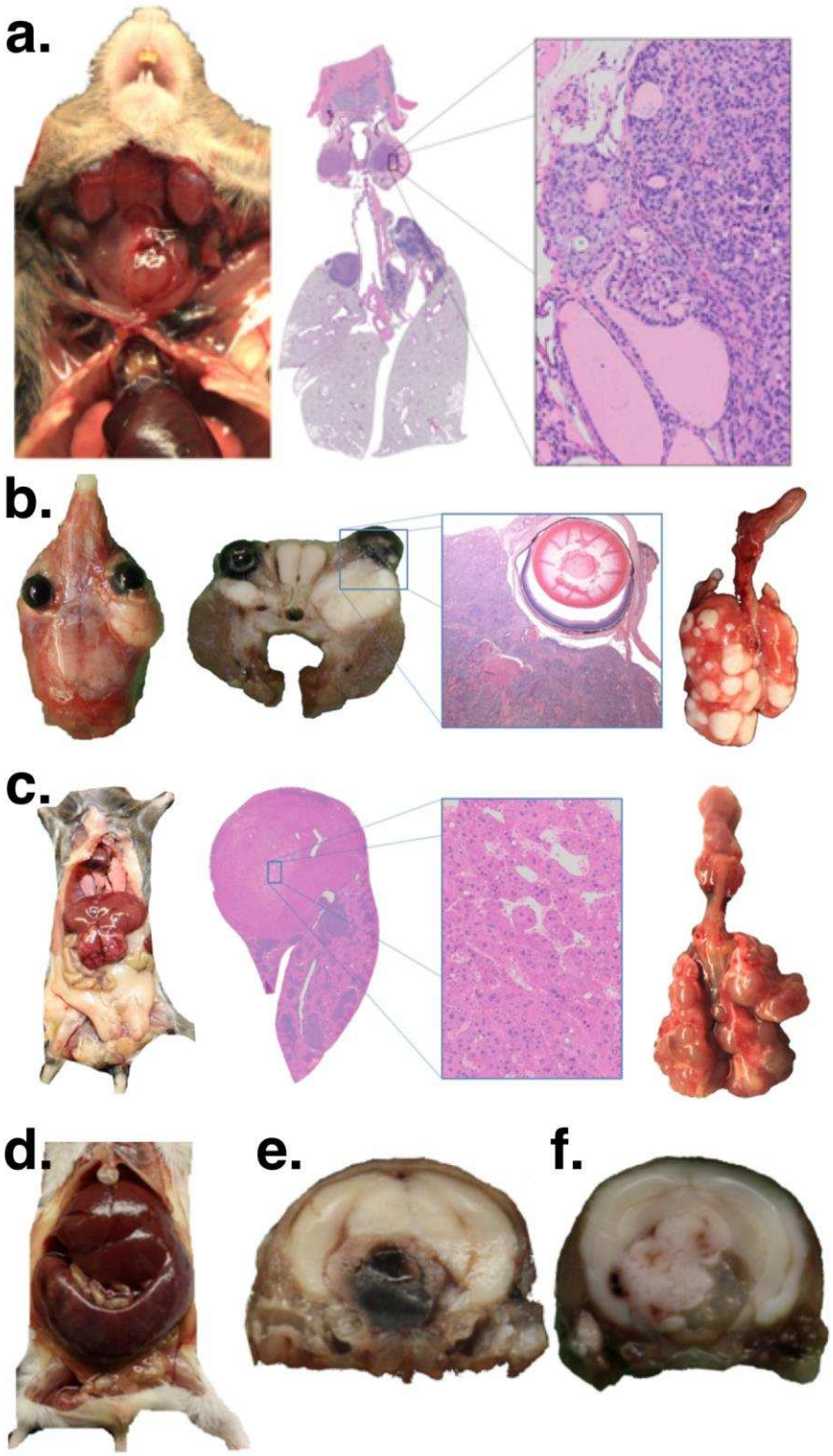

Figure 2.2: Representative gross and histologic pathology for a. thyroid adenoma, b. Harderian gland adenocarcinoma with pulmonary metastasis, c. hepatocellular carcinoma with pulmonary metastasis, d. splenomegaly with acute myeloid leukemia, e. pituitary adenoma f. pituitary adenoma.

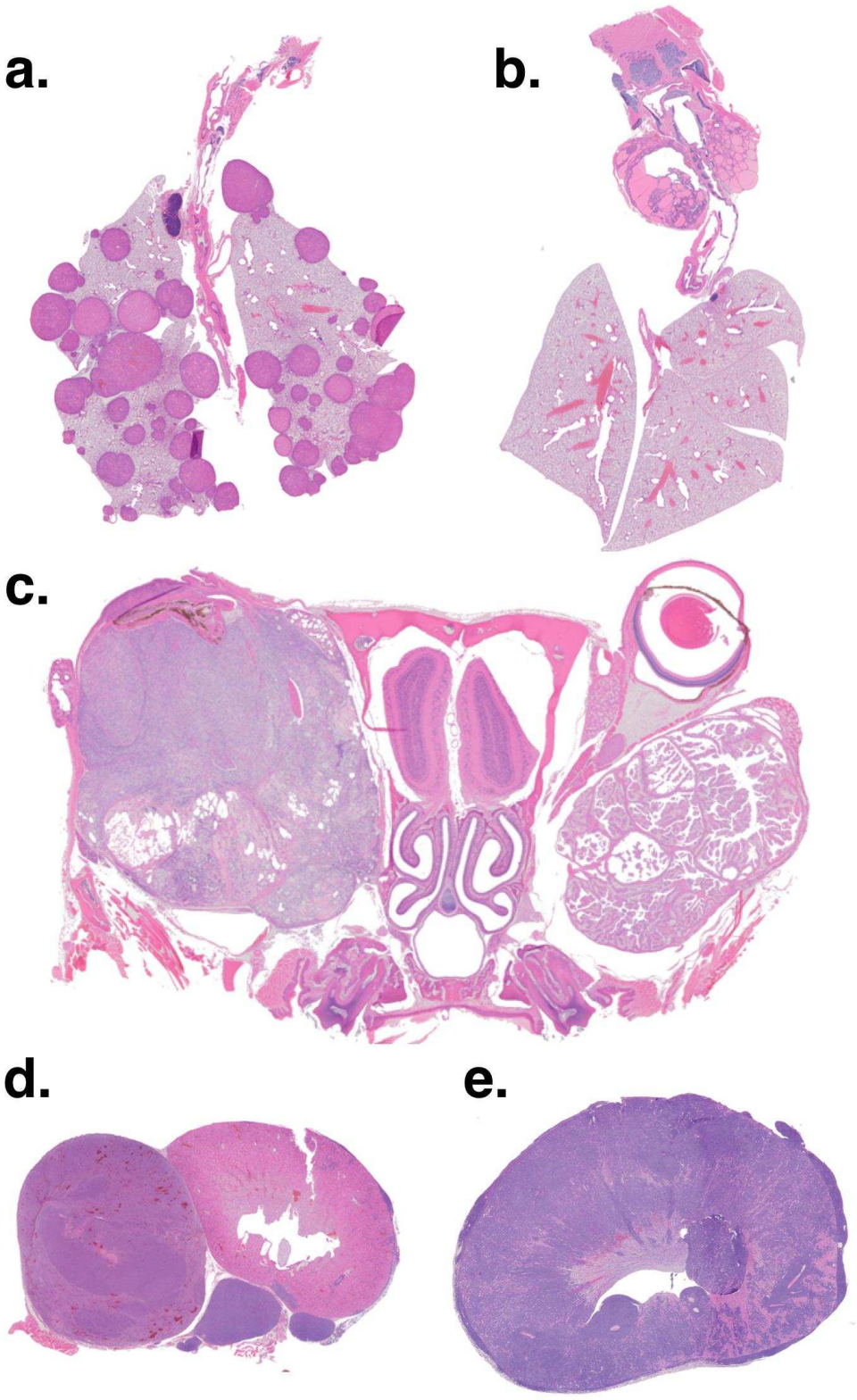

Figure 2.3: Representative histologic images for a. pulmonary metastases from a hepatocellular carcinoma, b. thyroid adenoma, c. Harderian gland adenocarcinoma (left) and adenoma (right), d. adrenal pheochromocytoma (left) adjacent to kidney, e, renal lymphoma.

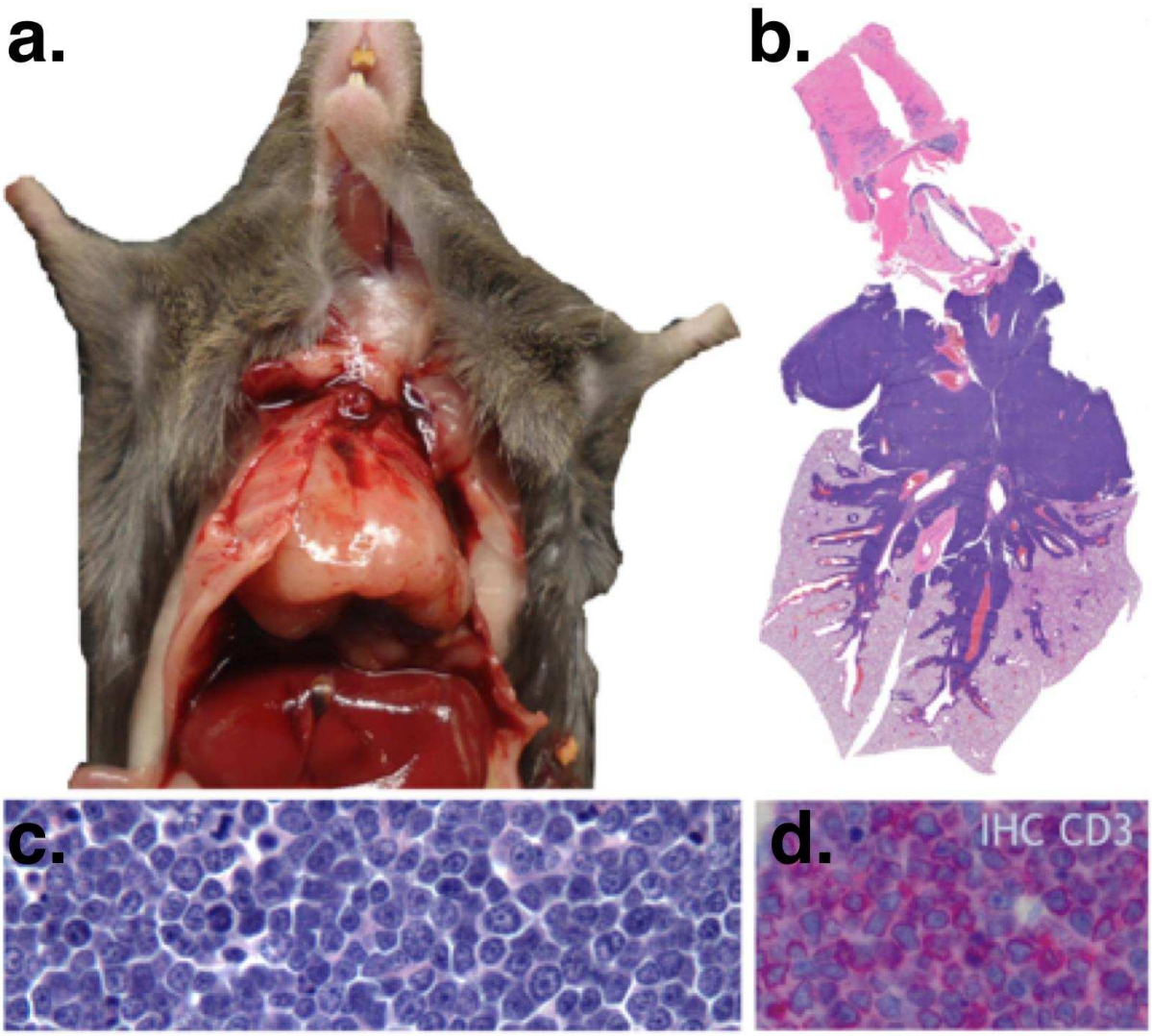

Figure 2.4: Gross, histologic, and immunohistochemical features of precursor T-cell lymphomblastic lymphoma: a. grossly enlarged thymus, b. effacement of the thymus by neoplastic lymphocytes, and c. uniform neoplastic lymphocytes with numerous mitotic figures, d. immunopositivity for CD3.

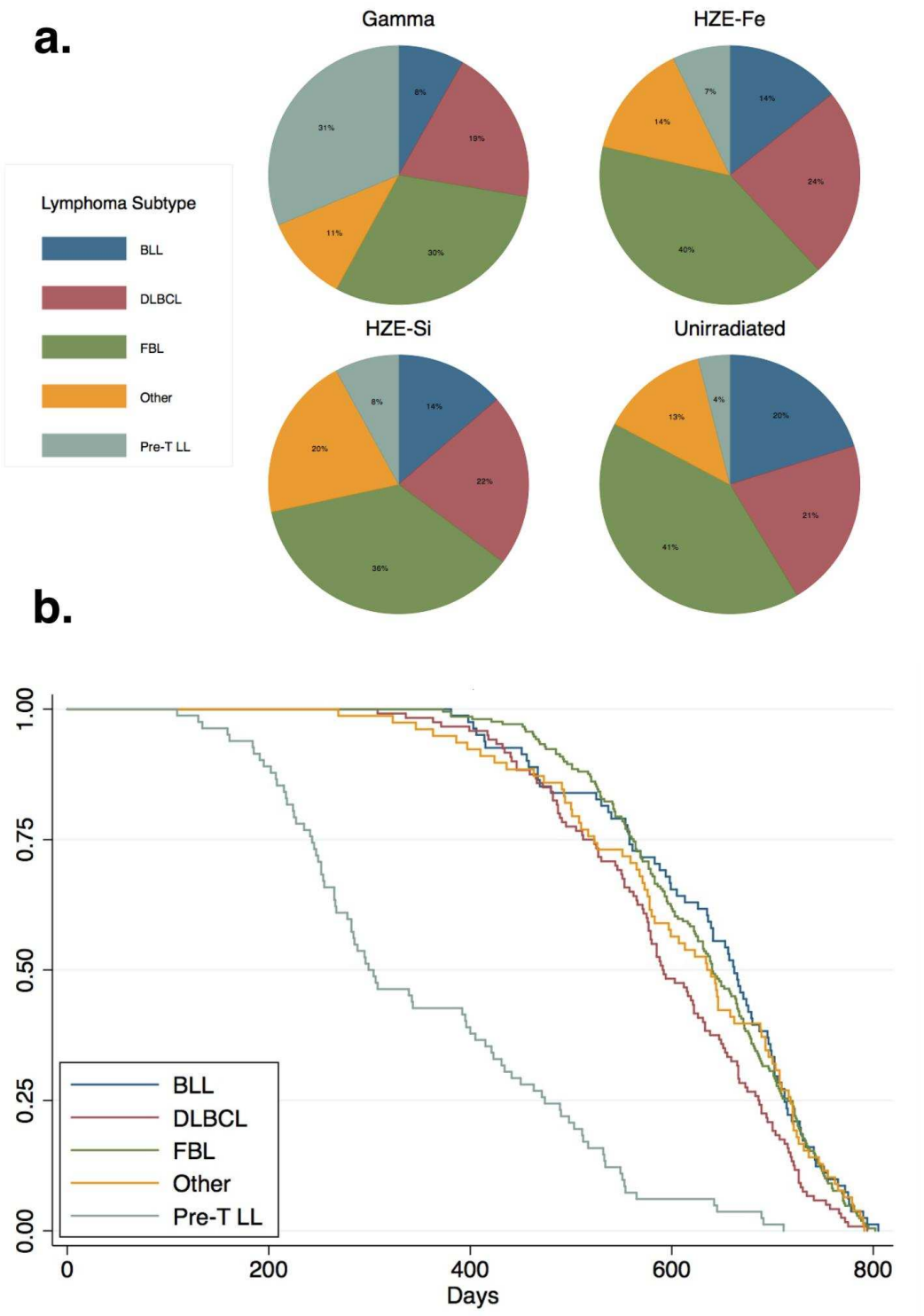

Figure 2.5: Lymphoma subtype data: a. distribution of lymphoma subtype by treatment group, b. Kaplan-Meier survival for mice diagnosed with each lymphoma subtype, including B-cell lymphoblastic lymphoma (BLL), Diffuse large B-cell lymphoma (DLBCL), follicular B cell lymphoma (FBL), Precursor T cell lymphoblastic lymphoma (PreT LL), and all other observed lymphomas combined.

Immunophenotyping lymphoid neoplasms

Tissue microarray constructions were utilized to immunophenotype and subcategorize lymphoid neoplasms, which were the most commonly diagnosed tumors in irradiated and unirradiated HS/Npt mice. Tissue microarray recipient blocks were constructed using the Arraymold® 150 x 1.5mm mold using Paraplast X-TRA® paraffin (Sigma Aldrich). Tissue identification and verification was performed for all cases by histologically analyzing Hematoxylin and Eosin stained sections along with the matching paraffin blocks. Identification of tissue sampling regions was performed by a veterinary pathologist. For each case, duplicate tissue cores were taken from multiple anatomic locations. Thirteen tissue microarrays were created, each of which contained six cores of normal tissue at one corner of the array (haired skin, spleen, thymus, or liver); these control tissues were present in a unique combination and allowed for (1) orientation of the resulting sections, (2) verification that the slide matched the block, and (3) positive controls for immunohistochemistry. **Figure 2.6** illustrates one tissue microarray as well as the resulting immunohistochemistry results for one thymic lymphoma and a core containing normal spleen. Immunohistochemistry for T-cell identification was performed using a rabbit monoclonal, anti-CD3 [SP7] antibody obtained from Abcam® (ab16669); this antibody was used at a concentration of 1:300. Immunohistochemistry for B-cell identification was performed using two rabbit monoclonal antibodies: an anti-CD45 antibody (ab10558) at a dilution of 1:1000 and an anti-PAX5 antibody (ab140341) at 1:50 dilution. All immunohistochemistry was performed on a Leica Bond-Max autostainer with the Leica bond polymer refine red detection system (Leica DS9390, Newcastle Upon Tyne, United Kingdom). In addition to defining the immunophenotype, lymphomas were characterized according to the Mouse Model of Human Cancer Consortium's (MMHCC) Bethesda protocols[27,28]. For these

protocols, anatomic location is important for the final diagnosis and, therefore, lymph node involvement was utilized from necropsy reports when necessary. Additional features included cell size, nuclear size, chromatic organization, mitotic figure frequency, and the presence or absence of a leukemic phase was defined by bone marrow involvement within the sternum or femur.

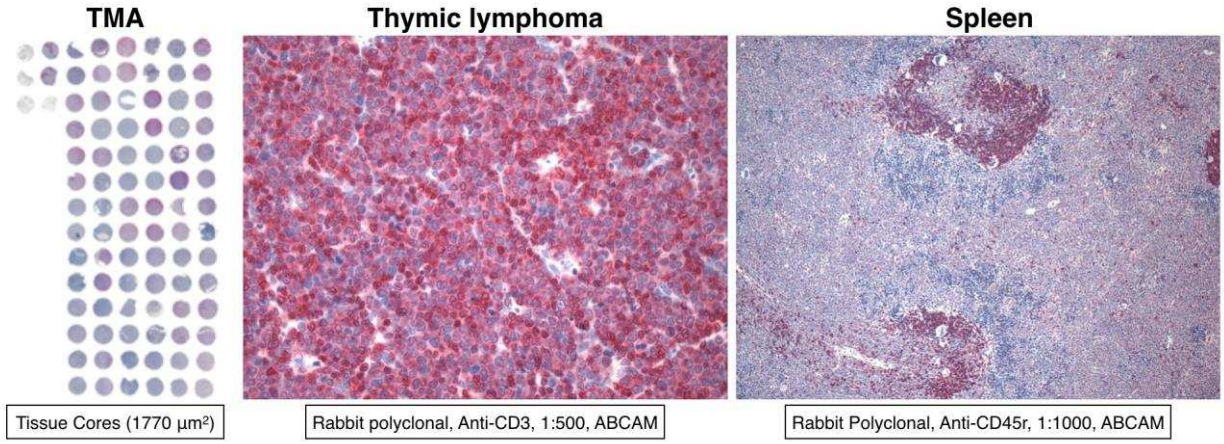

Figure 2.6: Immunophenotyping lymphoid neoplasms using Tissue microarrays (TMA) and immunohistochemistry for CD3 and Cd45r. Each core in the tissue microarray had an examination area of 1770 micrometers and all cases of lymphoma were examined in duplicate.

Histologic criteria for the most commonly diagnosed forms of lymphoma in HS/Npt—which are summarized in **Table 2.1**—are discussed briefly. Follicular B cell lymphoma (FBL) often involved the spleen, less commonly the mesenteric lymph nodes, and characteristically had increased numbers of infiltrating small T-cells. The nuclei within neoplastic cells in FBL were typically large, vesicular, and cleaved and mitotic figures were infrequent (less than one per 400x field). Diffuse large B cell lymphoma (DLBCL) had a similar anatomic distribution as FBL (typically involving the spleen and abdominal lymph nodes) and often also involved other organs, such as the thymus and mediastinal lymph nodes. The mitotic rate is higher for DLBCL, particularly in comparison to FBL, and mitotic figures often number three or more per 400x

field. DLBCL is composed of medium-sized cells with scant cytoplasm and round vesicular nuclei often containing a prominent nucleoli adherent to the nuclear membrane. B-cell lymphoblastic lymphoma (BLL) have very high mitotic activities, typically involve and wide variety of lymph nodes (mesenteric, mediastinal, mandibular, popliteal, etc), and are composed of uniform lymphoblastic cells with round nuclei and centrally located nucleoli. The most common form of T cell lymphoma, precursor T cell lymphoblastic lymphoma (Pre-T LL), invariably presented as markedly enlarged thymic tumors and were often the cause of morbidity-induced sacrifice in relatively young mice. These tumors often have up to 10 mitotic figures per 400x field and are composed of uniform, medium-sized cells with round nuclei.

Table 2.1. Lymphoma subtypes for HS/Npt mice in each radiation exposure group.

	Total ♂ = 934 ♀ = 916 n = 1850	HZE ♂ = 312 ♀ = 310 n = 622	γ ♂ = 313 ♀ = 302 n = 615	Unirradiated ♂ = 309 ♀ = 304 n = 613	HZE Fe ♂ = 161 ♀ = 153 n = 314	HZE Si ♂ = 151 ♀ = 157 n = 308	M:F
Lymphoid	570	172	195	203	84	88	274:307
Follicular B cell	209	66	59	84	34	32	101:108
Diffuse Large B cell	120	39	38	43	20	19	56:64
Lymphoblastic B cell	81	24	16	41	12	12	38:43
Histiocyte Associated B cell	13	3	3	7	1	2	3:10
Anaplasstic Plasmacytoma	4	1	2	1	0	1	2:2
Small B cell	13	6	4	3	2	4	6:7
Marginal Zone B cell	5	3	1	1	2	1	3:2
Precursor T cell	82	13	61	8	6	7	40:42
Small T cell	5	2	1	2	2	0	1:4
Anaplastic T cell	9	4	5	0	0	4	3:6
Other	29	11	5	13	5	6	14:15

Molecular characterization of AML

Droplet digital PCR was performed on cases of acute myeloid leukemia (AML) to assess deletion status via copy number variation for two genes: *Sfpi1* and *Asxl1*. These genes are both located on chromosome 2 at base pair locations 91,082,390–91,115,756 for *Sfpi1* and

153,345,845–153,404,007 for *Asxl1*. To establish a reference for normal diploid copy number in each AML sample, the copy number of *H2afx* was also determined. *H2afx* is located on chromosome 9 and deletions in this region have not been reported in murine acute myeloid leukemia. BioRad PrimePCR™ probes were used for all assays as follows: *Asxl1* ddPCR™ probe (dMmuCPE5100268), *Sfpi1* ddPCR™ probe (dMmuCPE5094900), and *H2afx* ddPCR™ probe (dMmuCPE5104287).

Ratios were created between the test gene and the reference gene (*Sfpi1*:*H2afx* and *Asxl1*:*H2afx*) to determine copy number with the assumption that the reference gene would not be deleted or amplified. Ideally, ratios of 1:1 represent equal copy numbers for both the test gene and the reference gene and ratios of 1:2 represent a deletion in one copy of the test gene. However, since the tumor samples contained neoplastic cells as well as stromal cells and other cells, the ideal 1:2 ratio was not commonly observed. This is because stromal cells, which occur at unknown proportions in each tumor and which should not have chromosomal deletions, artificially increase ratios for tumor samples in which a deletion is indeed present. To account for stromal cell contamination, a cutoff ratio of 3:4 was established. Tumor samples with ratios below 3:4 were considered to have a deletion in one copy of the test gene.

Metastatic disease quantification

For cases in which a solid tumor was identified, a standard section containing all lung lobes was processed and evaluated histologically (**Figure 2.7**). In cases where pulmonary metastases were observed, whole slide scanning was performed at 200x magnification using an Olympus VS120-S5 and the Olyvia software suite (http://www.olympusamerica.com/) to generate images for quantification of metastatic density. Analysis software, ImageJ

(https://imagej.nih.gov/ij/), was utilized to quantify the total area of normal lung as well as the total area of metastatic foci (**Figure 2.7**). Metastatic density is reported as a percentage of the total metastasis area divided by the total lung area.

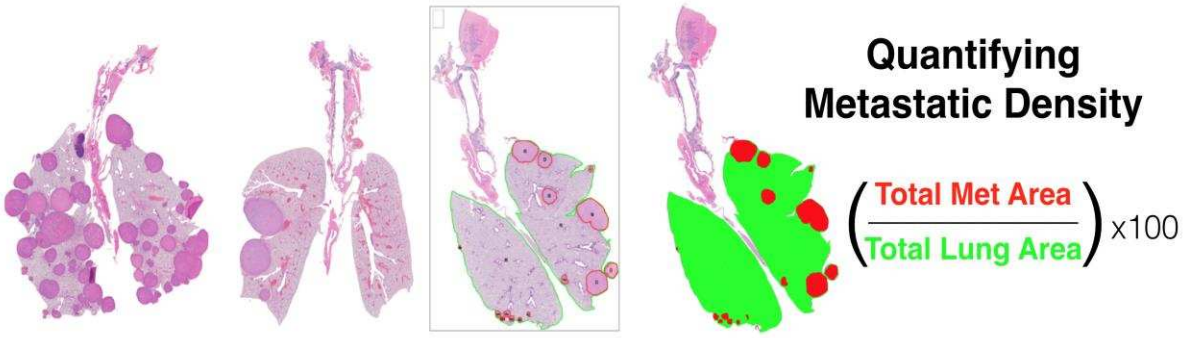

Figure 2.7: Metastatic densities were highly variable between individual mice. Quantifying metastatic densities was accomplished with whole slide image analysis.

RESULTS

Tumors were the predominant cause of morbidity and mortality for both HZE ion and γ-ray irradiated populations as well as for the population of unirradiated mice (**Figure 2.8**). Neoplasia was the cause of death for more than three out of every four mice and a wide variety of tumor diagnoses—82 neoplastic histotypes (**Appendix 1**)—were observed. This is consistent with the prediction that a population composed of individuals, each with a unique mosaic of susceptibility alleles from 8 inbred strains, will have a wider range of tumor phenotypes than the sum of each of the parental inbred strains. Although numerous tumor histotypes were observed, the majority of these tumor types were rare, occurring in less than 1% of the population.

Overall, the spectra of tumor histotypes produced in HZE ion irradiated and γ-ray irradiated populations is essentially identical; further, tumor types induced by radiation are mostly similar to those arising spontaneously (**Figure 2.8**). Tumor incidence in a lifetime

carcinogenesis study such as this must be interpreted as function of time-at-risk to acknowledge competing mortalities. Irradiated mice had significantly decreased overall survival times, and therefore decreased time at risk, compared to unirradiated controls (**Figure 2.9a**). Further, mice exposed to 0.4 Gy HZE ions had significantly increased median survival times than mice exposed to 3.0 Gy of γ-rays. Though these doses—at face value—seem disparate, their selection is based on preliminary dose-response studies which reveal that 0.4 Gy of HZE ions and 3.0 Gy γ-rays are each maximally tumorigenic in mouse carcinogenesis studies[29]. The reduced life spans for irradiated mice are at least partially the result of decreased tumor latencies and increased tumor incidences. Further, evidence to support the heritability in overall survival is provided by comparing the variability in survival between families (**Figure 2.9b**), which demonstrates that certain families have significantly shorter survival times as a group than others. HS/Npt mice are maintained in families so that individuals of the same family number are more closely related to one another than members from other families.

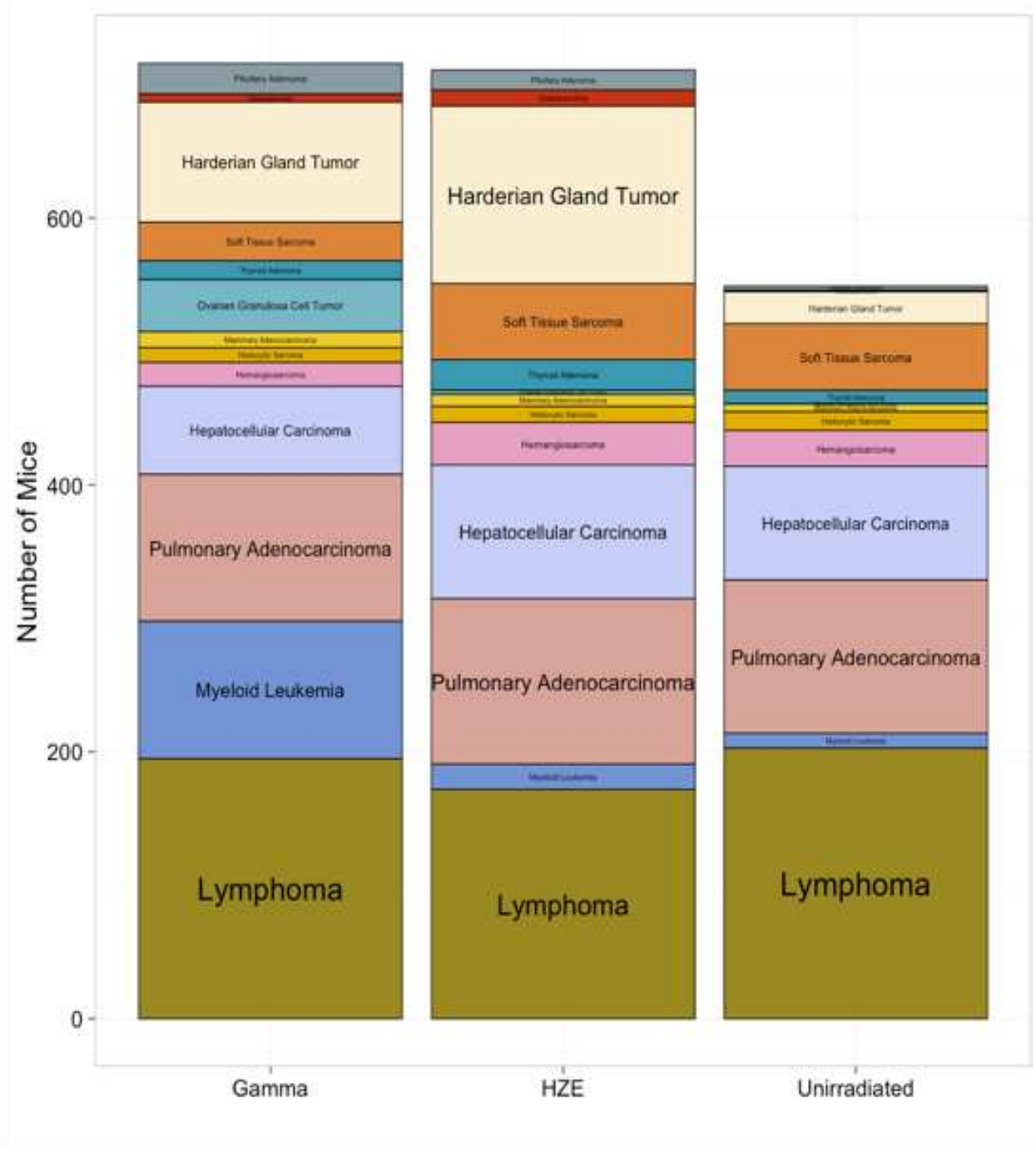

Figure 2.8. Burden of malignant tumors for each radiation exposure group: tumor types observed in gamma-irradiated mice also appear in HZE ion irradiated mice.

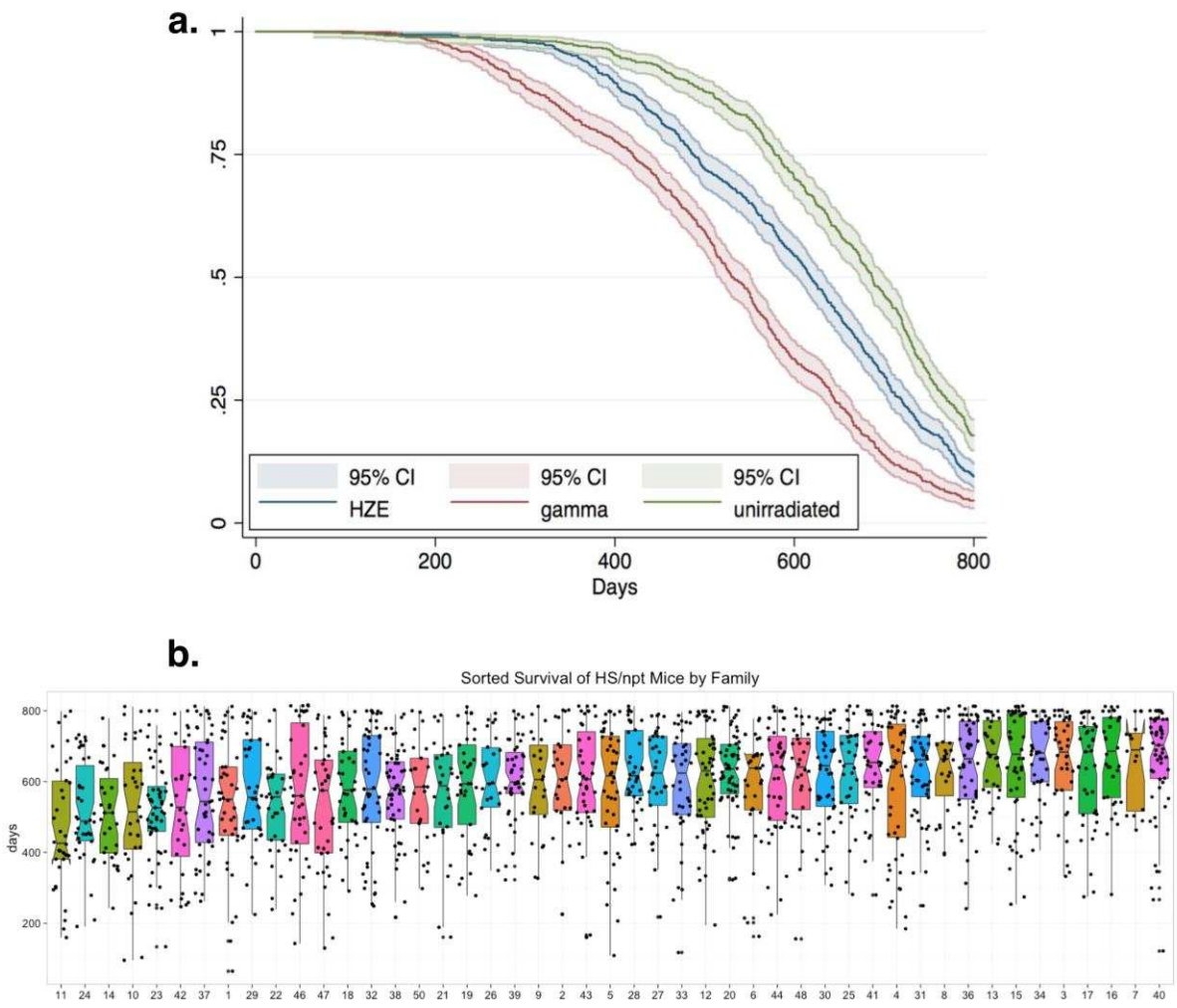

Figure 2.9: Overall survival for **a.** each radiation group of HS/Npt mice and **b.** overall survival for each HS/Npt family.

Although the tumor spectra are similar for each irradiated population, the different radiation qualities demonstrate varied efficiencies for producing specific tumor histotypes. γ-ray irradiated mice were at greater risk for hematological malignancies, pituitary tumors, and ovarian granulosa cell tumors than unirradiated mice; HZE ion irradiated mice demonstrated an intermediate susceptibility to these histotypes. For Harderian gland tumors, thyroid tumors, hepatocellular carcinomas, and sarcomas, HZE ion and γ-ray irradiated mice were at a similarly and significantly increased risk compared to unirradiated controls (supplementary materials).

Overall survival for females is significantly increased compared to males ($p = 2.7e-6$) with unirradiated females experiencing median survival times 56 days longer than males. In contrast, no significant difference is observed between γ-ray irradiated females and males ($p = 0.51$) or HZE ion irradiated females and males ($p = 0.056$). Irradiated female mice had significantly increased incidences of (1) malignant ovarian tumors, (2) mammary adenocarcinomas, (3) central nervous system tumors (pituitary adenomas, choroid plexus tumors, and ependymomas), (4) specific lymphoma subtypes (Diffuse Large B-cell Lymphomas, Lymphoblastic B cell lymphomas), and (5) certain sarcomas (osteosarcomas, leiomyosarcomas).

Although the tumor spectra observed, from a tumor histologic perspective, are similar for all groups of mice, the molecular events that occur in each tumor histotype can potentially be specific for each exposure group. The molecular events occurring in acute myeloid leukemias (AML) are discussed below.

Molecular characterization of acute myeloid leukemia

Radiation-induced acute myeloid leukemia (AML) is a well-characterized disease in mice[11,30,31], and is most commonly the result of a radiation-induced minimally deleted region on chromosome 2 containing the *Spi1* and a recurrent point mutation that inactivates the remaining *Spi1* allele[32]. To test the hypothesis that HZE ion-induced AML will contain the same molecular aberrations as γ-ray induced AML, *Spi1* copy number was investigated. As expected, the majority of AML cases in the γ-ray exposure group have a deletion in one copy of *Spi1*, which is distinct from the spontaneously occurring AML cases, in which a deletion was rare (**Figure 2.10**). Similar to γ-ray irradiated mice, mice exposed to HZE ions also have a significantly increased proportion of AML cases in which one copy of *Spi1* was deleted. We found that *Asxl1*

was not deleted in any sample in which *Spi1* was not also deleted, however, in 69% of cases with a *Spi1* deletion, *Asxl1* was also deleted (**Figure 2.10**). These results indicate that AML arises by similar molecular mechanisms following exposures to γ-rays or HZE ions.

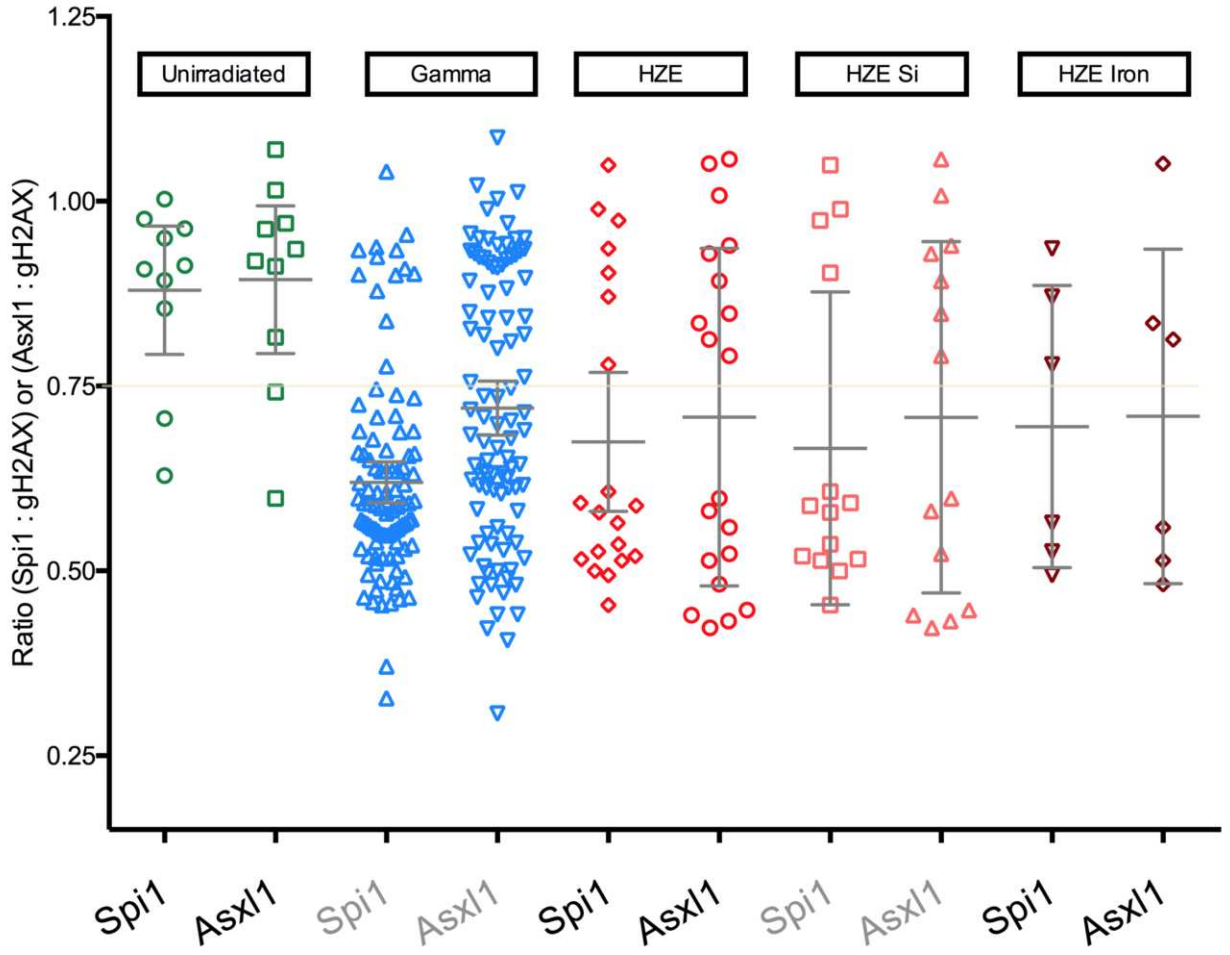

Figure 2.10: Copy number variation results derived from ratios of two test genes on chromosome 2, *Spi1* and *Asxl1*, compared to a housekeeping gene (*gH2AX*) for each exposure groups. Cases of AML that arise spontaneously commonly have 2 copies of each gene (a ratio of approximately 1:1). In contrast, for groups exposed to radiation, AMLs more commonly contain deletions in both genes (ratios of 0.5:1 are consistent with loss of one copy of the test gene). A cutoff ratio of 0.75 was utilized to designate deletion status.

Incidence of metastases are following to HZE ion or γ-ray exposure

To determine whether tumors that arise following HZE ion exposure are more likely to metastasize than their counterparts arising in unirradiated or γ-ray irradiated mice, two measures

were characterized and compared: metastatic events and metastatic density. The most common metastasizing tumor for all groups was hepatocellular carcinoma and comparisons are made between groups separately for this tumor type. In addition, comparisons are made between groups for all metastatic tumors types, which include hepatocellular carcinoma, Harderian gland adenocarcinoma, thyroid carcinoma, hemangiosarcoma, soft tissue sarcoma, renal cell carcinoma, osteosarcoma, ovarian granulosa cell tumor, and intestinal adenocarcinoma.

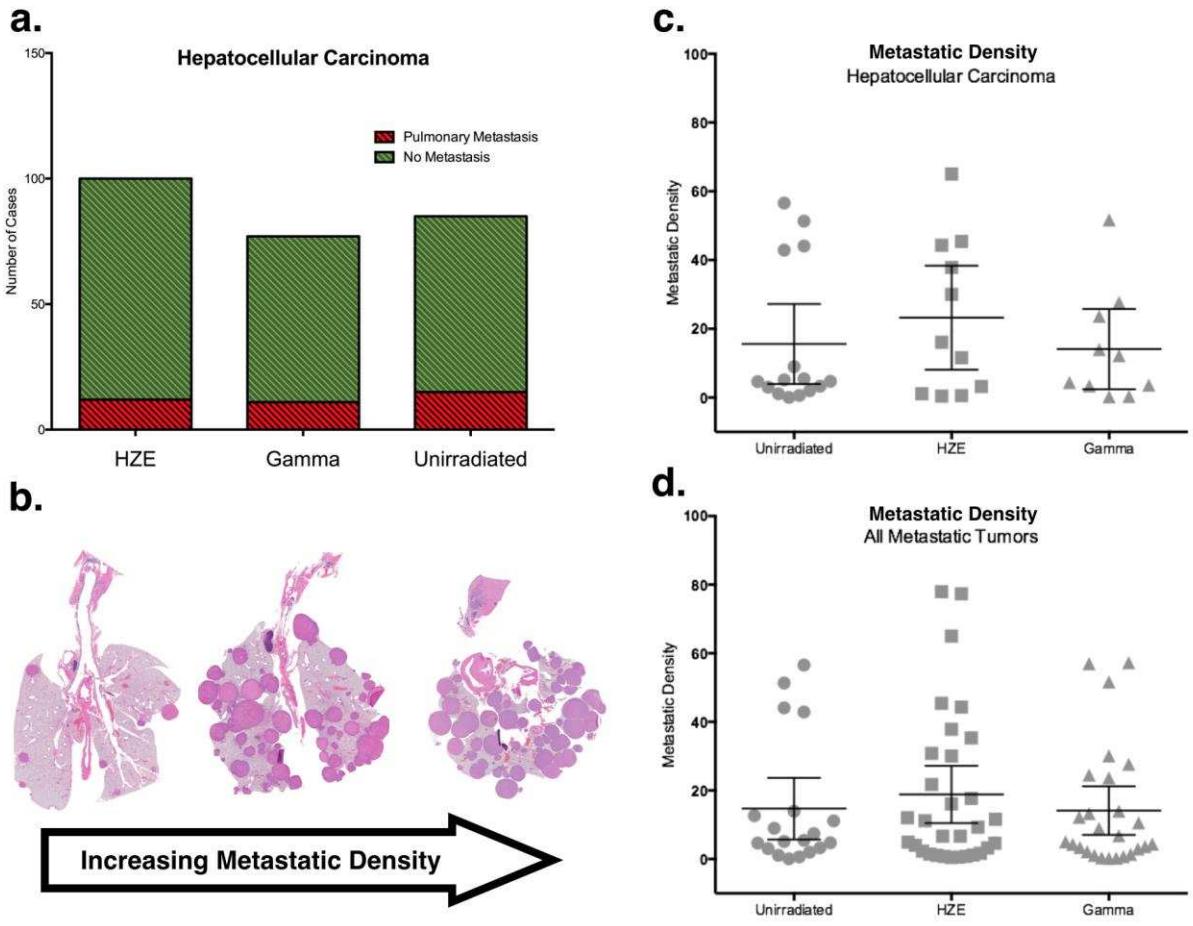

Figure 2.11: Metastatic characterization: a. Incidence of metastases in mice diagnosed with hepatocellular carcinoma for each exposure group (HZE, n = 100; Gamma, n = 66; Unirradiated, n = 85). No significant difference in incidence of metastatic disease was observed in populations bearing hepatocellular carcinomas. b. Examples of varying in metastatic densities for individual mice with hepatocellular carcinoma (lung, whole slide imaging), c. Hepatocellular carcinoma metastatic densities for each exposure group (Unirradiated, n = 15; HZE, n = 11; Gamma, n = 10). d Metastatic density for all neoplasms for each exposure group (Unirradiated, n = 19; HZE, n = 28; Gamma, n = 25).

Pulmonary metastases were observed in cases of hepatocellular carcinoma, Harderian gland adenocarcinoma, osteosarcoma, and ovarian granulosa cell tumor. Metastases were no more frequent in irradiated animals than in controls and there was no significant difference in metastatic incidence between HZE ion irradiated mice and γ-ray irradiated mice (**Figure 2.11a**). To further characterize colonization abilities for circulating tumor cells in different radiation exposure groups, pulmonary metastatic densities were calculated for each animal by utilizing whole-slide image analysis of all lung lobes to determine the pulmonary area occupied by metastatic cells. Individuals with pulmonary metastasis had a wide range of metastatic densities (**Figure 2.11b**) however, no significant difference in pulmonary metastatic density was observed between exposure groups for either hepatocellular carcinoma metastatic events (**Figure 2.11c)** or metastatic events for all tumor types (**2.11d**).

Tumor latency following irradiation was also analyzed using Kaplan-Meir survival statistics. As expected, tumors arising in both HZE ion and γ-ray irradiated mice show significantly decreased latencies in comparison to the unirradiated population (**Appendix 2**). However, HZE ions did not further decrease latencies when compared to γ-ray irradiated mice. Differences in tumor latency in this context indicate a decrease in time for tumor initiation or promotion. Since radiation is known to be efficient at both initiation and promotion, decreased latencies are expected for irradiated population. Tumor progression is not evaluated, however, using tumor latency, and our results do not demonstrate whether tumors arising in irradiated individuals are more likely to progress rapidly than those arising spontaneously.

DISCUSSION

Carcinogenesis following space radiation exposures is considered the primary impediment to human space exploration[7]. Compared to terrestrial radiation (including X-rays, γ-rays, and β particles), HZE ions have distinct ionization patterns that cluster along dense track structures as described by Dudley, et al[15]. resulting in unique forms of cell and tissue damage. Further, HZE particles travel at relativistic speeds and are highly penetrating, therefore, shielding such particles within spacecraft is essentially impossible[7].

Using genetically heterogeneous stock mice, we have demonstrated that the tumor types induced by γ-ray exposure are also induced by HZE ion exposures. Our results do not indicate that tumors arising in HZE ion exposed individuals are more malignant than spontaneous tumors of the same histotype, or tumors arising following γ-ray exposures. Finally, we find that female mice are at greater risk for radiogenic cancers—HZE ion or γ-ray induced—than males. These results are consistent with the current NASA model to calculate cancer risk from space radiation exposures[4].

Additionally, we present evidence that the molecular events that occur during tumorigenesis can be similar for HZE ion and γ-ray induced tumors. For AML, radiation of either type significantly increased the incidence of chromosomal 2 deletions compared to spontaneously arising tumors. This provides direct evidence that ionizing radiation, whether photon or particle, can increase the risk for hematological malignancies by inducing the same types of genomic lesions.

Historically, radiation carcinogenesis studies have employed genetically inbred mice. Due to the fact that radiation effects depend in part on how radiation and genes interact, genetically inbred mice tend to respond similarly regardless of the physical differences in track

structure and energy deposition between radiation types. Advantages to inbred mice include the fact that strains produce lower phenotypic variance and thus fewer mice are needed to detect statistical differences in radiation effects. However, disadvantages of using inbred mice include the fact that strain-specific responses may obscure the variability we expect in a genetically diverse population such as humans. With greater diversity within a screening population, the likelihood of identifying a genetically susceptible subpopulation is increased.

There are limitations to a mouse carcinogenesis study comparing acute γ-ray and HZE ion exposures. First, for cost-efficiency and logistics reasons, a single dose was employed for each radiation quality: 3.0 Gy for γ-ray exposures and 0.4 Gy for HZE ion exposures. Preliminary studies have demonstrated that these doses produce the maximum tumor incidence in inbred strains[29]. Because tumor susceptibility and association mapping were the primary goals of this study, doses were chosen with the goal of generating the greatest tumor incidences, and therefore the greatest power to detect significant QTL. But caution must be taken when comparing the two single dose groups, as it is impossible to untangle dose responses with such data. An additional benefit of the selected doses is that 0.4 Gy of HZE ions represents a realistic dose, received over 600 to 900 days, for a flight crew traveling to Mars. Second, the applicability of these findings to human populations is limited as mice serve only as models of carcinogenesis.

Permissible exposure limits for astronauts are based on the risk of death from cancer rather than cancer incidence. The incidence to mortality conversion used in the risk calculation is based on mortality from background cancers in the U.S. population. Thus, there is an assumption that radiogenic tumors are no more lethal than spontaneous tumors. However, there is accumulating evidence that HZE ion radiation can produce tumors with increased malignant

properties in mouse models[29,33,34]; this increase in malignancy following HZE ion exposures is not demonstrated in the present study.

References

1. Russo, D., Foley, T., Stroud, K., Connolly, J., Tillman, B., & Pickett, L. (2007, October). NASA space flight human system standards. In *Proceedings of the Human Factors and Ergonomics Society Annual Meeting* (Vol. 51, No. 21, pp. 1468-1470). Sage Publications.
2. de Gonzalez, A. B., Gilbert, E., Curtis, R., Inskip, P., Kleinerman, R., Morton, L., ... & Little, M. P. (2013). Second solid cancers after radiation therapy: a systematic review of the epidemiologic studies of the radiation dose-response relationship. *International Journal of Radiation Oncology* Biology* Physics*, *86*(2), 224-233.
3. United Nations. Scientific Committee on the Effects of Atomic Radiation. (2000). *Sources and effects of ionizing radiation: sources* (Vol. 1). United Nations Publications.
4. Cucinotta, F. A., Alp, M., Rowedder, B. & Kim, M.-H. Y. Safe days in space with acceptable uncertainty from space radiation exposure. *Life Sci Space Res (Amst)* **5,** 31–38 (2015).
5. Cucinotta, F. A., Kim, M. H. Y., Chappell, L. J., & Huff, J. L. (2013). How safe is safe enough? Radiation risk for a human mission to Mars. *PLoS One*, *8*(10), e74988.
6. Cucinotta, F. A. (2014). Space radiation risks for astronauts on multiple International Space Station missions. *PloS one*, *9*(4), e96099.
7. Durante, M., & Cucinotta, F. A. (2008). Heavy ion carcinogenesis and human space exploration. *Nature Reviews Cancer*, *8*(6), 465-472.
8. Board, S. S. (2006). *A risk reduction strategy for human exploration of space: a review of NASA's Bioastronautics Roadmap*. National Academies Press.
9. Bielefeldt-Ohmann, H., Genik, P. C., Fallgren, C. M., Ullrich, R. L., & Weil, M. M. (2012). Animal studies of charged particle-induced carcinogenesis. *Health physics*, *103*(5), 568-576.
10. Ando, K., Koike, S., Oohira, C., Ogiu, T., & Yatagai, F. (2005). Tumor induction in mice locally irradiated with carbon ions: a retrospective analysis. *Journal of radiation research*, *46*(2), 185-190.
11. Weil, M. M., Bedford, J. S., Bielefeldt-Ohmann, H., Ray, F. A., Genik, P. C., Ehrhart, E. J., ... & Callan, M. A. (2009). Incidence of acute myeloid leukemia and hepatocellular carcinoma in mice irradiated with 1 GeV/nucleon 56Fe ions. *Radiation research*, *172*(2), 213-219.
12. Imaoka, T., Nishimura, M., Kakinuma, S., Hatano, Y., Ohmachi, Y., Yoshinaga, S., ... & Shimada, Y. (2007). High relative biologic effectiveness of carbon ion radiation on induction of rat mammary carcinoma and its lack of H-ras and Tp53 mutations. *International Journal of Radiation Oncology* Biology* Physics*, *69*(1), 194-203.
13. Alpen, E. L., Powers-Risius, P., Curtis, S. B., & DeGuzman, R. (1993). Tumorigenic potential of high-Z, high-LET charged-particle radiations. *Radiation research*, *136*(3), 382-391.
14. Alpen, E. L., Powers-Risius, P., Curtis, S. B., DeGuzman, R., & Fry, R. J. M. (1994). Fluence-based relative biological effectiveness for charged particle carcinogenesis in mouse Harderian gland. *Advances in Space Research*, *14*(10), 573-581.
15. Fry, R. J. M., Powers-Risius, P., Alpen, E. L., & Ainsworth, E. J. (1985). High-LET radiation carcinogenesis. *Radiation Research*, *104*(2s), S188-S195.

16. Fry, R. J. M., Ullrich, R. L., Powers-Risius, P., Alpen, E. L., & Ainsworth, E. J. (1983). High-LET radiation carcinogenesis. *Advances in Space Research*, *3*(8), 241-248.
17. Hiromitsuwatanabe, T. O., Nishizaki, M., Fujimoto, N., Kido, S., Yoshimasaishimura, K. S., Kuramoto, K., ... & Katoh, O. (1998). Induction of ovarian tumors by heavy ion irradiation in B6C3F1 mice. *Oncology reports*, *5*, 1377-1380.
18. Burns, F. J., Jin, Y., Koenig, K. L., & Hosselet, S. (1993). The low carcinogenicity of electron radiation relative to argon ions in rat skin. *Radiation research*, *135*(2), 178-188.
19. Burns, F. J., Tang, M. S. E., Frenkel, K., Nádas, A., Wu, F., Uddin, A., & Zhang, R. (2007). Induction and prevention of carcinogenesis in rat skin exposed to space radiation. *Radiation and environmental biophysics*, *46*(2), 195-199.
20. Dicello, J. F., Christian, A., Cucinotta, F. A., Gridley, D. S., Kathirithamby, R., Mann, J., ... & Ricart-Arbona, R. (2004). In vivo mammary tumourigenesis in the Sprague–Dawley rat and microdosimetric correlates. *Physics in medicine and biology*, *49*(16), 3817.
21. Shellabarger, C. J., Baum, J. W., Holtzman, S., & Stone, J. P. (1985). Neon- 20 Ion- and X- Ray- Induced Mammary Carcinogenesis in Female Rats. *Annals of the New York Academy of Sciences*, *459*(1), 239-244.
22. Demarest, K., McCaughran, J., Mahjubi, E., Cipp, L., & Hitzemann, R. (1999). Identification of an acute ethanol response quantitative trait locus on mouse chromosome 2. *The Journal of neuroscience*, *19*(2), 549-561.
23. Johnsen, A. K., Valdar, W., Golden, L., Ortiz- Lopez, A., Hitzemann, R., Flint, J., ... & Benoist, C. (2011). Genome- wide and species- wide dissection of the genetics of arthritis severity in heterogeneous stock mice. *Arthritis & Rheumatism*, *63*(9), 2630-2640.
24. Valdar, W., Solberg, L. C., Gauguier, D., Burnett, S., Klenerman, P., Cookson, W. O., ... & Flint, J. (2006). Genome-wide genetic association of complex traits in heterogeneous stock mice. *Nature genetics*, *38*(8), 879-887.
25. Huang, G. J., Shifman, S., Valdar, W., Johannesson, M., Yalcin, B., Taylor, M. S., ... & Flint, J. (2009). High resolution mapping of expression QTLs in heterogeneous stock mice in multiple tissues. *Genome research*, *19*(6), 1133-1140.
26. Woods, L. C. S. (2014). QTL mapping in outbred populations: successes and challenges. *Physiological genomics*, *46*(3), 81-90.
27. Kogan, S. C., Ward, J. M., Anver, M. R., Berman, J. J., Brayton, C., Cardiff, R. D., ... & Haines, D. C. (2002). Bethesda proposals for classification of nonlymphoid hematopoietic neoplasms in mice. *Blood*, *100*(1), 238-245.
28. Morse, H. C., Anver, M. R., Fredrickson, T. N., Haines, D. C., Harris, A. W., Harris, N. L., ... & Ward, J. M. (2002). Bethesda proposals for classification of lymphoid neoplasms in mice. *Blood*, *100*(1), 246-258.
29. Weil, M. M., Ray, F. A., Genik, P. C., Yu, Y., McCarthy, M., Fallgren, C. M., & Ullrich, R. L. (2014). Effects of 28 Si ions, 56 Fe ions, and protons on the induction of murine acute myeloid leukemia and hepatocellular carcinoma. *PloS one*, *9*(8), e104819.
30. Mole, R. H., Papworth, D. G., & Corp, M. J. (1983). The dose-response for x-ray induction of myeloid leukaemia in male CBA/H mice. *British Journal of Cancer*, *47*(2), 285.
31. Ullrich, R. L., & Preston, R. J. (1987). Myeloid leukemia in male RFM mice following irradiation with fission spectrum neutrons or γ rays. *Radiation research*, *109*(1), 165-170.
32. Cook, W. D., McCaw, B. J., Herring, C., John, D. L., Foote, S. J., Nutt, S. L., & Adams, J. M. (2004). PU. 1 is a suppressor of myeloid leukemia, inactivated in mice by gene

deletion and mutation of its DNA binding domain. *Blood*, *104*(12), 3437-3444.
33. Datta, K., Suman, S., Kallakury, B. V., & Fornace Jr, A. J. (2013). Heavy ion radiation exposure triggered higher intestinal tumor frequency and greater β-catenin activation than γ radiation in APC Min/+ mice. *PLoS One*, *8*(3), e59295.
34. Illa-Bochaca, I., Ouyang, H., Tang, J., Sebastiano, C., Mao, J. H., Costes, S. V., ... & Barcellos-Hoff, M. H. (2014). Densely ionizing radiation acts via the microenvironment to promote aggressive Trp53-null mammary carcinomas. *Cancer research*, *74*(23), 7137-7148.

Chapter Three

Genomic mapping reveals overlap in genetic susceptibility for HZE ion and γ-ray induced tumors

SUMMARY

Cancer risk from galactic cosmic radiation exposure is considered a potential "showstopper" for a manned mission to Mars. Calculating the actual risks confronted by astronauts is complicated by our limited understanding of the carcinogenic effects of high charge, high energy (HZE) ions—a radiation type for which no human exposure data exists. The validity of applying human carcinogenesis data from γ-ray exposures to predict carcinogenesis from HZE ion exposures is unproven in genetically diverse populations, however, such human epidemiologic data currently presents the best estimates for radiation carcinogenesis and forms the basis for NASA cancer risk models. In this chapter, the results of genome wide association studies (GWAS) to identify quantitative trait loci (QTL) for neoplasia in HS/Npt mice are presented and compared for γ-ray exposed, HZE ion exposed, and unirradiated populations. Through a genetics approach using tumorigenesis data from a mouse model of population diversity, 51 QTL are identified for 11 tumor histotypes with a 95% confidence interval of 3.4 Mb and biologic effect sizes ranging from 0.75 – 7.68%. Comparative QTL analysis and QTL confidence intervals are determined using nonparametric resample model averaging. Genome-wide significance thresholds are derived from permutation analysis. For acute myeloid leukemia and hepatocellular carcinomas, tumor samples are molecularly characterized and, in combination with GWAS, this characterization provides insights into the molecular events of tumorigenesis

following radiation exposures. Finally, clustering procedures are utilized to compare whole genome scans to determine whether similarities exist between the genetic variants that predispose individuals to specific tumor histotypes or radiation induced tumors. We demonstrate that QTL controlling tumor susceptibilities following HZE ion exposures often overlap with the QTL for γ-ray induced tumors. This overlap indicates shared tumorigenesis mechanisms following γ-ray and HZE ion exposures and supports the use of human epidemiological data from γ-ray exposures to predict cancer risk from galactic cosmic rays.

INTRODUCTION

Interplanetary space is populated by densely ionizing particle radiation not naturally present on Earth[1]. Life on our planet has evolved under the protection of a geomagnetic field, which deflects the vast majority of high charge, high energy (HZE) ions. In the absence of human epidemiological data for exposures to this radiation type, uncertainties surround the estimates used to determine cancer risk for space flight crews that venture beyond low Earth orbit[2]. The current NASA model to calculate cancer risk from space radiation exposures is built predominantly upon epidemiological data from the Atomic bomb survivors, individuals who were exposed predominantly to γ-rays[3-5]. One key assumption in this model is that the molecular characteristics of the tumors will be similar for individuals exposed to different forms of ionizing radiation. However, notable physical differences exist between terrestrial radiation such as γ-rays—which are composed of sparsely ionizing photons—and the densely ionizing particle radiation found in space. The physical differences between space and terrestrial radiation raises the possibility that tumorigenesis following these distinct exposures may follow unique molecular pathways. If so, the resulting tumors would likely have variable biologic behaviors

and introduce distinctive biologic threats to astronauts. The best approximation for tumorigenesis in the space radiation environment is achieved with laboratory animals exposed to accelerator-produced HZE ions.

Previous HZE ion rodent carcinogenesis studies have informed our understanding of the relative effectiveness of HZE ions to produce tumors. In these studies, it has been noted that the tumors types that arise in HZE ion irradiated animals are the same as those that arise spontaneously or following γ-ray exposures for a given animal model[6]. Although this may seem to indicate that HZE ions produce the same tumors as γ-rays, potentially via the same molecular mechanisms, these studies have utilized inbred animals which are predisposed to particular tumor types[7-14]. These laboratory animals have been deliberately inbred in attempts to remove the confounding genetic variability present in natural populations. Inbred mouse and rat strains improve the statistical power of detecting significant differences in toxicity studies by reducing phenotypic variance. Because HZE ion carcinogenesis studies have only been performed on genetically homogeneous animals, the tumor spectra that might arise in genetically diverse populations is unknown. Modeling population diversity can be desirable for carcinogenesis studies which aim to differentiate the effects of distinct radiation types because strain-specific responses following radiation can obscure the variability we expect in a genetically diverse population, such as humans.

With the emergence of multi-parent outbreeding strategies that produce highly recombinant mouse populations with allelic variants from multiple founder strains[15-17], it is possible to model the effects of population diversity in carcinogenesis studies by minimizing the overwhelming effects of genetic background and increasing the phenotypic repertoire available within a test population. Such populations also allow for high precision genomic mapping[16,18].

Quantitative trait locus (QTL) mapping is a powerful forward-genetics approach that allows for unbiased testing of genetic variants that may influence gene-environment interactions for radiation effects[19,20]. Highly recombinant populations are designed for genetic mapping, therefore, QTL can be resolved to single megabase (Mb) resolution and complete sequence information can be utilized on genotyped individuals by imputing the genomic resources available for the founder strains.

Studying tumors that arise in irradiated, highly recombinant mouse populations presents a unique opportunity: the ability to determine whether the same QTL that make individuals within a population susceptible to a specific γ-ray induced tumors also make them susceptible to those tumor types following HZE ion exposures. If so, extrapolation of human epidemiological data from individuals exposed to γ-rays would be a realistic approach for risk calculation in the space radiation environment.

METHODS

Animals, phenotyping and radiation exposures

A workflow for the radiation exposures, phenotyping, and bioinformatics procedures is present in **Figure 3.1**. Male and female HS/Npt mice (n = 1850) were generated from breeding trios obtained from Oregon Health & Sciences University (Portland, OR). These outbred mice were generated via circular outbreeding procedure involving 48 families. All the mice for this study were produced in generation 71. Founder strains for the HS/Npt include A/J, AKR/J, BALB/cJ, C3H/HeJ, C57BL/6J, CBA/J, DBA/2J, and LP/J [21]. The mice were group housed (5 mice of the same sex per cage) in a climate-controlled facility with free access to food and sterile water, and a 12-hour light cycle. Mice were shipped to Brookhaven National Laboratories

(Upton, NY) where they were exposed to accelerator produced HZE ions, γ-rays, or sham irradiated at the NASA Space Radiation Laboratory at 7 to 12 weeks of age. Mice of both sexes were exposed to 0.4 Gy of 240 MeV/n ^{28}Si ions (n = 308) or 600 MeV/n ^{56}Fe ions (n = 314), 3 Gy of ^{137}Cs γ-rays (n = 615), or sham irradiated (n = 622). Following radiation exposure or sham irradiation, mice were shipped back to and housed in a vivarium in the Research Innovation Center at Colorado State University (Fort Collins, CO) and monitored twice daily for the duration of the study. The mice were phenotyped for cataractogenesis by slit lamp biomicroscopy and cancer development until they reached 800 days of age or became moribund. Moribund mice were euthanized with CO_2 according to the Colorado State University animal care and use committee guidelines. A laboratory technician was trained to systematically evaluate all organ systems and thorough necropsy and tissue collection procedures were performed on each mouse. For cases of splenomegaly, thymic masses, mammary masses, and liver masses, fresh sections of tumor were frozen at negative 80 degrees Celsius and small sections were mixed in RNA stabilization solutions (RNAlater®). All gross lesions were formalin-fixed, trimmed, and submitted for routine tissue processing (paraffin embedded, sectioned, and stained with hematolxylin and eosin) for histologic evaluation. Five coronal sections were grossly evaluated for each mouse following 48 hours of cranial decalcification.

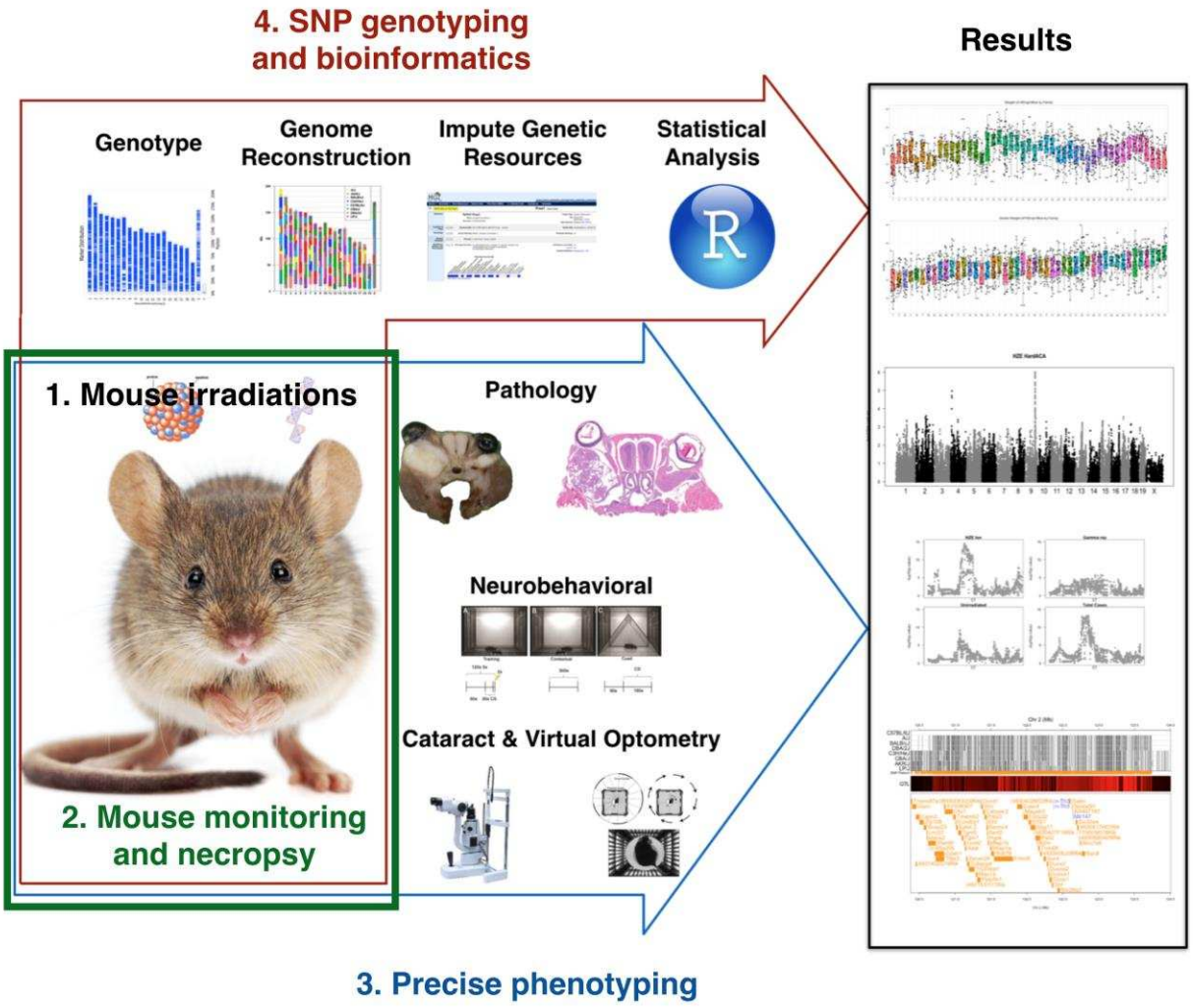

Figure 3.1: Workflow for mapping radiogenic QTL in Heterogeneous stock mice.

Genotyping

DNA was isolated from tail biopsies taken from each mouse at 3 to 4 weeks of age. DNA was extracted and purified using QIAGEN DNA extraction kit according to the manufacturer's instructions. GeneSeek (Lincoln, NE) performed genotyping assays using the Mega Mouse Universal Genotyping Array (MegaMUGA)[22] for a total of 1,878 mice. Nineteen 96 well plates were used for genotyping the 1,850 study mice. In addition, 28 inbred founder strain samples were scattered randomly within each plate for quality control. The MegaMUGA is built on the

Illumina Infinitum platform and consists of 77,808 single nucleotide polymorphic markers that are distributed throughout the genome with an average spacing of 33 kb (**Figure 3.2**). The marker density is sufficiently dense to capture the number of recombination events occurring in the HS/Npt population at generation 71.

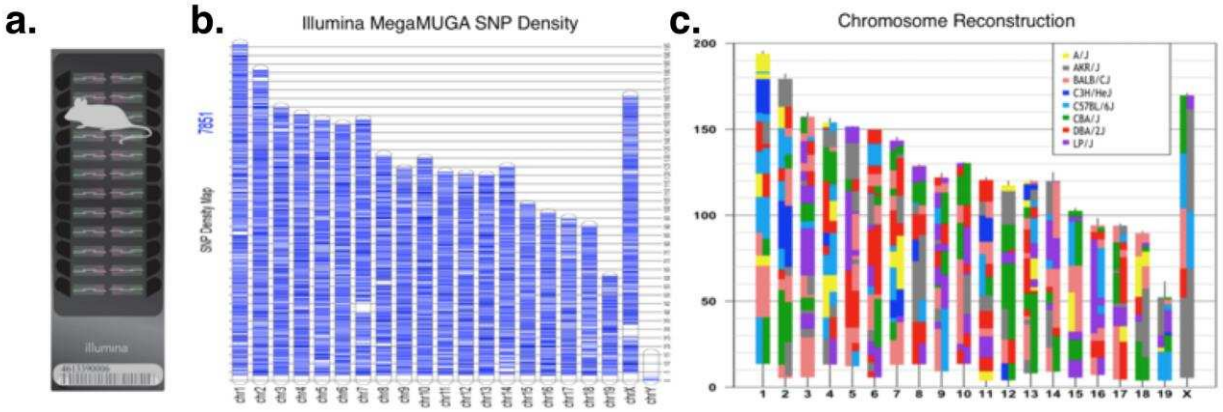

Figure 3.2: Genotyping: **a.** the MegaMUGA SNP array, **b.** the distribution of marker densities, and **c.** an example of genome reconstruction for a single HS/Npt mouse. Chromosomes are labeled along the horizontal axis and each color indicates one of the eight founder strains, which contributes to the mosaic of haplotypes; this mouse has a high degree of heterozygosity.

Genome reconstruction as mosaics of founder haplotypes

The heterogeneous stock mice are descendants of 8 inbred founder strains. For each mouse, allele calls from the MegaMUGA array are utilized to calculate descent probabilities using a hidden Markov model (HMM), in which the hidden states are the founder strains and the observed data are the genotypes. The HMM generates probabilistic estimates of the diplotype state(s) for each marker locus and produces a unique founder haplotype mosaic for each mouse[16]. A sample genome reconstruction is presented in **Figure 3.2**; these reconstructions serve as the scaffolding for imputing full sequencing information (mm10) from each founder strain.

Genome scans and QTL mapping

Association mapping was performed with mixed regression models using sex and cohort as covariates and adjusting for relatedness within the stock of mice by computing a matrix of expected allele sharing of founder haplotypes for each pair of mice [16]. Three statistical models were fit to account for the wide range of trait distributions in this study. A generalized linear regression model was fit for binomial distributions, such as neoplasia. Cox regression analysis was incorporated to model time-to-event distributions, such as cataract development and tumor latencies. Linear regression was utilized for normally distributed traits, such as neurobehavioral assays. Following genome wide association analyses, resample model averaging methods were utilized to identify QTL that are consistently reproduced within subsamples of the mapping population.

QTL significance thresholds, confidence intervals, effect sizes

Thresholds were determined using a permutation procedure in which the genotypes were fixed and the phenotype values were rearranged randomly within each sex. The distribution of the maximum negative log p-value of association under the null hypothesis that no associations exist (null model) was determined for each genome scan with permuted data. 1000 permutations were performed for each phenotype in each radiation exposure group, simulating effects arising from covariates, the linkage disequilibrium structure of the genome, and effects due to phenotype distribution. A threshold is determined as an estimate of the genome wide significance for which a type I statistical error will occur at a given frequency. Confidence intervals for each QTL were determined by nonparametric resample model averaging procedures using bootstrap aggregation with replacement. In this procedure, the mapping population is sampled to create a new data set

in which some individuals may be omitted and some may appear multiple times [23] and the locus with peak significance is recorded. Resampling is repeated 200 times for each phenotype to determine a 95% confidence interval for a given QTL. Effect sizes were calculated using the Tjur method for association mapping with logistic regression and pseudo-R^2 for mapping with Cox PH regression. Statistical significance for each model was assessed using a permutation strategy to randomize genotypes via resampling without replacement and maintaining covariates. Permutation analysis was performed (1000 tests) for each trait and exposure group to generate estimations of genome-wide significance thresholds. As genome scans with hundreds of thousands of imputed SNPs are computationally intensive, parallel computing was essential and accomplished using spot instances of resizable Elastic Compute Cloud (EC2) hosting resources.

Droplet digital PCR for copy number variation of Spi1 and Asxl1 in myeloid leukemia cells

Droplet digital PCR was performed on cases of acute myeloid leukemia (AML) to assess deletion status via copy number variation for two genes: *Sfpi1* and *Asxl1*. These genes are both located on chromosome 2 at base pair locations 91,082,390–91,115,756 for *Sfpi1* and 153,345,845–153,404,007 for *Asxl1* (mm10 reference genome). To establish a reference for normal diploid copy number in each AML sample, the copy number of *H2afx* was also determined with the assumption that each cell would contain two copies of this reference gene. *H2afx* is located on chromosome 9 and deletions in this region have not been reported in murine acute myeloid leukemia. BioRad PrimePCR™ probes were used for all assays as follows: *Asxl1* ddPCR™ probe (dMmuCPE5100268), *Sfpi1* ddPCR™ probe (dMmuCPE5094900), and *H2afx* ddPCR™ probe (dMmuCPE5104287). Ratios were created between the test gene and the reference gene (*Sfpi1*:*H2afx* and *Asxl1*:*H2afx*) to determine copy number with the assumption

that the reference gene would not be deleted or amplified. Ideally, ratios of 1:1 represent equal copy numbers for both the test gene and the reference gene and ratios of 1:2 represent a deletion in one copy of the test gene. However, since the tumor samples contained neoplastic cells as well as stromal cells and other cells, the ideal 1:2 ratio was not commonly observed. This is because stromal cells, which occur at unknown proportions in each tumor and which should not have chromosomal deletions, artificially increase ratios for tumor samples in which a deletion is indeed present. To account for stromal cell contamination, a cutoff ratio of 3:4 was established. Tumor samples with ratios below 3:4 were considered to have a deletion in one copy of the test gene.

Utilizing clustering procedures with whole genome scans

Comparisons were made between whole genome scans using Pearson correlations as a similarity measure with clustering based on average linkage. Significance of clustering results was estimated with 10,000 random permutations of the dataset. Each permutated data set simulates a null distribution of the maximally significant clustering based on a randomly assorted set of p-values for each genomic locus.

RESULTS

QTL mapping

To determine whether the genetic variants that increase tumor susceptibility following γ-ray irradiation also increase tumor susceptibility following HZE ion irradiation, genome-wide association mapping was performed for 18 tumor types. Only tumor types that occurred with an incidence of at least 1% were included for association mapping. Genomes were reconstructed for

each mouse using a probabilistic model to predict founder haplotypes from high-density genotype data[16]. Reconstructed genomes represent the unique accumulation of meiotic events for each individual and form a scaffold for the imputation of known sequencing information from the eight parental strains. Polygenic covariance among related individuals is of significant concern in multi-parent crosses and is corrected for during QTL mapping with a kinship term[16,24]. Mapping was performed using a linear mixed-effects model with the aforementioned kinship term to adjust for polygenic covariance between related mice. To determine the significance thresholds for a model in which no QTL is present, permutation analysis was performed for multiple phenotypes using each regression model. The 95% significance threshold was minimally variable between phenotypes with a mean threshold of $-\log(p) > 5.8$. This is consistent with the estimated 0.05 Bonferroni genome-wide corrected threshold of $-\log(p) > 6.0$, which is considered overly conservative for QTL mapping[25]. We use a significance threshold of $p \leq 0.05$ to select significant mapping associations.

At least one QTL was identified for 11 of the 18 tumor phenotypes examined, summarized in **Appendix 3**. For tumor incidence, 51 QTL were identified with an average confidence interval of 3.4 Mb. For QTL at the 95% confidence threshold, effect sizes average 3.7% with a range of 0.75 - 7.46%. For the majority of tumors, the genetic architecture of the phenotypic variance was complex with multiple QTL individually explaining only a small proportion of the total variance. Although loci with moderate effects on the phenotype were most common, 11 large effect QTL were observed for 7 tumor histotypes, with effect sizes greater than 5%.

To determine potential effects of genetic variants on tumor latency, mapping was also performed using proportional hazards regression; 39 QTL were identified for tumor latency

(**Appendix 4**), however QTL associated with latency predominantly mirrored the QTL already identified for tumor incidence, indicating that the genetic variants that control susceptibility to radiation induced tumors also affect latencies.

Neoplasia is a binomially distributed trait and, therefore, the power to detect significant associations is primarily dependent on tumor incidence and the QTL effect size. This leads to important considerations for the ultimate goal of this analysis: to determine similarities between QTL for specific neoplasms following unique radiation exposures. For some association mapping results, a significant peak was observed in one exposure group while only a suggestive peak present at the same locus in the alternative exposure group. In these cases, if the peak was more significant when combining radiation groups, the QTL was considered significant for all irradiated animals regardless of radiation quality. We speculate that the reason certain radiation qualities produce only suggestive QTL for certain tumor phenotypes is likely a function of decreased mapping power as a result of the variation in incidence between groups.

Comparing QTLs: Thyroid tumors following HZE ion and γ-ray exposures

To demonstrate the results contained within this dataset, we will now focus on a single tumor type. Thyroid tumors (**Figure 3.3a**) are a well-known radiation-induced entity for both humans and mice, however relatively little is known about genetic variants that increase susceptibility to this disease following radiation in mice. In HS/Npt mice, spontaneous thyroid adenomas occur at relatively low frequencies and have a uniformly late-onset, with tumors occurring between 700 and 800 days of age (**Figure 3.3b**). In contrast, thyroid tumors (including both adenomas and carcinomas) arising in HZE ion or γ-ray exposed mice occur at significantly increased incidences and with significantly earlier onsets, with tumors arising as early as 250

days of age (**Figure 3.3b**). Association mapping reveals a significant 3.4 Mb interval on chromosome 2 for HZE ion exposed animals (**Figure 3.3c and 3.3d**). The same locus is identified in the γ-ray irradiated population if the significance threshold is decreased to a level in which 30% of identified QTL will be false positives. Combining both irradiated populations and repeating genome-wide association mapping markedly increases the significance of the QTL identified on chromosome 2 (**Figure 3.3c and 3.3d**). This indicates that the susceptibility alleles present at this locus confer increased risk following exposure to either radiation quality. The protein-coding genes present within the QTL support interval on chromosome 2 are listed in **Figure 3.3e**, along with the strain specific SNP distributions.

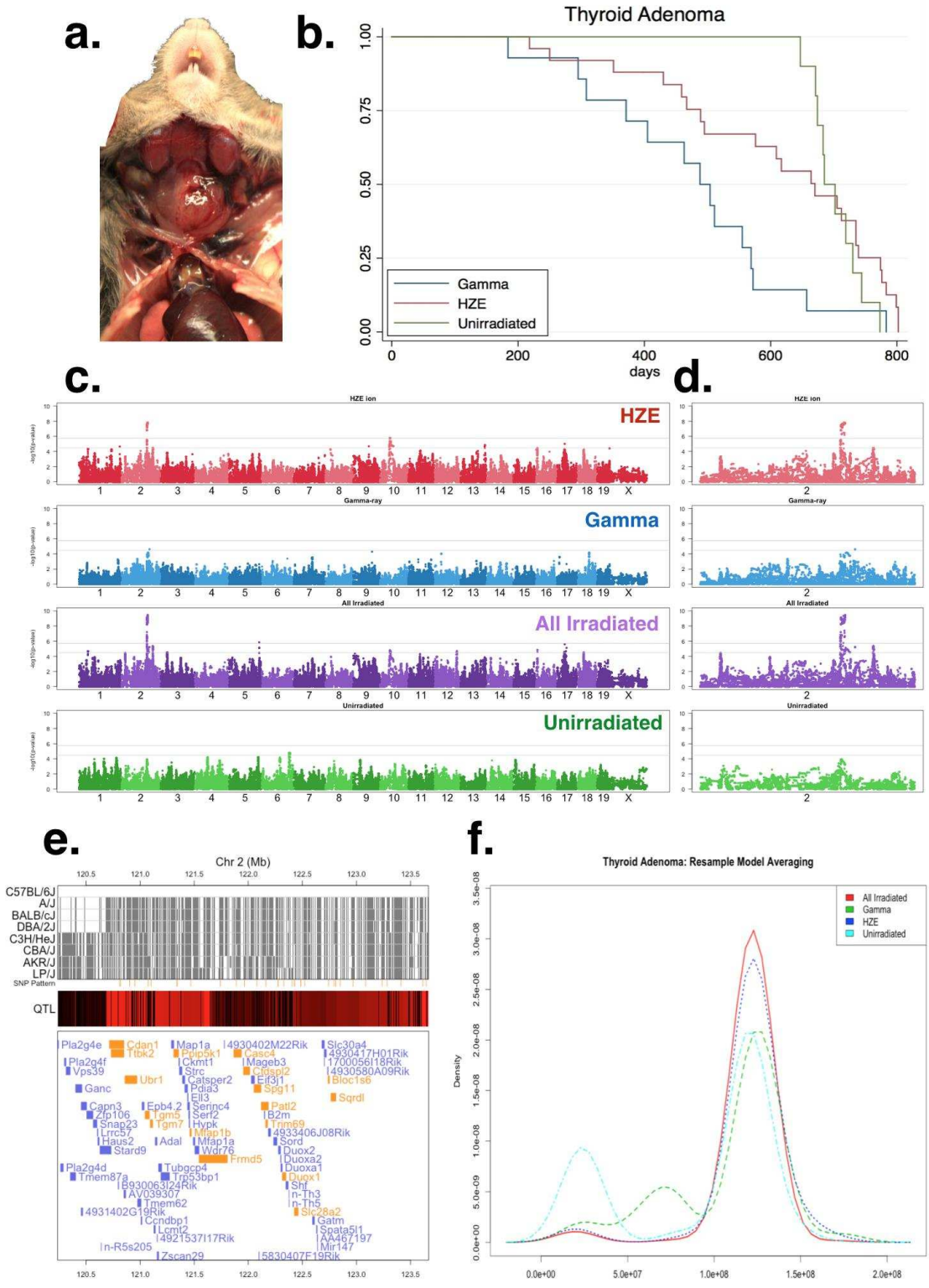

Figure 3.3: Thyroid adenoma bioinformatics results: a. gross image of an enlarged thyroid in HS/Npt mice, b. Kaplan-Meier survival for mice diagnosed with thyroid tumors by radiation exposure group, c. genome-wide association plots for each exposure group, d. an enlarged panel

demonstrating significant and suggestive chromosome 2 peaks for various exposures groups, e. the genes and founder SNP patterns present in the QTL support interval on chromosome 2 for all irradiated mice, f. resample model averaging procedure to demonstrate similarly significant chromosomal regions for each exposure group.

To further explore the possibility that the QTL identified on chromosome 2 controls susceptibility following γ-ray and HZE ion exposures, we utilized a nonparametric resample model averaging procedure[23] across the entire chromosome to identify genomic loci that consistently reappear in resampled populations. Briefly, genome scans are repeated for each new dataset created, in which some individuals will be sampled more than once and some not at all[23]. Resample model averaging consistently identifies the same locus for all groups of mice, regardless of radiation exposure (**Figure 3.3f**). Further, the resample model averaging procedure identifies the same locus for tumors arising spontaneously (**Figure 3.3f**). This indicates that germline genetic variants are more consequential for an individual's risk of developing thyroid cancer than whether or not an individual is exposed to radiation, of either quality.

Leukemogenic events are similar following HZE ion or γ-ray exposure

Acute myeloid leukemia (AML) is also a common radiation-induced tumor in both mice and humans[26,27]. In HS/Npt mice, myeloid leukemia often presented with splenomegaly (**Figure 3.4a**) and large numbers of circulating tumor cells. In concordance with previous studies in inbred strains[28], γ-ray exposures in HS/Npt mice are decidedly more efficient at inducing AML than HZE ion exposures, however AML was increased in both radiation groups when compared to the spontaneous incidence and survival times were similar for all groups (**Figure 3.4b**). Association mapping revealed a narrow QTL for AML incidence on chromosome 2 with a 95% confidence interval of 0.48 Mb (**Figure 3.4c and 3.4e**). This locus was observed in γ-ray

irradiated mice and significantly bolstered when grouping all irradiated animals together (**Figure 3.4c**).

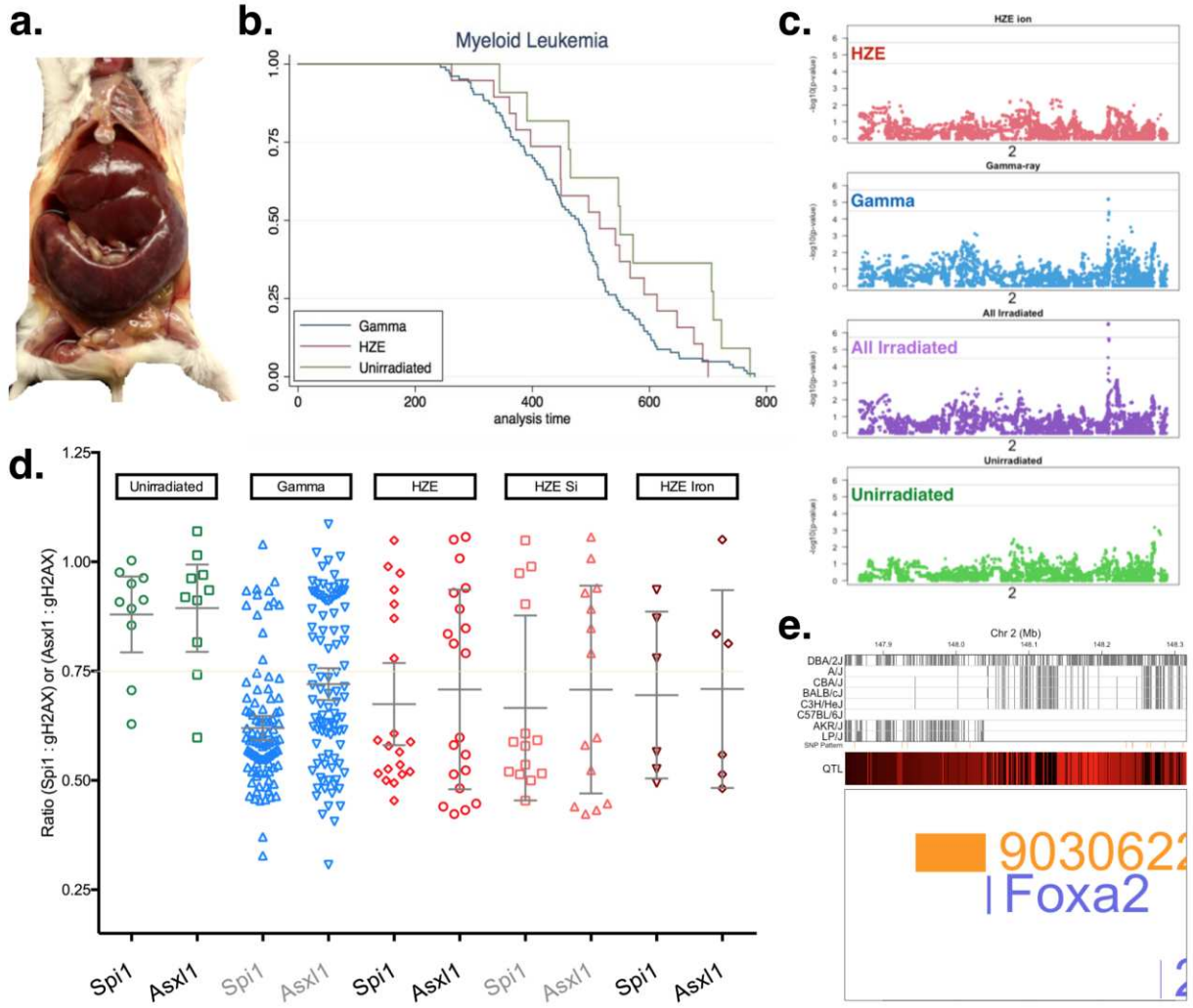

Figure 3.4: Acute myeloid leukemia: **a.** gross splenomegaly in an HS/Npt mouse diagnosed with splenic AML, **b.** Kaplan-Meier survival analysis for each exposure group, **c.** genome-wide association mapping results for chromosome 2 for each exposure group, **d.** copy number variation in AML samples expressed as *Spi1:gH2AX* and *Asxl1:gH2AX* demonstrating an increase in AML cases with each deletion for groups of HS/Npt mice exposed to radiation, **e.** the genes and founder SNP patterns present in the QTL support interval on chromosome 2 for all irradiated mice.

Radiation-induced AML is a well-characterized disease in mice[8,29,30], and is most commonly the result of a radiation-induced minimally deleted region, also on chromosome 2,

containing the *Spi1* gene and a recurrent point mutation that inactivates the remaining *Spi1* allele[31]. To test the hypothesis that HZE ion-induced AML will contain the same molecular aberrations as γ-ray induced AML, *Spi1* copy number was investigated. As expected, the majority of AML cases in the γ-ray exposure group had a deletion in one copy of *Spi1*, which was distinct from spontaneously occurring AML cases in which a deletion was rare (**Figure 3.4d**). Similar to γ-ray irradiated mice, mice exposed to HZE ions also have a significantly increased proportion of AML cases in which one copy of *Spi1* was deleted. This further supports the QTL data and indicates that AML arises by similar molecular mechanisms following exposures to sparsely or densely ionizing radiation.

Because the QTL identified on chromosome 2 is 62 Mb from *Spi1* and because radiation-induced deletions can be quite large, we considered the possibility that the chromosome 2 QTL was also deleted in many of the leukemias, leading to a loss of one copy of the susceptibility region. To test this hypothesis, we determined the copy number for a gene located at the distal end of the QTL support interval, *Asxl1*. We found that *Asxl1* was not deleted in any sample in which *Spi1* was not deleted, however, in 69% of cases with a *Spi1* deletion, *Asxl1*—and presumably the entire QTL region—was also deleted (**Figure 3.4d**). Thus, for the majority of cases, the AMLs that arise in irradiated animals are haploinsufficient for the entire QTL region.

Hierarchical clustering of genome scans

In addition to looking for similarities between individual selected QTL for HZE ion and γ-ray exposed populations, we also sought a more holistic method in which entire genome scans could be compared between groups in an unsupervised process. By using entire genome scans, we submit for comparison not only highly significant regions, but also the numerous loci

detected with lower confidence. To determine similarity of genetic associations profiles for all phenotypes and to detect possible coincident QTL, clustering procedures were utilized to compare genome-wide association scans between different radiation exposure groups.

To demonstrate and validate the methodology of QTL clustering, genome wide scans for coat colors in each treatment group are evaluated (**Figure 3.5**). As expected, genome wide scans for coat color are unaffected by radiation exposures, and therefore clustering is based entirely on coat phenotype rather than radiation exposure group. Utilizing the same procedure for neoplasia indicates that tumor types often clustered together as well, regardless of radiation exposure (**Figure 3.6**). Radiation-induced thyroid adenomas and mammary adenocarcinomas and all hepatocellular carcinoma genome scans cluster together. This finding supports the hypothesis that host genetic factors are more important in determining neoplasm incidence than radiation exposure type.

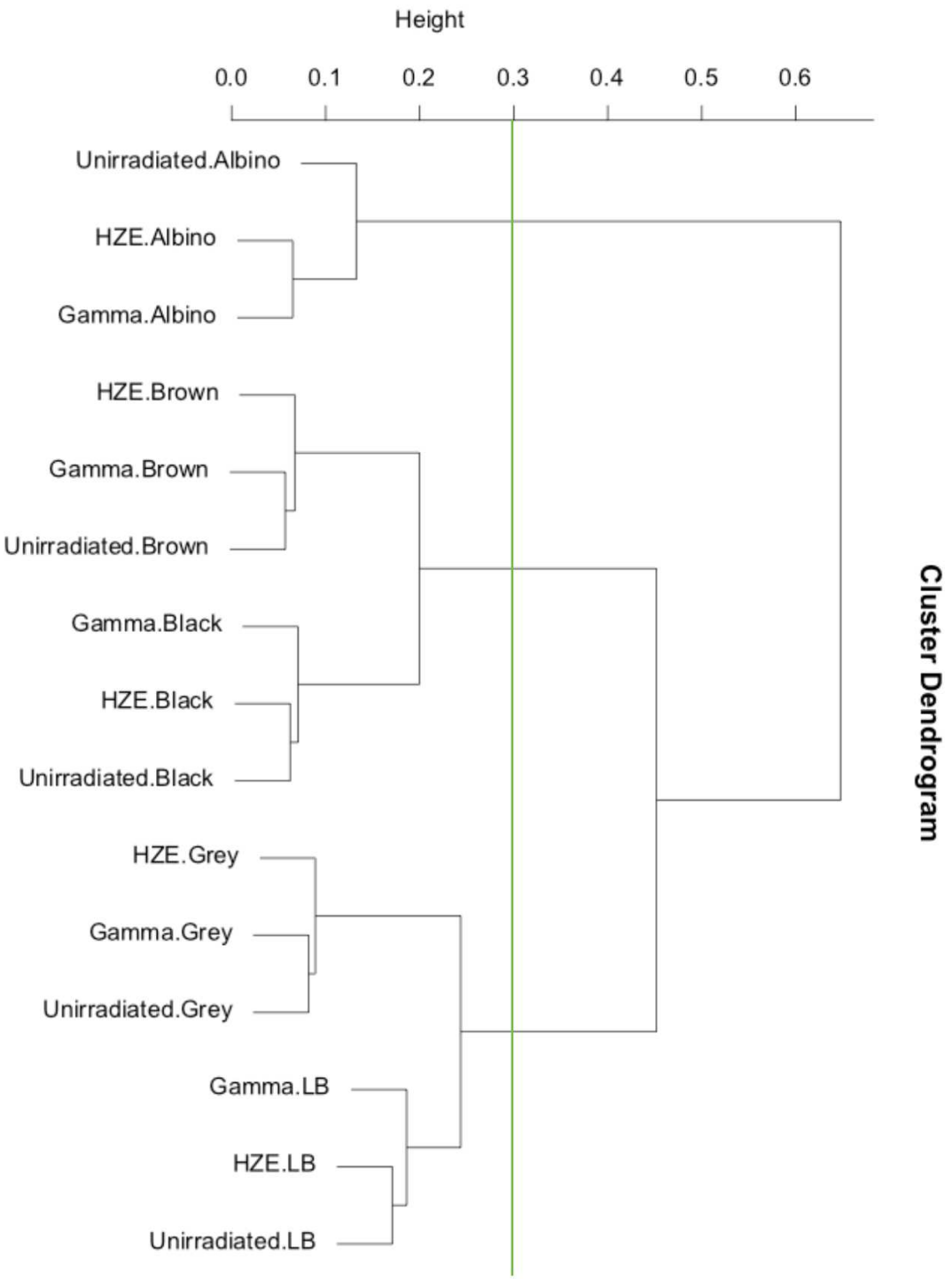

Figure 3.5: Coat color clustering. Unsupervised hierarchical clustering of genome wide association scans using Pearson's correlations. Indicated by a green line is the 95% confidence level of minimum dendrogram heights, estimated using permutation of p-values and marker positions.

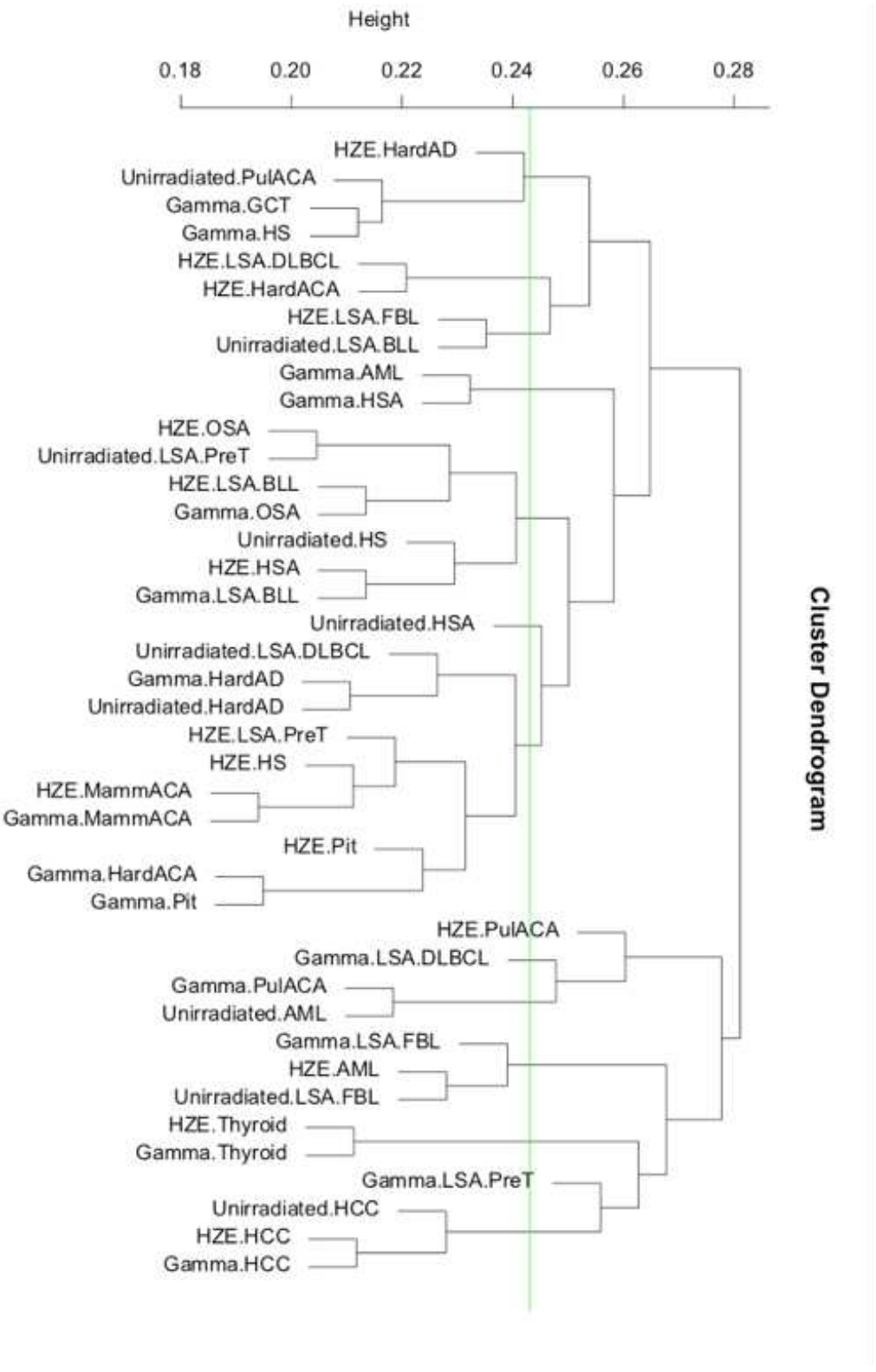

Figure 3.6: Tumor clustering. Unsupervised hierarchical clustering of genome wide association scans using Pearson's correlations. Indicated by a green line is the 95% confidence level of minimum dendrogram heights, estimated using permutation of p-values and marker positions.

DISCUSSION

Forward-genetics approaches allow for a hypothesis-free (unbiased) search of the entire genome for multiple genetic associations within a given phenotype. In contrast, common genetically engineered mouse models rely on a reverse-genetics approach in which a given gene is mutated and the resulting phenotypes are then described. Forward-genetics is only possible with a mouse model that contains abundant genetic and phenotypic diversity, which has been goal of research communities creating highly recombinant mouse populations such as the Heterogeneous Stock and Diversity Outbred mice.[16,18,32-35] As the shortest interval into which a QTL can be mapped is equal to the distance between the closest pair of recombinants surrounding the causal variant in the mapping population, highly recombinant outbred mouse populations such as the HS/Npt enable much higher resolution QTL mapping by decreasing that distance. Personalized approaches to cancer risk assessments may eventually allow for greater reductions in uncertainties when generating space radiation cancer risk estimates[36].

The combination of GWAS and molecular characterization of tumors has produced insights into tumorigenesis pathways for irradiated HS/Npt mice. γ-ray exposures are known to predispose certain strains of mice to acute myeloid leukemia (AML) by producing a deletion—sometimes a very large deletion—that commonly involves *Spi1*. To determine whether HZE ions produce similar molecular lesions, AML samples from all exposure groups were molecularly characterized to detect deletions in *Spi1*. Although HZE ions are found to be less efficient than γ-rays, radiation of either quality increases AML incidence and significantly increases the proportion of AML with *Spi1* deletions in comparison to spontaneously arising AML. GWAS in AML identified a QTL approximately 62 Mb distal to *Spi1*, establishing the possibility that the QTL region may be deleted along with *Spi1*. We demonstrate that this entire 62 Mb region,

including the entire QTL, is often deleted in radiation-induced AML, thus implicating QTL haploinsufficiency as a step during leukemogenesis for heterozygous outbred mice.

Applying clustering methods with Pearson correlation distance measures, we compare genome wide association scans for tumor phenotypes between exposure groups and find that tumor histotypes often cluster together regardless of radiation exposures. These results indicate shared tumorigenesis mechanisms following γ-ray and HZE ion exposures and support the use of human epidemiological data from γ-ray exposures to predict cancer risk from galactic cosmic rays.

In broader terms, to our knowledge this work is the first of its kind in that highly recombinant mouse models created for genetic mapping have not been previously utilized in lifetime carcinogenesis studies. Mapping QTL for carcinogenesis provides inherent challenges due to the structure of the binomial data, potential confounding causes of death following irradiation, the fundamental stochastic nature of radiation tumorigenesis, and incomplete penetrance of a potential allelic variant. Despite these challenges, we were able to map 51 QTL for 11 neoplastic subtypes and many of the identified loci are novel.

The results presented here indicate that host genetic factors dictate risk for tumor development following radiation exposures, regardless of radiation quality. Therefore, subpopulations at increased cancer risk following terrestrial radiation exposures are likely to substantially overlap with subpopulations at increased cancer risk following exposures to the space radiation environment.

References

1. Zeitlin, C., Hassler, D. M., Cucinotta, F. A., Ehresmann, B., Wimmer-Schweingruber, R. F., Brinza, D. E., ... & Burmeister, S. (2013). Measurements of energetic particle radiation in transit to Mars on the Mars Science Laboratory. *Science*, *340*(6136), 1080-1084.
2. National Council on Radiation Protection and Measurements, & Fry, R. J. (2000). Radiation Protection Guidance for Activities in Low-earth Orbit: Recommendations of the National Council on Radiation Protection and Measurements. National Council on Radiation Protection and Measurements.
3. de Gonzalez, A. B., Gilbert, E., Curtis, R., Inskip, P., Kleinerman, R., Morton, L., ... & Little, M. P. (2013). Second solid cancers after radiation therapy: a systematic review of the epidemiologic studies of the radiation dose-response relationship. *International Journal of Radiation Oncology* Biology* Physics*, *86*(2), 224-233.
4. United Nations. Scientific Committee on the Effects of Atomic Radiation. (2000). *Sources and effects of ionizing radiation: sources* (Vol. 1). United Nations Publications.
5. Cucinotta, F. A., Alp, M., Rowedder, B., & Kim, M. H. Y. (2015). Safe days in space with acceptable uncertainty from space radiation exposure. *Life sciences in space research*, *5*, 31-38.
6. Bielefeldt-Ohmann, H., Genik, P. C., Fallgren, C. M., Ullrich, R. L., & Weil, M. M. (2012). Animal studies of charged particle-induced carcinogenesis. *Health physics*, *103*(5), 568-576.
7. Ando, K., Koike, S., Oohira, C., Ogiu, T., & Yatagai, F. (2005). Tumor induction in mice locally irradiated with carbon ions: a retrospective analysis. *Journal of radiation research*, *46*(2), 185-190.
8. Weil, M. M., Bedford, J. S., Bielefeldt-Ohmann, H., Ray, F. A., Genik, P. C., Ehrhart, E. J., ... & Callan, M. A. (2009). Incidence of acute myeloid leukemia and hepatocellular carcinoma in mice irradiated with 1 GeV/nucleon 56Fe ions. *Radiation research*, *172*(2), 213-219.
9. Imaoka, T., Nishimura, M., Kakinuma, S., Hatano, Y., Ohmachi, Y., Yoshinaga, S., ... & Shimada, Y. (2007). High relative biologic effectiveness of carbon ion radiation on induction of rat mammary carcinoma and its lack of H-ras and Tp53 mutations. *International Journal of Radiation Oncology* Biology* Physics*, *69*(1), 194-203.
10. Alpen, E. L., Powers-Risius, P., Curtis, S. B., & DeGuzman, R. (1993). Tumorigenic potential of high-Z, high-LET charged-particle radiations. *Radiation research*, *136*(3), 382-391.
11. Alpen, E. L., Powers-Risius, P., Curtis, S. B., DeGuzman, R., & Fry, R. J. M. (1994). Fluence-based relative biological effectiveness for charged particle carcinogenesis in mouse Harderian gland. *Advances in Space Research*, *14*(10), 573-581.
12. Fry, R. J. M., Powers-Risius, P., Alpen, E. L., & Ainsworth, E. J. (1985). High-LET radiation carcinogenesis. *Radiation Research*, *104*(2s), S188-S195.
13. Fry, R. J. M., Ullrich, R. L., Powers-Risius, P., Alpen, E. L., & Ainsworth, E. J. (1983). High-LET radiation carcinogenesis. *Advances in Space Research*, *3*(8), 241-248.
14. Hiromitsuwatanabe, T. O., Nishizaki, M., Fujimoto, N., Kido, S., Yoshimasaishimura, K. S., Kuramoto, K., ... & Katoh, O. (1998). Induction of ovarian tumors by heavy ion

irradiation in B6C3F1 mice. *Oncology reports*, *5*, 1377-1380.
15. Woods, L. C. S. (2014). QTL mapping in outbred populations: successes and challenges. *Physiological genomics*, *46*(3), 81-90.
16. Gatti, D. M., Svenson, K. L., Shabalin, A., Wu, L. Y., Valdar, W., Simecek, P., ... & Chesler, E. J. (2014). Quantitative trait locus mapping methods for diversity outbred mice. *G3: Genes| Genomes| Genetics*, *4*(9), 1623-1633.
17. Mott, R., & Flint, J. (2008). Prospects for complex trait analysis in the mouse. *Mammalian Genome*, *19*(5), 306-308.
18. Valdar, W., Solberg, L. C., Gauguier, D., Burnett, S., Klenerman, P., Cookson, W. O., ... & Flint, J. (2006). Genome-wide genetic association of complex traits in heterogeneous stock mice. *Nature genetics*, *38*(8), 879-887.
19. Svenson, K. L., Gatti, D. M., Valdar, W., Welsh, C. E., Cheng, R., Chesler, E. J., ... & Churchill, G. A. (2012). High-resolution genetic mapping using the Mouse Diversity outbred population. *Genetics*, *190*(2), 437-447.
20. Mott, R., & Flint, J. (2013). Dissecting quantitative traits in mice. *Annual review of genomics and human genetics*, *14*, 421-439.
21. Demarest, K., McCaughran, J., Mahjubi, E., Cipp, L., & Hitzemann, R. (1999). Identification of an acute ethanol response quantitative trait locus on mouse chromosome 2. *The Journal of neuroscience*, *19*(2), 549-561.
22. Morgan, A. P., Fu, C. P., Kao, C. Y., Welsh, C. E., Didion, J. P., Yadgary, L., ... & Giusti-Rodriguez, P. (2015). The mouse universal genotyping array: from substrains to subspecies. *G3: Genes| Genomes| Genetics*, g3-115.
23. Valdar, W., Holmes, C. C., Mott, R., & Flint, J. (2009). Mapping in structured populations by resample model averaging. *Genetics*, *182*(4), 1263-1277.
24. Cheng, R., Parker, C. C., Abney, M., & Palmer, A. A. (2013). Practical considerations regarding the use of genotype and pedigree data to model relatedness in the context of genome-wide association studies. *G3: Genes| Genomes| Genetics*, g3-113.
25. Churchill, G. A., & Doerge, R. W. (1994). Empirical threshold values for quantitative trait mapping. *Genetics*, *138*(3), 963-971.
26. Mole, R. H. (1986). Radiation-induced acute myeloid leukemia in the mouse: experimental observations in vivo with implications for hypotheses about the basis of carcinogenesis. *Leukemia research*, *10*(7), 859-865.
27. Preston, D. L., Kusumi, S., Tomonaga, M., Izumi, S., Ron, E., Kuramoto, A., ... & Thompson, D. E. (1994). Cancer incidence in atomic bomb survivors. Part III: Leukemia, lymphoma and multiple myeloma, 1950-1987. *Radiation research*, *137*(2s), S68-S97.
28. Weil, M. M., Ray, F. A., Genik, P. C., Yu, Y., McCarthy, M., Fallgren, C. M., & Ullrich, R. L. (2014). Effects of 28 Si ions, 56 Fe ions, and protons on the induction of murine acute myeloid leukemia and hepatocellular carcinoma. *PloS one*, *9*(8), e104819.
29. Mole, R. H., Papworth, D. G., & Corp, M. J. (1983). The dose-response for x-ray induction of myeloid leukaemia in male CBA/H mice. *British Journal of Cancer*, *47*(2), 285.
30. Ullrich, R. L., & Preston, R. J. (1987). Myeloid leukemia in male RFM mice following irradiation with fission spectrum neutrons or γ rays. *Radiation research*, *109*(1), 165-170.
31. Cook, W. D., McCaw, B. J., Herring, C., John, D. L., Foote, S. J., Nutt, S. L., & Adams, J. M. (2004). PU. 1 is a suppressor of myeloid leukemia, inactivated in mice by gene deletion and mutation of its DNA binding domain. *Blood*, *104*(12), 3437-3444.

32. Valdar, W., Solberg, L. C., Gauguier, D., Cookson, W. O., Rawlins, J. N. P., Mott, R., & Flint, J. (2006). Genetic and environmental effects on complex traits in mice. *Genetics*, *174*(2), 959-984.
33. Valdar, W., Flint, J., & Mott, R. (2006). Simulating the collaborative cross: power of quantitative trait loci detection and mapping resolution in large sets of recombinant inbred strains of mice. *Genetics*, *172*(3), 1783-1797.
34. Churchill, G. A., Gatti, D. M., Munger, S. C., & Svenson, K. L. (2012). The diversity outbred mouse population. *Mammalian genome*, *23*(9-10), 713-718.
35. Bogue, M. A., Churchill, G. A., & Chesler, E. J. (2015). Collaborative Cross and Diversity Outbred data resources in the Mouse Phenome Database. *Mammalian Genome*, *26*(9-10), 511-520.
36. Locke, P. A., & Weil, M. M. (2016). personalized Cancer risk assessments for space radiation exposures. *Frontiers in oncology*, *6*.

Chapter Four

Overlap in genetic susceptibility to cataractogenesis following HZE ion and γ-ray exposures

SUMMARY

Cataractogenesis in the space radiation environment poses a significant health risk for astronauts, as the lens of the eye is known to be one of the most sensitive areas of the body to radiation-induced late effects. Cataractogenesis has been documented in numerous human populations exposed to the types of radiation found on Earth. In assessing cataractogenesis risk for astronauts, the unique forms of ionizing radiation in space must be characterized. The forms of radiation present in space, known as high energy and high charge (HZE) ions, deposit energy along dense linear tracks. This high linear energy transfer (LET) particle radiation is in contrast to the low LET photon radiation that currently forms the bulk of our understanding for radiation cataractogenesis. Populations exposed to low LET radiation, such as γ-rays, have provided epidemiologic data that has informed dose limits for cataractogenesis. Limited cataractogenesis data is also available for astronauts exposed to space radiation, and these data demonstrate that relatively low levels of space radiation are capable of producing increased incidences of and decreased latencies for cataract formation. Genetic susceptibility is a known risk factor for cataractogenesis following low LET exposures and likely also plays a role in high LET exposures, however, sufficient data is not available to analyze the role of genetic susceptibility for cataractogenesis following high LET exposures in humans.

To determine whether genetic susceptibility to cataracts is similar for high and low LET radiation exposures, we utilize genome wide association mapping (GWAS) in an animal model

of genetic diversity to compare quantitative trait loci (QTL) for cataractogenesis following high or low LET irradiations. 1,850 HS/Npt stock mice of both sexes are irradiated with 0.4 Gy of 240 MeV/n ^{28}Si or 600 MeV/n ^{56}Fe ions or 3.0 Gy of ^{137}Cs γ-rays, or sham irradiated at Brookhaven National Laboratories, NASA Space Radiation Laboratory (NSRL) facility. Each mouse is genotyped for 77,808 single nucleotide polymorphisms (SNP) and genomes are reconstructed for sequencing imputation using a hidden Markov chain for founder probabilities at each defined SNP. The progression of radiation-induced ocular changes is followed by dilated slit lamp biomicroscopy and each mouse is examined up to seven times post-irradiation. Tumors are the predominant cause of morbidity and mortality for both exposure groups; therefore, time-at-risk for cataracts is corrected for using proportional hazards regression models during GWAS.

Progressive, radiation-associated lens changes, consistent with posterior subcapsular cataract (PSC), are noted in both HZE ion and γ-ray exposed populations. Prevalence and severity of PSCs in irradiated animals increases significantly in comparison to unirradiated controls, which, have very mild to no posterior lens changes. 14 QTL were identified for radiation-induced cataracts and substantial overlap is identified between HZE ion and γ-ray exposed populations. In addition, 4 QTL were identified for spontaneous cataractogenesis. These results indicate that the susceptibility to radiation-induced cataractogenesis is highly heritable and that individuals within a population that are sensitive to cataractogenesis following low LET irradiation are also sensitive following high LET exposures.

INTRODUCTION

The lens is a transparent and avascular tissue that derives nutrients from the aqueous humor and vitreous[1] and refracts light to a point source on the retina in the normal eye[2]. The lens

is enveloped by a basement membrane and has only a single epithelial cell layer on the anterior surface. This anterior epithelium contains the progenitors of the lens fiber cells[3]. At the peripheral germinative zone, epithelial cells differentiate into mature lens fiber cells throughout life. This maturation process involves shedding of organelles, including the nucleus, to achieve translucency. As these lens fiber cells lack nuclei and mitochondria, they depend on the overlying epithelial cells for nutrient transport and energy[2]. Lens transparency is influenced by cytoplasmic hydration, intracellular ionic strength, and other metabolic functions within the lens[2,4,5]. The initial event of cataract formation is thought to be damage to the lens epithelial cells[6-8].

The development of cataracts is a complex biological phenomenon that results in vision deficits due to alterations in the proteins that compose the lens. The World Health Organization estimates that there are 285 million visually impaired individuals worldwide—39 million of whom are blind—and an estimated 33% of these cases are the result of cataracts[9]. Cataract formation is remarkably common with age—96% of humans greater than 60 years develop cataracts[10]—however, several risk factors have been identified that accelerate cataract formation[11]. These risk factors include genetic predisposition[12,13], co-morbidities such as diabetes mellitus, adverse reactions to certain drugs, dietary deficiencies, uveitis, trauma, and exposure to ionizing or non-ionizing radiation[2,14]. For astronaut risk prediction, ionizing radiation exposure is the most significant factor increasing risk over the general population.

Cataractogenesis following exposure to ionizing radiation was recognized soon after the discovery of X-rays[15] and radiation was demonstrated to produce lens changes in experimental animals as early as 1897[16]. Since that time, researchers have been aware that ionizing radiation exposure can accelerate cataract formation[17-24]. Ionizing radiation is remarkably efficient at

producing lens opacities, which is evidenced by multiple studies of radiation-exposed populations. These studies include Chernobyl accident liquidators[25], atomic bomb survivors[26], cyclotron workers[27], interventional medical personnel[28-31], patients undergoing CT scans[32] or receiving radiotherapy for cancer treatment or bone marrow transplantation[33-38], and astronauts[39,40]. Data from medical exposure studies have helped establish thresholds for cataract formation; however, it is important to mention that cataractogenesis is likely a stochastic event without a single threshold. Independent studies have demonstrated that all patients receiving a single 10 Gy dose[38], 7.5 Gy dose[33], or 14 Gy dose[34] developed cataracts, indicating the threshold dose for cataracts is somewhere below these levels. Furthermore, cataract latency has been found to be inversely related to dose, meaning that cataracts developed more rapidly for individuals exposed to higher doses[41]. Atomic bomb data indicate a clear relationship between cataract incidence and dose[42] and estimated thresholds have been reported as low as 0.6 to 1.5 Gy[43,44]. Together, these observations have been utilized to establish dose limits for the lens[45-47] and it appears that a single dose of 2 Gy or more is definitively cataractogenic for exposed populations[48]. However, individual susceptibility to radiation-induced cataractogenesis is widely variable[12] and no single dose limit can be defined for a single individual.

The risk of cataract formation for astronauts exposed to the space radiation environment is of particular concern, as space radiation exposures has been demonstrated to increase cataractogenesis[49,50]. Astronaut data (n = 295) spanning over 3 decades indicates that relatively low doses of space radiation can result in increased cataract incidence as well as a decrease in latency for cataract formation[39]. These astronaut studies indicate a significant association between cataract formation and radiation quality, however estimating the effects of contributory risk factors, such as genetic predisposition, is difficult with such a small sample size.

Experimental studies using mouse models have indicated that genetics play a significant role in exposures to both low and high LET radiation, but these studies have utilized inbred, genetically engineered mouse (GEM) models[23,50-52]. Such GEM models indicate that similar genetic pathways play a role in spontaneous and radiation-induced cataractogenesis and that radiation can worsen and hasten cataractogenesis, however, GEM mice on the same genetic backgrounds are highly predisposed to a specific set of phenotypes.

This study aims to utilize genetic diverse populations of mice in cataract GWAS to determine whether genetic susceptibilities to cataractogenesis overlap in populations exposed to qualitatively distinct radiation types.

METHODS

Animals, phenotyping, and radiation exposures

A workflow for the radiation exposures, phenotyping, and bioinformatics procedures is presented in **Figure 3.1**. Male and female HS/Npt mice (n = 1850) were generated from breeding pairs obtained from Oregon Health & Sciences University (Portland, OR). These outbred mice were generated via circular outbreeding procedure involving 48 families. All the mice for this study were produced in generation 71. Founder strains for the HS/Npt include A/J, AKR/J, BALB/cJ, C3H/HeJ, C57BL/6J, CBA/J, DBA/2J, and LP/J[53]. The mice were group housed (5 mice of the same sex per cage) in a climate-controlled facility with free access to food and sterile water, and a 12-hour light cycle. Mice were shipped to Brookhaven National Laboratories (Upton, NY) where they were exposed to accelerator produced HZE ions, γ-rays, or sham irradiated at the NASA Space Radiation Laboratory at 7 to 12 weeks of age. HS/Npt stock mice of both sexes were exposed to 0.4 Gy of 240 MeV/n ^{28}Si ions (n = 308) or 600 MeV/n ^{56}Fe ions

(n = 314), 3 Gy of ^{137}Cs γ-rays (n = 615), or sham irradiated (n = 622). Following radiation exposure or sham irradiation, mice were returned to Colorado State University Research Innovation Center vivarium (Fort Collins, CO) and monitored twice daily for the duration of the study. Mice were cared for in accordance with the recommendations of the Guide for the Care and Use of Laboratory Animals. The Colorado State University (CSU) and the Brookhaven National Laboratory Institutional Animal Care and Use Committees (IACUC) approved experimental protocols and animal handling and care.

Mice were examined approximately every two months, for more than 100 weeks post-irradiation, or until animals died or were euthanized due to comorbid conditions. Irradiation status and genotype were blinded to observers until the completion of the study. Radiation associated lens changes were monitored by slit-lamp biomicroscopy and analyzed using a modified version of the Merriam-Focht scoring criteria (Merriam and Focht, 1962). This 0-4 scoring range depends upon the fact that radiation- associated lens changes develop in a characteristically sequential fashion with the earliest changes, stage 0.5, consisting of less than four dots, vacuoles or diffuse opacities around the central suture in the posterior subcapsular region, and progressing, over time, to stage 4, when there is a complete opacification of the lens. A score of 2.0 or higher is thought to be vision impairing. As animals were not examined weekly, values for weeks where no assessment was made were filled in using the score obtained at the last observation. Approximately 5-10 min prior to the dilated slit lamp exam, one to two drops each of 1% cyclopentolate and 2.5% phenylephrine HCl were placed in each eye. Examinations were performed roughly every two months on each mouse by one of two veterinary ophthalmology residents. Interobserver variability was minimal and a third expert observer was utilized to regularly compare findings from the two primary ophthalmologists.

To account for co-morbidities and time at risk, cataractogenesis endpoints were analyzed using time-to-event procedures and genome wide mapping was performed with proportional hazards regression models

Genotyping

DNA was isolated from tail biopsies taken from each mouse at 4 to 5 weeks of age. DNA was extracted and purified using a QIAGEN DNA extraction kit according to the manufacturer's instructions. GeneSeek (Lincoln, NE) performed genotyping assays using the Mega Mouse Universal Genotyping Array (MegaMUGA) for a total of 1,878 mice. The MegaMUGA is built on the Illumina Infinitum platform and consists of 77,808 single nucleotide polymorphic markers that are distributed throughout the genome with an average spacing of 33 kb. The marker density is sufficiently dense to capture the number of recombination events occurring in the HS/Npt population at generation 71.

Genome reconstruction as mosaics of founder haplotypes

The heterogeneous stock mice are descendants of 8 inbred founder strains. For each mouse, allele calls from the MegaMUGA array are utilized to calculate descent probabilities using a hidden Markov model (HMM), in which the hidden states are the founder strains and the observed data are the genotypes. The HMM generates probabilistic estimates of the diplotype state(s) for each marker locus and produces a unique founder haplotype mosaic for each mouse. A sample genome reconstruction is presented in **Figure 3.2**; these reconstructions serve as the scaffolding for imputing full sequencing information (mm10 reference genome) from each founder strain.

Genome scans and QTL mapping

Association mapping was performed with mixed regression models using sex and cohort as covariates and adjusting for relatedness within the stock of mice by computing a matrix of expected allele sharing of founder haplotypes for each pair of mice [54]. Three statistical models were fit to account for the wide range of trait distributions in this study. A generalized linear regression model was fit for binomial distributions, such as neoplasia. Cox regression analysis was incorporated to model time-to-event distributions, such as cataract development and tumor latencies. Linear regression was utilized for normally distributed traits, such as neurobehavioral assays. Following genome wide association analyses, resample model averaging methods were utilized to identify QTL that are consistently reproduced within subsamples of the mapping population.

QTL significance thresholds, confidence intervals, effect sizes

Thresholds were determined using a permutation procedure in which the genotypes were fixed and the phenotype values were rearranged randomly within each sex. The distribution of the maximum negative log p-value of association under the null hypothesis that no associations exist (null model) was determined for each genome scan with permuted data. 1000 permutations were performed for each phenotype in each radiation exposure group, simulating effects arising from covariates, the linkage disequilibrium structure of the genome, and effects due to phenotype distribution. A threshold is determined as an estimate of the genome wide significance for which a type I statistical error will occur at a given frequency. Confidence intervals for each QTL were determined by nonparametric resample model averaging procedures using bootstrap aggregation with replacement. In this procedure, the mapping population is sampled to create a new data set

in which some individuals may be omitted and some may appear multiple times and the locus with peak significance is recorded. Resampling is repeated 200 times for each phenotype to determine a 95% confidence interval for a given QTL. Effect sizes were calculated using the Tjur method for association mapping with logistic regression and pseudo-R^2 for mapping with Cox PH regression. Statistical significance for each model was assessed using a permutation strategy to randomize genotypes via resampling without replacement and maintaining covariates. Permutation analysis was performed (1000 tests) for each trait and exposure group to generate estimations of genome-wide significance thresholds. As genome scans with hundreds of thousands of imputed SNPs are computationally intensive, parallel computing was essential and accomplished using spot instances of resizable Elastic Compute Cloud (EC2) hosting resources.

RESULTS

Cataract latency is significantly decreased for HS/Npt mice exposed to either HZE ions or γ-rays in comparison to unirradiated controls (**Figure 4.1**). No significant difference was observed between onset for cataracts following 0.4 Gy of HZE ion irradiation or 3.0 Gy of γ-ray irradiation, however, these two doses may not be equivalent for cataract induction. Though these doses seem disparate, their selection was optimized to produce maximum tumorigenesis, as the primary phenotyping goal for this project was tumorigenesis. Preliminary dose-response studies indicate that 0.4 Gy of HZE ions and 3.0 Gy γ-rays are each maximally tumorigenic in mouse carcinogenesis studies[55], however the maximally cataractogenic dose for HS/Npt mice has not been established. Nevertheless, ionizing radiation of either type produced significantly increased cataract incidence, as well as earlier cataract onset, compared to spontaneously occurring

cataracts; this indicates that radiation-induced cataract GWAS have the potential to map radiation-specific cataractogenesis susceptibility loci.

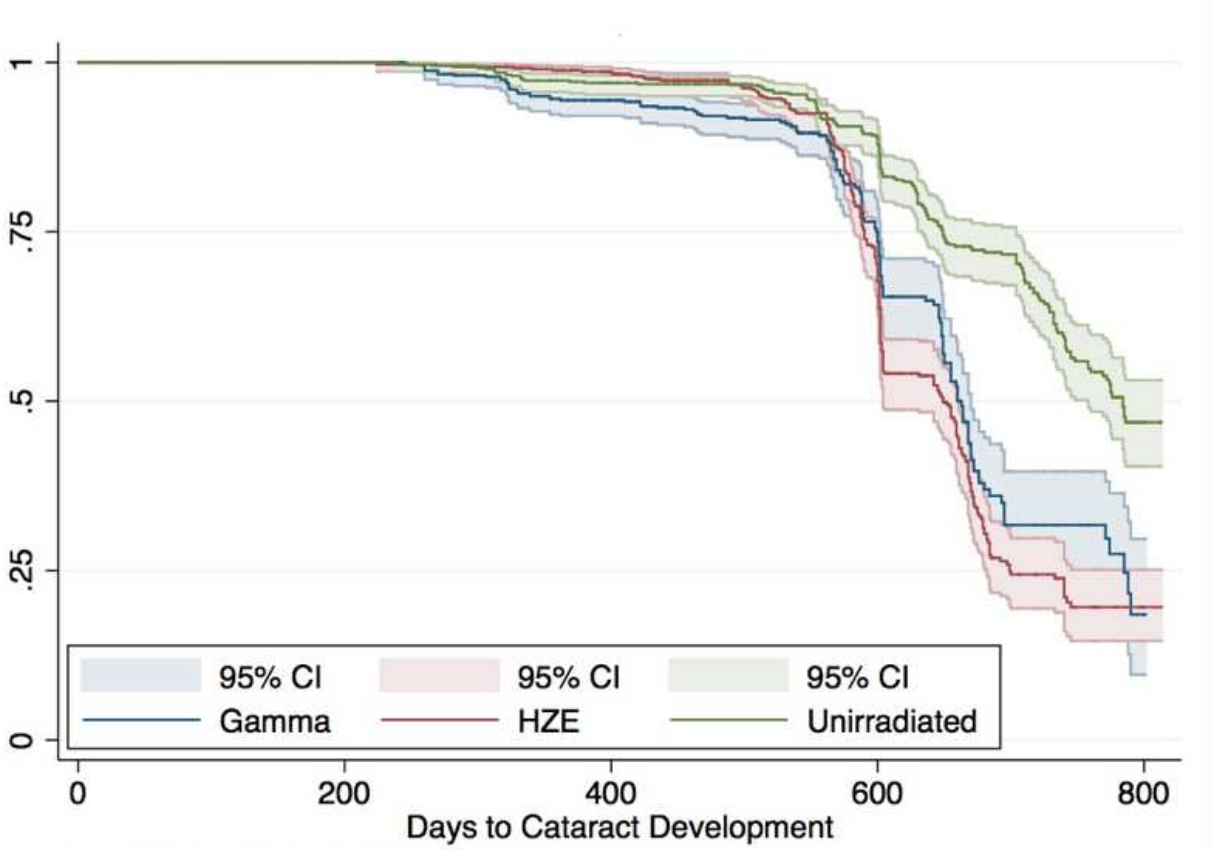

Figure 4.1: Kaplan-Meier analysis for latency of cataract formation (Merriam Focht score of 2.0 or higher).

Variable survival times are observed for individual HS/Npt mice for this study, from 94 to 800 days. This survival variability has the potential to skew binomial incidence data; e.g., if a cataract susceptible mouse dies prior to developing cataracts, this mouse may erroneously be considered cataract free using a binomial count analysis. To best control survival variability, proportional hazards regression analysis with censoring is utilized during cataract QTL mapping. In **Figure 4.2,** the genome wide association mapping results for HZE ion exposed

(n = 622), γ-ray exposed (n = 615), HZE ion and γ-ray exposed (n = 1,237), unirradiated (n = 613), and all mice (n = 1,850) are presented.

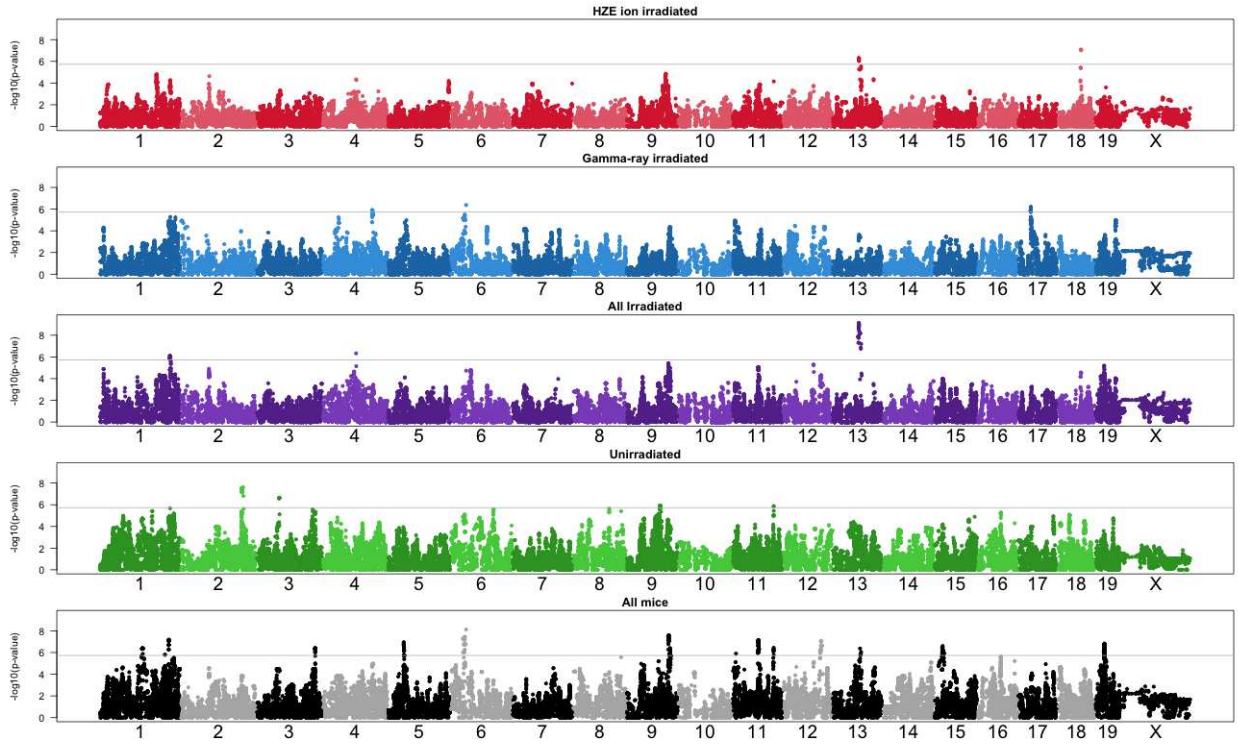

Figure 4.2: Genome wide association mapping with proportional hazards regression for cataractogenesis in each exposure group. Significance thresholds were developed using permutation analysis and the 95% confidence threshold is demarcated with a grey line for each panel.

Cataractogenesis in HS/Npt mice is a complex, highly heritable trait with a total of 18 QTL identified at 95% significance and an average QTL effect size of 2.7% (range: 1.3 – 5.2%). Detailed information on location, QTL support intervals, significance, and effects can be found in **Appendix 5**. Of these QTL, four appear to be predominantly associated with radiation (chromosomes 4, 13, 17, and 18), three are most significantly associated with cataracts arising spontaneously (chromosomes 2, 3, and 9), and the remaining genomic loci appear to confer risk

for all mice, regardless of radiation exposure. For simplicity, results will be presented for a single QTL, and similar information is provided for all additional QTL in **Appendix 5**.

The most significant cataractogenesis QTL is observed on chromosome 13 when grouping all irradiated mice (-log10 p-value = 9.1) (**Figure 4.3a**); this locus is identified in HZE ion irradiated mice and approaches significance in γ-ray exposed mice. When grouping all irradiated mice together, this locus is significantly bolstered, indicating that this genomic region is confers susceptibility to cataractogenesis following radiation of either quality. The support interval for the chromosome 13 QTL is 3.61 Mb and is located at basepairs 64314474 – 67923771 (mm10 reference genome). The QTL support interval contains one gene previously identified as having contributory effects for human and murine cataractogenesis: *Cdc14b*[24]. This gene is a strong candidate for radiation-induced cataractogenesis, as Cdc14b is involved in defective DNA damage response, which is widely accepted as a likely mechanism of radiation induced cataractogenesis[24].

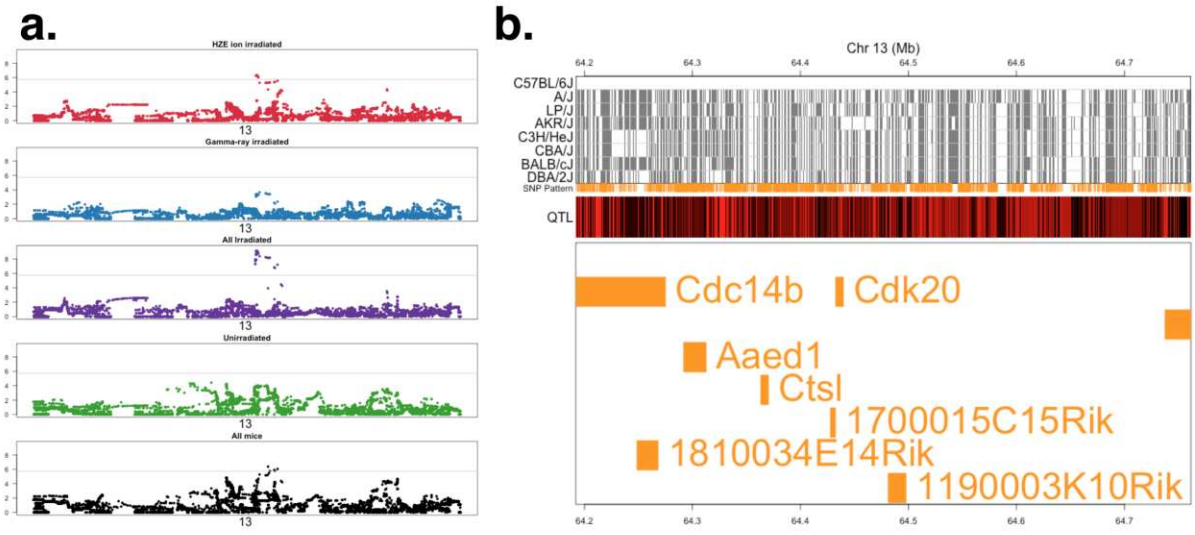

Figure 4.3: Genome wide association chromosome 13 results for cataractogenesis in HS/Npt mice.

To further investigate whether overlap is present for genomic loci controlling susceptibility to cataractogenesis in distinct exposure groups, a resample model averaging procedure was employed for each exposure group to identify a distribution of the most significant genetic loci in resampled populations. Results of these procedures for chromosome 13 are illustrated as histograms (**Figure 4.4)**, with bin sizes of 150 SNPs. Overlap in HZE ion and γ-ray irradiated mice is observable as an overrepresentation of SNPs near 64 Mb region. For the all irradiated group, nearly all resampled populations produced a SNP within 5 Mb the 64 Mb region. Mapping peak SNPs for spontaneous arising cataracts produced a wide variety of loci.

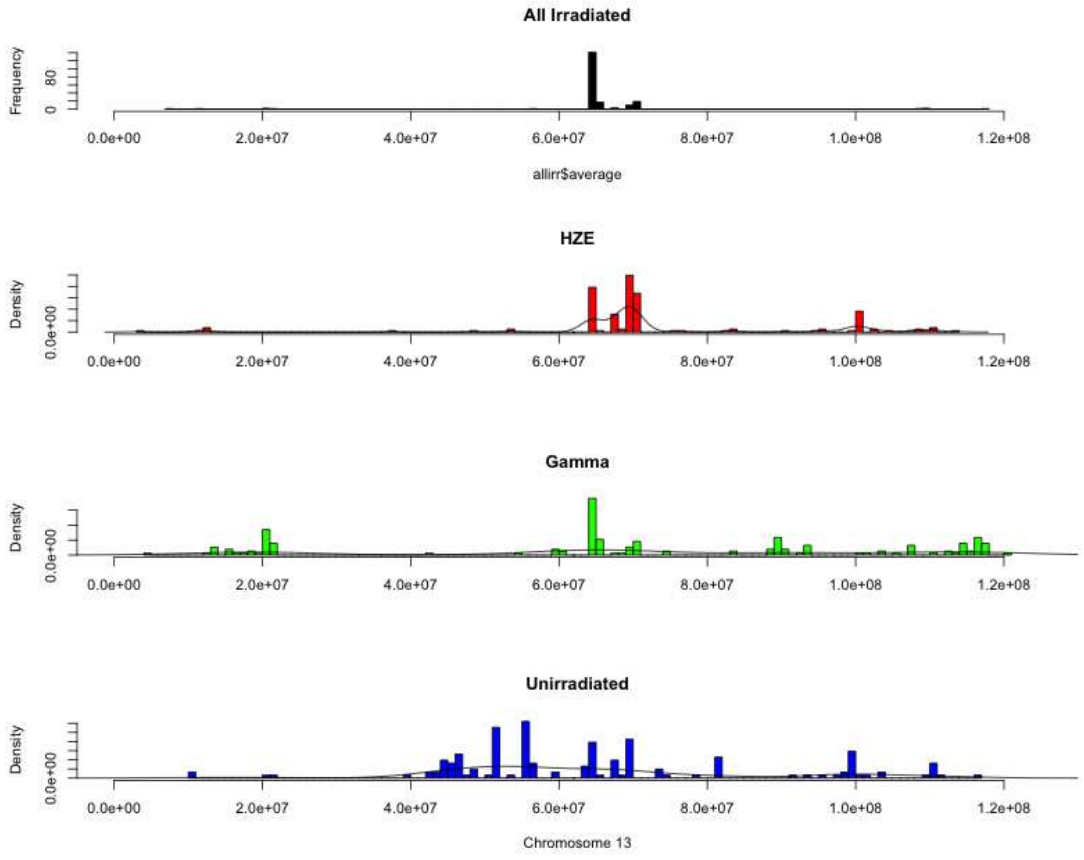

Figure 4.4: Results of QTL mapping with resample modeling averaging to determine the distribution of the genomic loci that are most significantly related to cataractogenesis for each exposure group.

DISCUSSION

The precise mechanism of radiation cataractogenesis is unclear, but genomic damage resulting in altered cell division, RNA transcription, and abnormal cell differentiation is considered to be the principal injury[56]. Populations are composed of individuals with a range in sensitivity for different radiation late effects, including the risk for cataract development[57]. In genetically diverse populations, such as humans, polymorphism and heterozygosity for genes involved in cell cycle checkpoint control, DNA damage recognition, or DNA repair may contribute to cataractogenesis susceptibility[58]. The work presented here indicates that some overlap exists for genetic susceptibility to cataracts following HZE ion and γ-ray irradiation; however, because unique QTL were identified in each radiation group—chromosome 18 QTL for HZE ion exposures and chromosome 17 QTL for γ-ray exposures—the possibility that distinct genetic polymorphisms control susceptibility for different radiation qualities exists.

Cataractogenesis following irradiation likely involves oxidative stress resulting in DNA damage, protein damage, or lipid peroxidation, however the mechanisms are not fully understood. Radiation-induced cataracts were originally thought to represent a deterministic effect; once a deterministic threshold dose is achieved cataract incidence increases as a function of increasing dose. Cataractogenesis can be the result of lens protein aggregation [59] or due to cellular pathology within the lens epithelium, lens germinal epithelium, or lens fiber cells[60,61]. In a deterministic model, cataractogenesis presumably arises following radiation-induced cell death, which requires a minimum killing dose (threshold) and severity is a consequence of the extent of cell loss. However, there is reason to believe that radiation-induced cataracts actually represent a stochastic effect, whereby no threshold exists. For stochastic phenomena, the probability of an effect within an exposed population increases with increasing dose, and any dose—no matter

how small—can increase the probability of an effect. Radiation carcinogenesis is considered stochastic as the radiation presumably increases the mutation rate in cells, leading to an increased probability of cancerous transformation. Interestingly, neoplasia of the lens has not been reported[62,63] and the lens responds to carcinogenic agents with opacification[63]. Genetic susceptibility effects are also regarded as stochastic effects.

Cataracts can be classified according to the anatomic location of opacities within the lens. Posterior subcapsular cataracts (PSC) are historically associated with radiation exposure in humans and are also induced by radiation consistently across species[41]. Following irradiation, there is an initial formation of opacities on the posterior lens capsule followed by small vacuoles and diffuse punctate opacities on the posterior lens sutures. Over time, these opacities and vacuoles coalesce into a posterior subcapsular cataract[21]. Eventually, progression of the cataract extends to the anterior subcapsular and cortical regions, resulting in vision loss. Rate of progression is shown to be affected by dose, age, environment, genetics, sex, and sex hormone while time of onset is inversely related to dose[20,23,64-69]. Cataract progression can be documented by serial slit-lamp biomicroscopy exams. The Merriam-Focht classification system that was initially described in 1962 depends on the assumption of a sequential progression to radiation cataracts. The system has been widely used by many researchers in both animal models [20,21,23,25,57,70] as well as in human populations[25,29,57,70]. Though many species have been used as animal models to study radiation cataracts, rodents have been used most commonly.

It should be noted that, of the strains that contributed to the HS/Npt population, several founder strains are predisposed to specific ocular diseases that could result in cataract development. C57BL/6J strain is known to have microphthalmia (https://www.jax.org/strain/000664), which could be associated with other ocular abnormalities.

The C3H/HeJ strain is homozygous for a retinal degeneration allele (https://www.jax.org/strain/000659), which has been associated with cataractogenesis due to toxic lenticular changes[2]. The CBA/J strain is also known for being affected by retinal degeneration as well (https://www.jax.org/strain/000656). The DBA/2J strain is known to develop pigmentary dispersion, iris atrophy, anterior synechia, and increased intraocular pressure (https://www.jax.org/strain/000671), which can be responsible for cataractogenesis[2].

Astronauts face not only acute risks during space missions, but also long-term late effects such as cancer and cataracts from exposure to space radiation. There are important differences in the energy deposition patterns between terrestrial low LET radiation (X rays or γ-rays) and high LET heavy ions in space[39]. The present study demonstrates that susceptibility to radiation-induced cataracts is highly heritable and indicates that individuals genetically predisposed to radiation-induced cataracts on Earth are also more susceptible in the space radiation environment. These results indicate that epidemiologic data from humans exposed to terrestrial radiation can be extrapolated to risk predictions in for cataractogenesis in the space radiation environment.

References

1. Harding, J. J., & Crabbe, M. J. C. (1984). The lens: development, proteins, metabolism and cataract. *The Eye, Davson, H.(Ed), 1*.
2. Gelatt, K. N., Gilger, B. C. & Kern, T. J. *Veterinary Ophthalmology*. (Wiley-Blackwell, 2013).
3. Jaffe, N. S., & Horwitz, J. H. (1992). Lens biochemistry. *Lens and cataract. Gower Medical Publishing, New York*, *4*, 1320.
4. Hejtmancik, J. F., & Piatigorsky, J. (2000). Lens proteins and their molecular biology. *Principles and practice of ophthalmology*, 1409-1428.
5. Kuszak, J. R., & Brown, H. G. (1994). Embryology and anatomy of the lens. *Principles and practice of ophthalmology: basic sciences (Edited by: Albert DM, Jakobiec FA) Philadelphia, WB Saunders Company*, 82-96.
6. Cogan, D. G., Donaldson, D. D., & Reese, A. B. (1952). Clinical and pathological characteristics of radiation cataract. *AMA archives of ophthalmology*, *47*(1), 55-70.
7. von Sallmann, L. (1957). The lens epithelium in the pathogenesis of cataract: The XIII Edward Jackson memorial lecture. *American journal of ophthalmology*, *44*(2), 159-170.
8. Worgul, B. V., Merriam Jr, G. R., Medvedovsky, C., & Brenner, D. J. (1989). Accelerated heavy particles and the lens: III. Cataract enhancement by dose fractionation. *Radiation research*, *118*(1), 93-100.
9. Lindfield, R., Kocur, I., Limburg, H., & Foster, A. (2012). Global initiative for the elimination of avoidable blindness. In *The Epidemiology Of Eye Disease* (pp. 601-606).
10. Luntz, M. H. (1992). Clinical types of cataract. *Duane's clinical ophthalmology*, *1*, 1-20.
11. Potts, A. M. (1979). Cataract—a semantic trap. In *Progress in Anterior Eye Segment Research and Practice* (pp. 229-233). Springer Netherlands.
12. Brown, N. A., Shun-Shin, G. A., Lewis, P., Cramp, W. A., Arlett, C., Cole, J., ... & Stephens, G. (1989). Relationship of cataract to radiation sensitivity. *British journal of ophthalmology*, *73*(12), 955-959.
13. Hammond, C. J., Snieder, H., Spector, T. D., & Gilbert, C. E. (2000). Genetic and environmental factors in age-related nuclear cataracts in monozygotic and dizygotic twins. *New England Journal of Medicine*, *342*(24), 1786-1790.
14. Asbell, P. A., Dualan, I., Mindel, J., Brocks, D., Ahmad, M., & Epstein, S. (2005). Age-related cataract. *The Lancet*, *365*(9459), 599-609.
15. Bendel, I., Schuettman, W., & Arndt, D. (1978). Cataract of lens as late effect of ionizing radiation in occupationally exposed persons. In *Late biological effects of ionizing radiation*.
16. Chalupecky, H. (1897). Über die Wirkung der Röntgenstrahlen auf das Auge und die Haut. *Zentralbl Prakt Augenheilk*, *21*, 234-239.
17. Desjardins, A. U. (1931). Action of roentgen rays and radium on the eye and ear. *Am. J. Roentgenol*, *26*, 639-679.
18. Bellows, J. G. (1944). *Cataract and Anomalies of the Lens*. Kimpton.
19. Lerman, S. (1962). Radiation cataractogenesis. *New York State Journal of Medicine (US)*, *62*.
20. Merriam, G. R., Szechter, A., & Focht, E. F. (1972). The Effects of Ionizing Radiations on

the Eye1. In *Radiation Effects and Tolerance, Normal Tissue* (pp. 346-385). Karger Publishers.
21. Worgul, B. V., & Rothstein, H. (1977). Mechanism of Radiocataracto-gensis. *Medikon*, *6*(6), 5.
22. Koch, H. R., & Hockwin, O. (1980). Radiation cataractogenesis. In *Radiant Energy and the Eye* (pp. 286-302). MacMillan New York, USA.
23. Kleiman, N. J., David, J., Elliston, C. D., Hopkins, K. M., Smilenov, L. B., Brenner, D. J., ... & Lieberman, H. B. (2007). Mrad9 and atm haploinsufficiency enhance spontaneous and X-ray-induced cataractogenesis in mice. *Radiation research*, *168*(5), 567-573.
24. Blakely, E. A., Kleiman, N. J., Neriishi, K., Chodick, G., Chylack, L. T., Cucinotta, F. A., ... & Kanamoto, T. (2010). Radiation cataractogenesis: epidemiology and biology. *Radiation research*, *173*(5), 709-717.
25. Worgul, B. V., Kundiyev, Y. I., Sergiyenko, N. M., Chumak, V. V., Vitte, P. M., Medvedovsky, C., ... & Shylo, S. A. (2007). Cataracts among Chernobyl clean-up workers: implications regarding permissible eye exposures. *Radiation research*, *167*(2), 233-243.
26. Cogan, D. G., Martin, S. F., & Kimura, S. J. (1949). Atom bomb cataracts. *American Association for the Advancement of Science. Science*, 654-5.
27. Abelson, P. H., & Kruger, P. G. (1949). Cyclotron-induced radiation cataracts. *American Association for the Advancement of Science. Science*, 655-7.
28. UNSCEAR, S. *Effects of Ionizing Radiation: 2000 Report to the General Assembly, with Scientific Annexes, Vol. II: Effects*. *Radiation Research* (United Nations, 2000).
29. Vano, E., Kleiman, N. J., Duran, A., Rehani, M. M., Echeverri, D., & Cabrera, M. (2010). Radiation cataract risk in interventional cardiology personnel. *Radiation research*, *174*(4), 490-495.
30. Miller, D. L., Vañó, E., Bartal, G., Balter, S., Dixon, R., Padovani, R., ... & De Baère, T. (2010). Occupational radiation protection in interventional radiology: a joint guideline of the Cardiovascular and Interventional Radiology Society of Europe and the Society of Interventional Radiology. *Cardiovascular and interventional radiology*, *33*(2), 230-239.
31. Rehani, M. M., Ciraj-Bjelac, O., Al-Naemi, H. M., Al-Suwaidi, J. S., El-Nachef, L., Khosravi, H. R., ... & Shaaban, M. (2012). Radiation protection of patients in diagnostic and interventional radiology in Asian countries: Impact of an IAEA project. *European journal of radiology*, *81*(10), e982-e989.
32. Klein, B. E., Klein, R., Linton, K. L., & Franke, T. (1993). Diagnostic x-ray exposure and lens opacities: the Beaver Dam Eye Study. *American journal of public health*, *83*(4), 588-590.
33. Merriam, G. R., & Focht, E. F. (1957). A clinical study of radiation cataracts and the relationship to dose. *Am. J. Roentgenol. Radium Therapy Nuclear Medicine*, *77*.
34. Merriam, G. R., Szechter, A., & Focht, E. F. (1972). The Effects of Ionizing Radiations on the Eye1. In *Radiation Effects and Tolerance, Normal Tissue* (pp. 346-385). Karger Publishers.
35. Henk, J. M., Whitelocke, R. A. F., Warrington, A. P., & Bessell, E. M. (1993). Radiation dose to the lens and cataract formation. *International Journal of Radiation Oncology* Biology* Physics*, *25*(5), 815-820.
36. Britten, M. J. A., Halnan, K. E., & Meredith, W. J. (1966). Radiation cataract—new evidence on radiation dosage to the lens. *The British journal of radiology*, *39*(464), 612-

617.
37. Morita, K., & Kawabe, Y. (1979). Late Effects on the Eye of Conformation Radiotherapy for Carcinoma of the Paranasal Sinuses and Nasal Cavity 1. *Radiology*, *130*(1), 227-232.
38. Calissendorff, B., Bolme, P., & El Azazi, M. (1991). The development of cataract in children as a late side-effect of bone marrow transplantation. *Bone marrow transplantation*, *7*(6), 427-429.
39. Cucinotta, F. A., Manuel, F. K., Jones, J., Iszard, G., Murrey, J., Djojonegro, B., & Wear, M. (2001). Space radiation and cataracts in astronauts. *Radiation research*, *156*(5), 460-466.
40. Chylack Jr, L. T., Peterson, L. E., Feiveson, A. H., Wear, M. L., Manuel, F. K., Tung, W. H., ... & Cucinotta, F. A. (2009). NASA study of cataract in astronauts (NASCA). Report 1: Cross-sectional study of the relationship of exposure to space radiation and risk of lens opacity. *Radiation research*, *172*(1), 10-20.
41. Blakely, E. A. (2012). Lauriston S. Taylor Lecture on Radiation Protection and Measurements: What Makes Particle Radiation so Effective?. *Health physics*, *103*(5), 508.
42. Choshi, K., Takaku, I., Mishima, H., Takase, T., Neriishi, S., Finch, S. C., & Otake, M. (1983). Ophthalmologic changes related to radiation exposure and age in adult health study sample, Hiroshima and Nagasaki. *Radiation research*, *96*(3), 560-579.
43. Junk, A. K., Kundiev, Y., & Vitte, P. (1998). *Ocular radiation risk assessment in populations exposed to environmental radiation contamination* (Vol. 50). Springer Science & Business Media.
44. Otake, M., & Schull, W. J. (1982). The relationship of gamma and neutron radiation to posterior lenticular opacities among atomic bomb survivors in Hiroshima and Nagasaki. *Radiation research*, *92*(3), 574-595.
45. Vennart, J. (1991). The 1990 Recommendations of the International Commission on Radiological Protection. *Journal of Radiological Protection*, *11*(3), 199.
46. ICORPCORE *Radiosensitivity and spatial distribution of dose*. (Annals of the ICRP, 1969).
47. ICORPCORE *Recommendations of the International Commission on Radiological Protection*. (Annals of the ICRP, 1977).
48. Wilde, G., & Sjöstrand, J. (1997). A clinical study of radiation cataract formation in adult life following γ irradiation of the lens in early childhood. *British journal of ophthalmology*, *81*(4), 261-266.
49. Joseph, J. A., Hunt, W. A., Rabin, B. M., & Dalton, T. K. (1992). Possible" Accelerated Striatal Aging" Induced by Heavy-Particle Irradiation: Implications for Manned Space Flights. *Radiation research*, *130*(1), 88-93.
50. Worgul, B. V., Smilenov, L., Brenner, D. J., Vazquez, M., & Hall, E. J. (2005). Mice heterozygous for the ATM gene are more sensitive to both X-ray and heavy ion exposure than are wildtypes. *Advances in Space Research*, *35*(2), 254-259.
51. Worgul, B. V., Smilenov, L., Brenner, D. J., Junk, A., Zhou, W., & Hall, E. J. (2002). Atm heterozygous mice are more sensitive to radiation-induced cataracts than are their wild-type counterparts. *Proceedings of the National Academy of Sciences*, *99*(15), 9836-9839.
52. Hall, E. J., Brenner, D. J., Worgul, B., & Smilenov, L. (2005). Genetic susceptibility to radiation. *Advances in Space Research*, *35*(2), 249-253.
53. Demarest, K., McCaughran, J., Mahjubi, E., Cipp, L., & Hitzemann, R. (1999). Identification of an acute ethanol response quantitative trait locus on mouse chromosome

2. *The Journal of neuroscience*, *19*(2), 549-561.
54. Gatti, D. M., Svenson, K. L., Shabalin, A., Wu, L. Y., Valdar, W., Simecek, P., ... & Chesler, E. J. (2014). Quantitative trait locus mapping methods for diversity outbred mice. *G3: Genes| Genomes| Genetics*, *4*(9), 1623-1633.
55. Weil, M. M., Ray, F. A., Genik, P. C., Yu, Y., McCarthy, M., Fallgren, C. M., & Ullrich, R. L. (2014). Effects of 28 Si ions, 56 Fe ions, and protons on the induction of murine acute myeloid leukemia and hepatocellular carcinoma. *PloS one*, *9*(8), e104819.
56. Huff, J., Carnell, L., Blattnig, S., Chappell, L., Kerry, G., Lumpkins, S., ... & Werneth, C. (2016). Evidence Report: Risk of Radiation Carcinogenesis.
57. Rehani, M. M., Vano, E., Ciraj-Bjelac, O., & Kleiman, N. J. (2011). Radiation and cataract. *Radiation protection dosimetry*, *147*(1-2), 300-304.
58. ICRP, I. (2012). Statement on tissue reactions/Early and late effects of radiation in normal tissues and organs–threshold doses for tissue reactions in a radiation protection context. *ICRP Publication*, *118*, 1-2.
59. Benedek, G. B. (1997). Cataract as a protein condensation disease: the Proctor Lecture. *Investigative ophthalmology & visual science*, *38*(10), 1911-1921.
60. Lovicu, F. J., Ang, S., Chorazyczewska, M., & McAvoy, J. W. (2005). Deregulation of lens epithelial cell proliferation and differentiation during the development of TGFβ-induced anterior subcapsular cataract. *Developmental neuroscience*, *26*(5-6), 446-455.
61. Benedek, G. B. (1971). Theory of transparency of the eye. *Applied optics*, *10*(3), 459-473.
62. Kleinstein, R. N., & Lehman, H. F. (1977). Incidence and Prevalence of Eye Cancer*. *Optometry & Vision Science*, *54*(1), 49-51.
63. World Cancer Report 2014. 1–632 (2013).
64. Merriam Jr, G. R., & Focht, E. F. (1962). A clinical and experimental study of the effect of single and divided doses of radiation on cataract production. *Transactions of the American Ophthalmological Society*, *60*, 35.
65. Merriam Jr, G. R., & Szechter, A. (1973). The effect of age on the radiosensitivity of rat lenses. *Transactions of the American Ophthalmological Society*, *71*, 88.
66. Kelly, S. P., Thornton, J., Edwards, R., Sahu, A., & Harrison, R. (2005). Smoking and cataract: review of causal association. *Journal of Cataract & Refractive Surgery*, *31*(12), 2395-2404.
67. Taylor, H. R. (1989). THE BIOLOGICAL EFFECTS OF UV- B ON THE EYE. *Photochemistry and photobiology*, *50*(4), 489-492.
68. Schein, O. D., West, S., Munoz, B., Vitale, S., Maguire, M., Taylor, H. R., & Bressler, N. M. (1994). Cortical lenticular opacification: distribution and location in a longitudinal study. *Investigative ophthalmology & visual science*, *35*(2), 363-366.
69. Dynlacht, J. R. (2013). The role of age, sex and steroid sex hormones in radiation cataractogenesis. *Radiation research*, *180*(6), 559-566.
70. Ciraj- Bjelac, O., Rehani, M. M., Sim, K. H., Liew, H. B., Vano, E., & Kleiman, N. J. (2010). Risk for radiation- induced cataract for staff in interventional cardiology: Is there reason for concern?. *Catheterization and Cardiovascular Interventions*, *76*(6), 826-834.

Chapter Five

Determining Dose Rate Effects on Carcinogenesis: Differences in the Tumor Spectrum Following Single or Fractionated Radiation Exposures

SUMMARY

In this study, we demonstrate that repeated 2-Gy fractions of γ-ray radiation more commonly produce neoplasms arising from endothelial or osteocyte precursors, in contrast to single large-dose exposures, which more commonly produce fibrosarcomas or malignant fibrous histiocytomas. There is a general lack of *in vivo* data describing differences in second cancer histotype, incidence, and latency after fractionated irradiation in comparison with single large-dose exposures. These results indicate that different cell types respond differently to radiation, depending on delivery schedule.

To investigate differences in tumor histotype, incidence, latency, and strain susceptibility in mice exposed to single-dose or clinically relevant, fractioned-dose γ-ray radiation, C3Hf/Kam and C57BL/6J mice were locally irradiated to the right hindlimb with either single large doses between 10 and 70 Gy or fractionated doses totaling 40 to 80 Gy delivered at 2-Gy/d fractions, 5 d/wk, for 4 to 8 weeks. The mice were closely evaluated for tumor development in the irradiated field for 800 days after irradiation, and all tumors were characterized histologically.

A total of 210 tumors were induced within the radiation field in 788 mice. An overall decrease in tumor incidence was observed after fractionated irradiation (16.4%) in comparison with single-dose irradiation (36.1%). Sarcomas were the pre- dominant postirradiation tumor observed (n = 201), with carcinomas occurring less frequently (n = 9). The proportion of mice

developing tumors increased significantly with total dose for both single-dose and fractionated schedules, and latencies were significantly decreased in mice exposed to larger total doses. C3Hf/Kam mice were more susceptible to tumor induction than C57BL/6J mice after single-dose irradiation; however, significant differences in tumor susceptibilities after fractionated radiation were not observed. For both strains of mice, osteosarcomas and hemangiosarcomas were significantly more common after fractionated irradiation, whereas fibrosarcomas and malignant fibrous histiocytomas were significantly more common after single- dose irradiation.

This study investigated the tumorigenic effect of acute large doses in comparison with fractionated radiation in which both the dose and delivery schedule were similar to those used in clinical radiation therapy. Differences in tumor histotype after single-dose or fractionated radiation exposures provide novel in vivo evidence for differences in tumor susceptibility among stromal cell populations.

INTRODUCTION

Inbred mouse strains differ in their susceptibilities to various radiogenic tumors, including thymic lymphoma, myeloid leukemia, mammary tumors, pulmonary adenocarcinoma, hepatocellular carcinoma, and osteosarcoma[1-9]. The strain differences in susceptibilities are thought to be due to the differing genetic backgrounds of the strains, and in some cases specific genetic polymorphisms have been identified that may be responsible[7,10-13]. Most of these studies on strain differences involve single, acute, whole-body exposures, although there are exceptions such as the use of internal emitters in the study of osteosarcoma and the use of dose fractionation to induce thymic lymphomas. The total doses in most, but not all, studies are 3 Gy or less. To the best of our knowledge, research into mouse strain and tumor histotype differences involving

fractionated exposures to high total doses, similar to those experienced by radiation therapy patients, have not been reported.

Here we report on tumorigenesis in 2 inbred murine strains, C3Hf/Kam and C57BL/6J, exposed to single-dose or fractionated irradiation of γ-rays up to 70 or 80 Gy delivered to a hindlimb.

METHODS

Mice

C57BL/6J and C3Hf/Kam male mice, bred and maintained in the Experimental Radiation Oncology specific-pathogen- free mouse colony, were 3 to 4 months old at the beginning of experiments. The mice, housed 5 per cage, were exposed to 12-hour light/dark cycles and given free access to sterilized pelleted food (Prolab Animal Diet; Purina, Indianapolis, IN) and sterilized water. The facilities were approved by the Association for Assessment and Accreditation of Laboratory Animal Care and in accordance with current regulations of the US Department of Agriculture and Department of Health and Human Services, and the experimental protocol was approved by and in accordance with guidelines established by the University of Texas MD Anderson Cancer Center Institutional Animal Care and Use Committee.

Irradiation

A preclinical model consisting of development of solid tumors in the limbs of C3H mice exposed locally to ionizing radiation was used to study radiation-induced tumorigenesis[14-17]. Right hindlimbs of mice were exposed to local irradiation in air with single doses of γ-rays ranging from 10 to 70 Gy, or with 2-Gy fractions given daily for 5 days per week for a total of

40, 50, 60, 70, and 80 Gy. For single-dose radiation, mice were grouped for analysis according to exposures as follows: 10 to 29 Gy, 30 to 39 Gy, 40 to 49 Gy, 50 to 59 Gy, and 60 to 70 Gy, as detailed in **Table E1** (available at www.redjournal.org). Only C3Hf/Kam mice were exposed to single-dose radiation from 60 to 70 Gy, therefore the results from this dose range were not included in the statistical analysis comparing tumor incidence be- tween strains. Radiation was delivered from a small-animal irradiator with 2 parallel-opposed ^{137}Cs sources at a dose rate of 6.4 to 8 Gy/min. During irradiation, unanesthetized mice were immobilized in a jig, and the right rear thigh was centered in a circular radiation field 3 cm in diameter.

Assessment of hindlimb tumors

Mice were observed for development of tumors in the irradiated limbs at 2-week intervals until 800 days after irradiation. Tumor incidence was defined as the proportion of mice developing hindlimb tumors out of the total number of mice receiving a given dose of radiation. All tumors were analyzed histologically by a veterinary pathologist (blinded to treatment and mouse strain) using 5-mm sections from formalin-fixed, paraffin-embedded tissues routinely processed and stained with hematoxylin and eosin. Osteosarcomas were characterized as tumors composed of malignant mesenchymal cells associated with brightly eosinophilic, fibrillar to homogeneous, tumor osteoid matrix (**Figure 5.1A**). Hemangiosarcomas were composed of atypical, plump endothelial cells forming irregularly anastomosing vascular spaces containing erythrocytes (**Fig. 5.1B**). Fibrosarcomas were composed of spindle-shaped cells separated by variable amounts of lightly eosinophilic collagenous stroma; spindle- shaped cells were arranged in interweaving fascicles forming a characteristic herringbone pattern (**Fig. 5.1C**). Malignant fibrous histiocytomas were pleomorphic with fusiform to rounded cells and typically contained

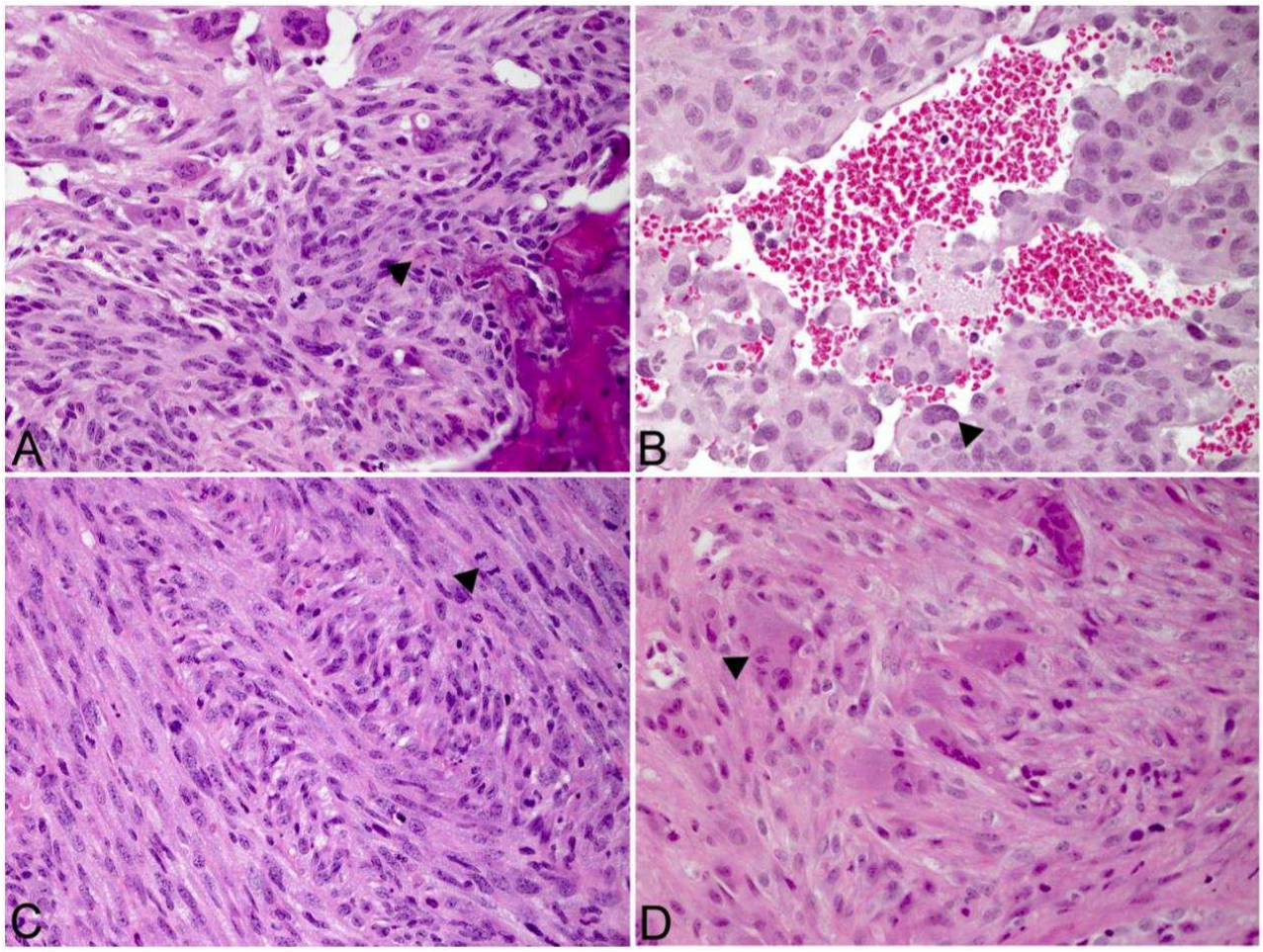

Figure 5.1: Representative tumor histopathology, hematoxylin and eosin. (A) Osteosarcoma. Neoplastic osteocytes surround and are encased in brightly eosinophilic tumor osteoid (arrowhead), which progressively transitions to immature woven bone. Multinucleated osteoclasts are scattered throughout the tumor. (B) Hemangiosarcoma. Atypical endothelial cells form irregularly anastomosing vascular channels containing erythrocytes, and nuclei of neoplastic cells often bulge into vascular channels (arrowhead). (C) Fibrosarcoma. Neoplastic spindle cells are arranged in fascicles that interweave to form a herringbone pattern. Cells are separated by variable amounts of lightly eosinophilic, collagenous stroma, and mitotic figures are common (arrowhead). (D) Malignant fibrous histiocytoma. Pleomorphic cells with fibroblastic and histiocytic differentiation are separated by sparse eosinophilic, collagenous stroma. Moderate to marked anisocytosis and anisokaryosis is observed, and multinucleated giant cells are frequent (arrowhead).

numerous multinucleated giant cells (**Fig. 5.1D**). Representative histopathology for additional tumor histotypes can be found in **Figures E1 and E2** (available online at www.redjournal.org).

Sarcomas lacking diagnostic features of the previously mentioned subtypes were assigned the diagnosis of undifferentiated sarcoma.

Statistical analysis

Comparisons were made between tumor histotype, radiation dosing schedule, tumor-free survival times, tumor latencies, and mouse strain. Chi-squared tests were used to compare categorical variables. Logistic regression was used to compare proportions of tumors induced by increasing doses for single-dose or fractionated radiation. Kaplan-Meier survival analyses were used to determine differences in tumor-specific survival between strains and differences in tumor-specific survival between tumor histotypes and radiation delivery. Tumor latencies between mouse strains, radiation dose groups, and tumor histotypes were compared using analysis of variance. Statistical analyses were per- formed using STATA software (version 11.2; StataCorp, College Station, TX) and Graphpad Prism (version 6.0d; GraphPad Software, La Jolla, CA). All values were considered significant at $P < 0.05$.

RESULTS

Tumor incidence

After single-dose exposures between 10 and 70 Gy, 163 of 451 mice (36.1%) developed hindlimb tumors. Tumor incidences showed a similar increase for each increasing dose group when combining C3Hf/Kam and C57BL/6J mice (**Figure 2A**; $P < 0.001$). Single-dose exposures were significantly more effective at inducing hindlimb tumors in comparison with similar total doses received in 2-Gy fractions ($P < 0.001$). For hindlimbs irradiated with fractionated exposures, 55 tumors were induced in 335 mice (16.4%). The 5 fractionated dosing groups each

showed a consecutive increase in tumor incidence with increasing dose (**Figure 5.2A**), to culminate in a 38% tumor incidence for the 80-Gy group. Over the dose ranges investigated for single-dose irradiation, increases in tumor incidences were observed up to 50 Gy for C57BL/6J mice and up to 60 Gy for C3Hf/Kam mice, with evidence of a plateau in the dose response for larger doses (**Figure 2B**). Over the dose ranges investigated for fractionated irradiation, no evidence for a plateau in the dose response was observed (**Figure 5.2 A, B**).

Tumor latency

Latency was defined as the number of days between the date of irradiation and tumor development. For fractionated irradiation, the day of the final fraction was defined as day 0. For single-dose irradiation, the first tumors appeared at 216 days after irradiation for C3Hf/KAM and at 348 days for C57BL/6J. For fractionated irradiation, the first tumors appeared at 256 days after the last fraction for C3Hf/KAM and at 384 days for C57BL/6J. A decrease in latency was observed with increasing dose for both single-dose (**Figure 5.3A**; P = 0.024) and fractionated dosing schedules (**Figure 5.3B**; P = 0.026). After single-dose irradiation, the mean tumor latency time for C3Hf/Kam mice was significantly decreased compared with C57BL/6J mice (**Figure 5.4A**; P = 0.002); no significant difference in latency was observed between the 2 strains after fractionated radiation (**Figure 5.4B**; P = 0.858). The latencies for different sarcoma histotypes were not significantly different (**Figure 5.5A, B**); however, the latency for carcinomas was significantly prolonged in comparison with the latencies for sarcomas as a group (**Figure E3**).

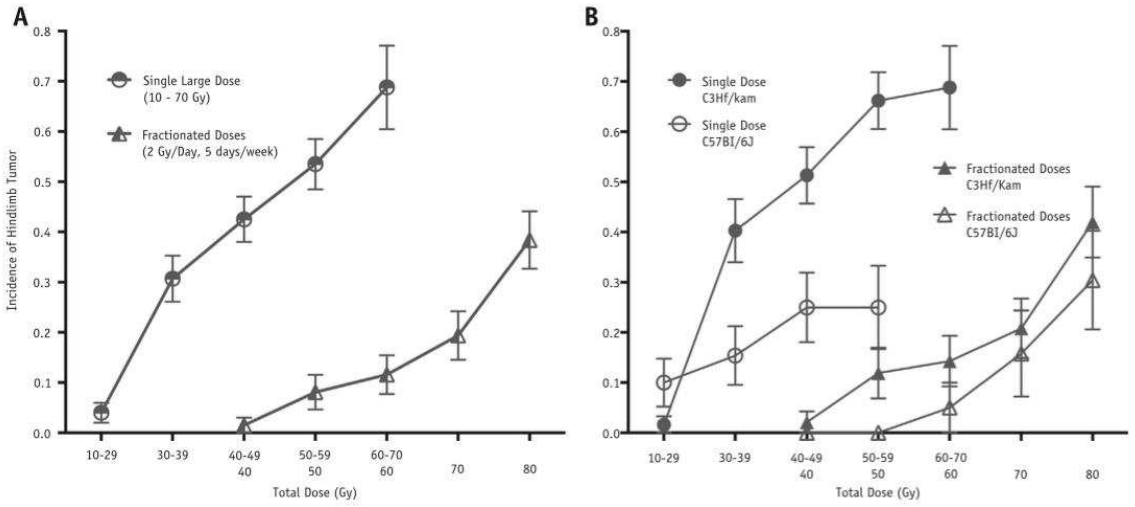

Figure 5.2: Incidence of hindlimb tumors by radiation dose. (A) Incidences of hindlimb tumors are significantly increased in mice exposed to a single large dose of radiation in comparison with mice exposed to fractionated radiation ($P < 0.001$). (B) Incidences of hindlimb tumors by radiation dose and mouse strain. C3Hf/Kam mice have a significantly higher incidence of hindlimb tumors after single-dose exposures than C57BL/6J mice ($P < 0.001$). No significant difference in tumor incidence is observed between C3Hf/Kam and C57BL/6J mice after fractionated exposures. Single doses are grouped as 10 to 29, 30 to 39, 40 to 49, and 50 to 59 Gy. Fractionated doses were given as 2 Gy/d, 5 d/wk for 4 to 8 weeks and are listed as total doses of 40, 50, 60, 70, and 80 Gy.

Tumor histotype

All 210 tumors observed were categorized histologically, as summarized in Table 1. After fractionated exposures, both C57BL/6J and C3Hf/Kam mice were more likely to develop osteosarcoma ($P < 0.001$) and hemangiosarcomas ($P < 0.001$) than other tumor types (**Figure 5.5C**). Of the tumors produced by fractionated radiation, 63% were osteosarcoma or hemangiosarcoma; in comparison, these tumor types constituted only 8% of all tumors after single-dose exposures. The most common tumors induced by single- dose radiation were fibrosarcoma and malignant fibrous histiocytoma, each of which was significantly more common after single-dose irradiation ($P < 0.001$). Fibrosarcomas and malignant fibrous histiocytomas constituted 59% of the tumors after single-dose exposures, in comparison with 7% after

fractionated exposures. Additionally, squamous cell carcinomas were more commonly observed in mice given 2-Gy fractions than in mice given single large doses (P = 0.036).

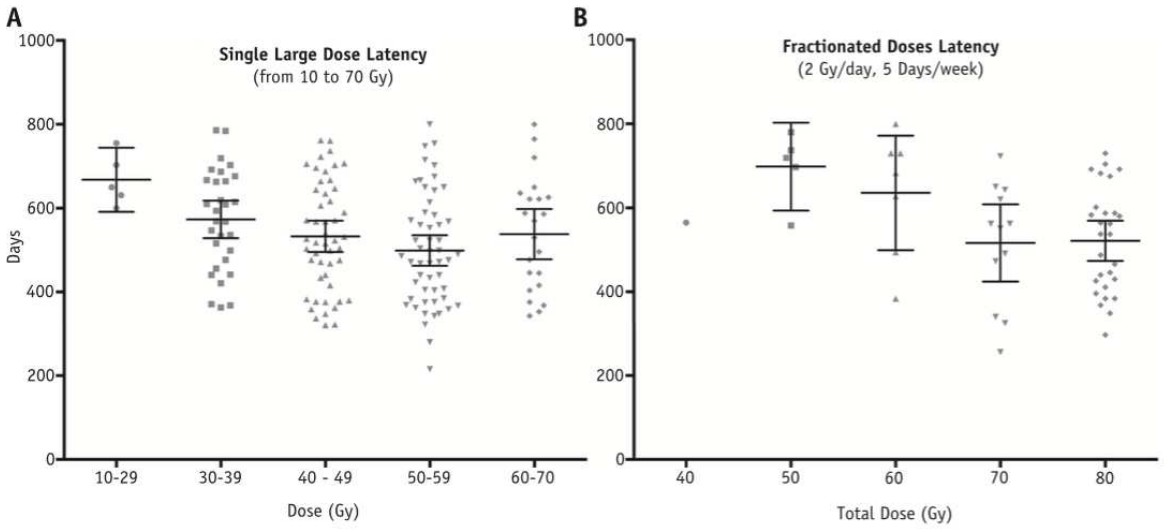

Figure 5.3: Decreasing tumor latencies with increasing dose after (A) single exposures of 10 to 70 Gy or (B) fractionated exposure of 2 Gy/day fractions given 5 days/week for 4 to 8 weeks. Mice receiving higher total single doses have significantly decreased tumor latencies (*P* = 0.024), measured as the number of days between irradiation and tumor development. Mice receiving higher total fractionated doses also have significantly decreased tumor latencies (*P* = 0.026).

Strain susceptibility

After single-dose exposure, significant differences in tumor incidences (**Figure 5.2B**; P < 0.001) and tumor latencies (**Figure 4A**; P = 0.002) were observed between C3Hf/Kam and C57BL/ 6J mice. For fractionated exposures, tumor incidences and latencies were similarly increased and decreased, respectively; however, these changes were not statistically significant (**Figure 2B and 4B**). For both strains of mice, osteosarcomas and hemangiosarcomas were significantly more common after fractionated irradiation, whereas fibrosarcomas and malignant fibrous histiocytomas were significantly more common after single-dose irradiation.

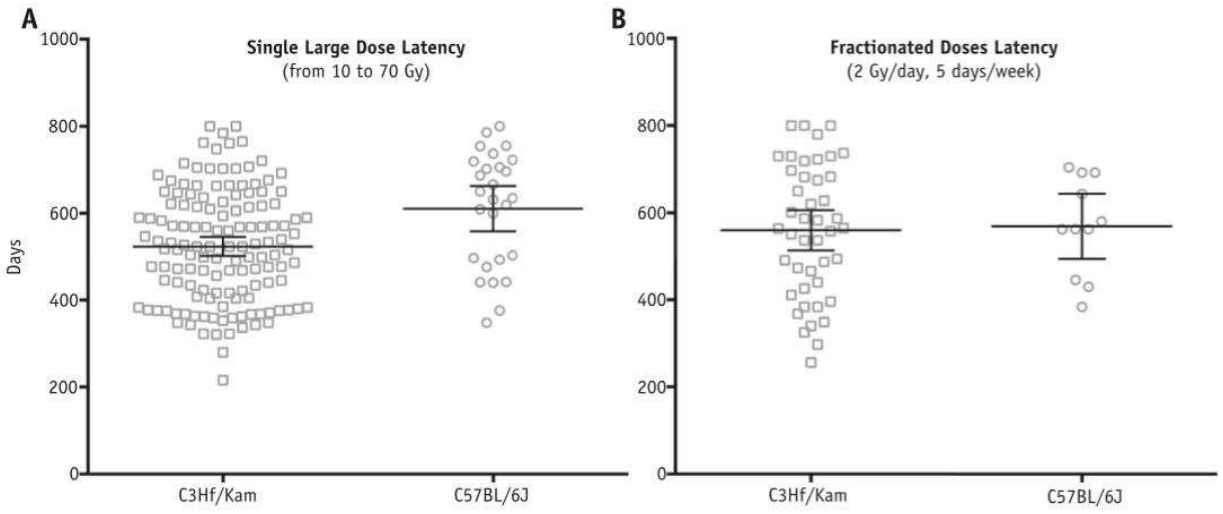

Figure 5.4: Tumor latencies after (A) single exposures of 10 to 70 Gy or (B) fractionated exposure of 2-Gy/d fractions given 5 d/wk for 4 to 8 weeks separated by mouse strain (C3Hf/Kam or C57BL/6J). C3Hf/Kam mice have significantly decreased tumor latencies in comparison with C57BL/6J mice after single-dose exposures (P = .002) but not after fractionated exposures (P = 0.858).

DISCUSSION

In this study we demonstrate that repeated 2-Gy fractions more commonly produce neoplasms arising from endothelial or osteocyte precursors, in contrast to single large-dose exposures, which more commonly produce fibrosarcomas or malignant fibrous histiocytomas. Differences in tumor histotypes after single-dose and fractionated radiation exposures provide novel in vivo evidence for variability in susceptibility amongst stromal cell populations. Investigations into the cell of origin for sarcomas have identified progenitor cells for the development of specific sarcoma subtypes[18,19]; our work suggests that certain histotype-specific progenitor cells may have differential susceptibilities to the late effects of radiation based on dose fractionation.

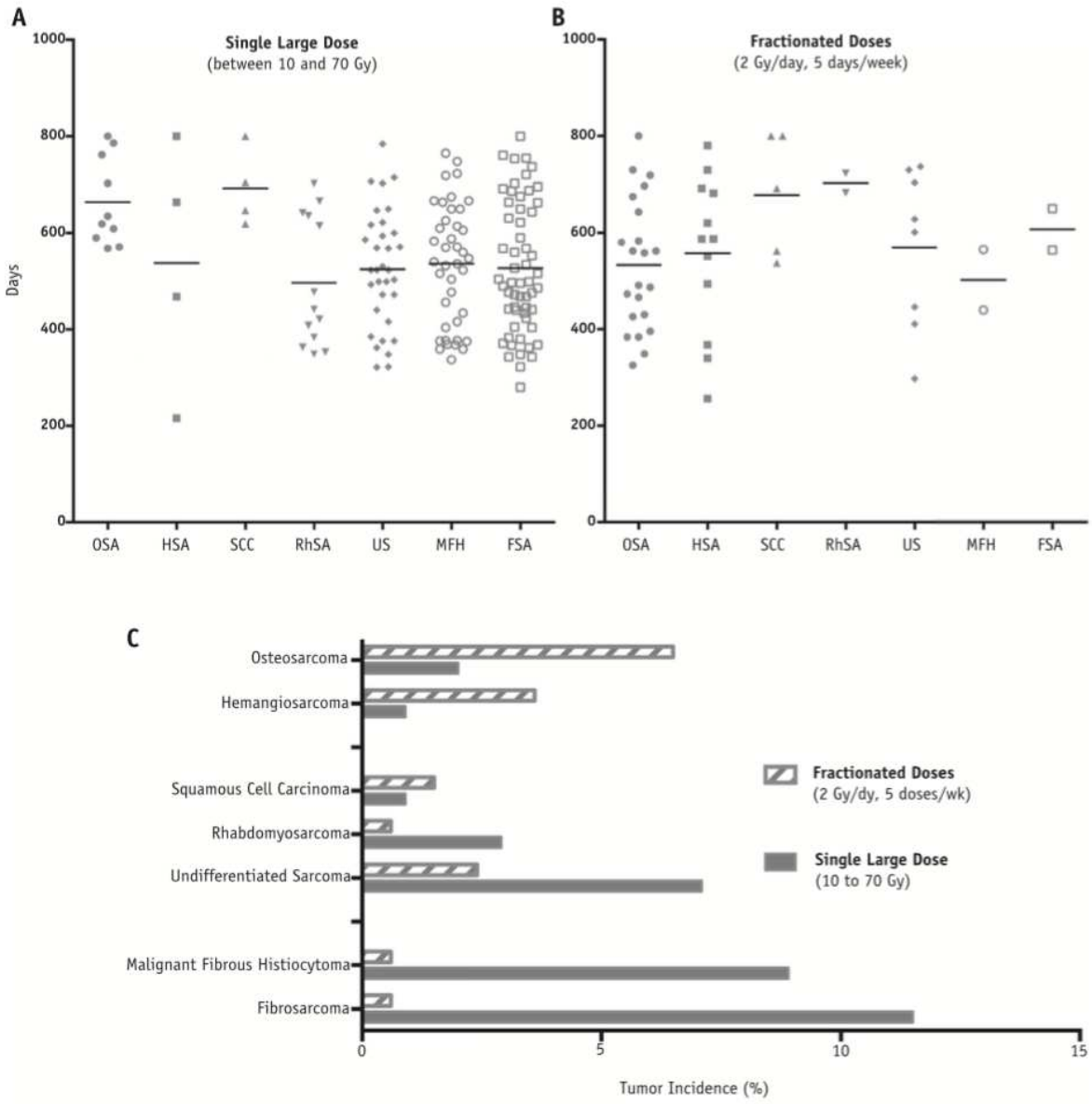

Figure 5.5: Tumor histotypes arising in locally γ-irradiated hindlimbs compared by dose schedule. Latency of tumors separated by histotype after (A) single exposures of 10 to 70 Gy or (B) fractionated exposures of 2-Gy/d fractions given 5 d/wk for 4 to 8 weeks and (C) tumor incidences separated by dose scheduling. Osteosarcomas (P<.001), hemangiosarcomas (P<.001), and squamous cell carcinomas (P=.036) were significantly more common after fractionated irradiation, whereas fibrosarcomas (P<.001) and malignant fibrous histiocytomas (P<.001) were significantly more common after single large-dose irradiation. FSA = fibrosarcoma; HAS = hemangiosarcoma; MFH = malignant fibrous histiocytoma; OSA = osteosarcoma; RhSA = rhabdomyosarcoma; SCC = squamous cell carcinoma; US = undifferentiated sarcoma.

Table 5.1: Histology of γ-irradiation–induced tumors of the hindlimbs of locally irradiated mice, separated by radiation dose scheduling

Table 1 Histology of γ-irradiation—induced tumors of the hindlimbs of locally irradiated mice, separated by radiation dose scheduling

Histologic diagnosis	Multifractionated dose	Single dose	χ^2 *P*
Osteosarcoma	22	9	<.001
Hemangiosarcoma	12	4	<.001
Squamous cell carcinoma	5	4	.036
Myxosarcoma	1	1	.430
Rhabdomyosarcoma	2	13	.255
Undifferentiated sarcoma	8	32	.358
Carcinosarcoma	0	1	-
Malignant fibrous histiocytoma	2	40	<.001
Fibrosarcoma	2	52	<.001
Mice developing tumors	54	156	<.001
Total no. of mice	337	452	
C3Hf/Kam	236	304	
C57BL/6J	101	148	

Values are n. Multifractionated dose given as 2-Gy/d fractions, 5 d/wk for 4 to 8 weeks. Single-dose irradiation includes acute doses from 10 to 70 Gy. All doses used in each radiation dose schedule are included.

Sarcomas were one of the original solid tumors to be associated with radiation therapy in the 1920s[20,21] and continue to be a rare but highly fatal hazard of modern radiation therapy[22]. Conventionally, radiation therapy is delivered as 2- to 2.5-Gy fractions (Monday-Friday) for 1 to 7 weeks[23], which is similar to the fractionation schedule used in our study (2 Gy/d, 5 d/wk, for 4-8 weeks). Radiation fractionation is thought to increase the efficacy of tumor cell killing by increasing the number of tumor cells irradiated during radiosensitive phases of the cell cycle and by allowing tumor reoxygenation between each fraction, which increases the accumulated non-

repairable damage in tumor cells per unit dose[24,25]. Fractionated radiation therapy also has the advantage of allowing non-neoplastic cells time to repair[24,25]; however, accumulated damage to non-targeted cells may lead to a second primary neoplasm. In addition, the protracted time period between fractionated doses allows for the replenishment of radiation-depleted cells, including potential target cells for neoplastic transformation, thereby expanding the number of cells at risk. Because of the increased success of cancer therapies, increasing numbers of cancer survivors are at risk for developing second primary malignancies within radiation treatment fields, which include post-irradiation sarcomas[22]. However, uncertainties surrounding post-irradiation sarcomas exist owing to their relative rarity. These uncertainties include the variation in risk by sarcoma histotype, the shape of the dose response curve, and potential genetic susceptibility.

In the present study, osteosarcomas and hemangiosarcomas were significantly more common after clinically relevant fractionated radiation, whereas fibrosarcomas and malignant fibrous histiocytomas were significantly more common after single large doses of radiation. These results are consistent with previous studies in which mice exposed to single or hypofractionated large doses of γ-rays were most commonly diagnosed with fibrosarcomas and malignant fibrous histiocytomas[26,27]. Potential explanations for the observed differences in tumor cell-of-origin after fractionated or single-dose irradiation include: (1) differential cell type susceptibility to apoptosis, necrosis, or senescence after irradiation; (2) differential cell type repair capabilities; (3) differential post-irradiation immune- modulatory effects on different cell types; or (4) differential cell type responses to growth factors, cytokines, or hormones after fractionated or single-dose irradiation. In vitro, changes in transcription in normal human coronary artery endothelial cells exposed to single-dose or fractionated radiation have been examined[28,29]. Palayoor et al.[29] demonstrated that exposure of endothelial cell cultures to 5 2-Gy

fractions resulted in robust transcriptional changes in comparison with a single 10-Gy dose. Genes regulating cell cycle, DNA replication, DNA damage stimulus, DNA repair, and genes related to immune response were significantly altered after exposure to fractionated radiation in comparison with single-dose radiation[29].

Similar to the mice in this study, tumor histotypes arising in humans exposed to fractionated radiation are commonly osteosarcoma and angiosarcoma (angiosarcoma is a category that includes hemangiosarcoma and lymphangiosarcoma). Studies of childhood post-irradiation sarcomas reveal that the most frequent second solid cancer occurring in children treated with radiation therapy is osteosarcoma[30]. In adult breast cancer patients treated with fractionated radiation therapy (2 Gy/d, 5 weekly fractions) with median doses of 50-55 Gy, the most common tumor was angiosarcoma, followed by undifferentiated sarcoma and osteosarcoma[31].

In our study the risk of post-irradiation sarcoma after clinically relevant fractionated exposures increased with total doses up to 80 Gy, with no evidence of a plateau. Similarly, in humans, studies of childhood post-irradiation sarcomas provide clear evidence of increased risks with no evidence of a decrease in slope with doses up to 60 Gy[30,32,33]. For breast cancer patients in adulthood, increased risk of post-irradiation sarcomas is also associated with increasing dose[34]. After single-dose irradiation, evidence of a plateau in tumor incidence was observed at doses higher than 50 Gy for C57BL/6J mice and at doses higher than 60 Gy for C3Hf/Kam mice. The risk of developing sarcomas is influenced by genetic susceptibility in humans and mice; however, only a few specific examples of a genetic susceptibility to radiation-related sarcomas are present in the literature[13,35,36]. Susceptibility to radiation-induced osteosarcoma has been associated with a common promoter variant in Rb1 in mice[13]. In humans treated for

retinoblastoma with radiation therapy, there is an increased risk of sarcomas in the radiation field[35,36]. Additional evidence for genetic susceptibility to sarcoma can be observed in the differential solid object tumorigenesis in different strains of mice, in which there is a marked difference in tumorigenesis after implanted foreign bodies[37]. Genetic susceptibility to radiation-induced sarcoma in mice was revealed in the present study as an increased incidence and decreased latencies of post-irradiation sarcomas in the C3Hf/Kam strain compared with C57BL/6 after single-dose irradiation. No significant differences were observed between these 2 strains after fractionated irradiation; however, fewer tumors and different histotypes were induced after fractionated exposures, which decreased the power of the statistical analysis; and although not significant, the incidences of tumors were similarly increased in C3Hf/Kam mice compared with C57BL/6 mice (Figure 1B).

Conclusions

Osteosarcoma, hemangiosarcoma, and squamous cell carcinoma are significantly more common in mice after exposure to radiation in fractions of 2 Gy/d. In contrast, fibrosarcomas and malignant fibrous histiocytomas are significantly more common after single large doses of radiation (10-70 Gy). Genetic susceptibility to radiation- induced sarcomas was observed as a difference in tumor incidences and latencies between C3Hf/Kam and C57BL/ 6J mice.

References

1. Kaplan, H. S., Hirsch, B. B., & Brown, M. B. (1956). Indirect Induction of Lymphomas in Irradiated Mice IV. Genetic Evidence of the Origin of the Tumor Cells from the Thymic Grafts. *Cancer Research*, *16*(5), 434-436.
2. Storer, J. B., Mitchell, T. J., & Fry, R. J. M. (1988). Extrapolation of the relative risk of radiogenic neoplasms across mouse strains and to man. *Radiation research*, *114*(2), 331-353.
3. Szymanska, H., Sitarz, M., Krysiak, E., Piskorowska, J., Czarnomska, A., Skurzak, H., ... & Demant, P. (1999). Genetics of susceptibility to radiation- induced lymphomas, leukemias and lung tumors studied in recombinant congenic strains. *International journal of cancer*, *83*(5), 674-678.
4. Rosemann M, Kuosaite V, Nathrath M, et al. The genetics of radiation- induced osteosarcoma. Radiat Prot Dosimetry 2002;99:257-259.
5. Okumoto, M., Nishikawa, R., Imai, S., & Hilgers, J. (1990). Genetic analysis of resistance to radiation lymphomagenesis with recombinant inbred strains of mice. *Cancer research*, *50*(13), 3848-3850.
6. Boulton, E., Cole, C., Knight, A., Cleary, H., Snowden, R., & Plumb, M. (2003). Low-penetrance genetic susceptibility and resistance loci implicated in the relative risk for radiation-induced acute myeloid leukemia in mice. *Blood*, *101*(6), 2349-2354.
7. Darakhshan, F., Badie, C., Moody, J., Coster, M., Finnon, R., Finnon, P., ... & Ullrich, R. (2006). Evidence for complex multigenic inheritance of radiation AML susceptibility in mice revealed using a surrogate phenotypic assay. *Carcinogenesis*, *27*(2), 311-318.
8. Ponnaiya, B., Cornforth, M. N., & Ullrich, R. L. (1997). Radiation-induced chromosomal instability in BALB/c and C57BL/6 mice: the difference is as clear as black and white. *Radiation research*, *147*(2), 121-125.
9. Weil, M. M., Bedford, J. S., Bielefeldt-Ohmann, H., Ray, F. A., Genik, P. C., Ehrhart, E. J., ... & Callan, M. A. (2009). Incidence of acute myeloid leukemia and hepatocellular carcinoma in mice irradiated with 1 GeV/nucleon 56Fe ions. *Radiation research*, *172*(2), 213-219.
10. Mori, N., Matsumoto, Y., Okumoto, M., Suzuki, N., & Yamate, J. (2001). Variations in Prkdc encoding the catalytic subunit of DNA-dependent protein kinase (DNA-PKcs) and susceptibility to radiation-induced apoptosis and lymphomagenesis. *Oncogene*, *20*(28), 3609-3619.
11. Yu, Y., Okayasu, R., Weil, M. M., Silver, A., McCarthy, M., Zabriskie, R., ... & Ullrich, R. L. (2001). Elevated breast cancer risk in irradiated BALB/c mice associates with unique functional polymorphism of the Prkdc (DNA-dependent protein kinase catalytic subunit) gene. *Cancer research*, *61*(5), 1820-1824.
12. Perez-Losada, J., Wu, D., DelRosario, R., Balmain, A., & Mao, J. H. (2012). Allele-specific deletions in mouse tumors identify Fbxw7 as germline modifier of tumor susceptibility. *PloS one*, *7*(2), e31301.
13. Rosemann, M., Gonzalez-Vasconcellos, I., Domke, T., Kuosaite, V., Schneider, R., Kremer, M., ... & Atkinson, M. J. (2014). A Rb1 promoter variant with reduced activity contributes to osteosarcoma susceptibility in irradiated mice. *Molecular cancer*, *13*(1), 1.

14. Hunter, N. R., Guttenberger, R., & Milas, L. (1992). Modification of radiation-induced carcinogenesis in mice by misonidazole and WR-2721. *International Journal of Radiation Oncology* Biology* Physics*, *22*(4), 795-798.
15. Milas, L., Hunter, N., Stephens, L. C., & Peters, L. J. (1984). Inhibition of radiation carcinogenesis in mice by S-2-(3-aminopropylamino)-ethylphosphorothioic acid. *Cancer research*, *44*(12 Part 1), 5567-5569.
16. Suit, H. D., Sedlacek, R., Fagundes, L., Goitein, M., & Rothman, K. J. (1978). Time distributions of recurrences of immunogenic and nonimmunogenic tumors following local irradiation. *Radiation research*, *73*(2), 251-266.
17. Urano, M., Kenton, L. A., & Kahn, J. (1988). The effect of hyperthermia on the early and late appearing mouse foot reactions and on the radiation carcinogenesis: effect on the early and late appearing reactions. *International Journal of Radiation Oncology* Biology* Physics*, *15*(1), 159-166.
18. Hatley, M. E., Tang, W., Garcia, M. R., Finkelstein, D., Millay, D. P., Liu, N., ... & Olson, E. N. (2012). A mouse model of rhabdomyosarcoma originating from the adipocyte lineage. *Cancer cell*, *22*(4), 536-546.
19. Blum, J. M., Añó, L., Li, Z., Van Mater, D., Bennett, B. D., Sachdeva, M., ... & Cardona, D. M. (2013). Distinct and overlapping sarcoma subtypes initiated from muscle stem and progenitor cells. *Cell reports*, *5*(4), 933-940.
20. Beck, A. (1922). Zur frage des Rontgensarkoms, zugleich ein Beitrag zur pathogenese des Sarkoms. *Munchener Med Wochenschr*, *69*, 623-5.
21. Martland, H. S., & Humphries, R. E. (1973). Osteogenic sarcoma in dial painters using luminous paint. *CA: A Cancer Journal for Clinicians*, *23*(6), 368-374.
22. de Gonzalez, A. B., Kutsenko, A., & Rajaraman, P. (2012). Sarcoma risk after radiation exposure. *Clinical sarcoma research*, *2*(1), 1.
23. Demaria, S., & Formenti, S. C. (2012). Radiation as an immunological adjuvant: current evidence on dose and fractionation. *Frontiers in oncology*, *2*, 153.
24. Pajonk, F., Vlashi, E., & McBride, W. H. (2010). Radiation resistance of cancer stem cells: the 4 R's of radiobiology revisited. *Stem cells*, *28*(4), 639-648.
25. Withers, H. R. (1975). The four R's of radiobiology. *Advances in radiation Biology*, *5*, 241-271.
26. Ando, K., Koike, S., Oohira, C., Ogiu, T., & Yatagai, F. (2005). Tumor induction in mice locally irradiated with carbon ions: a retrospective analysis. *Journal of radiation research*, *46*(2), 185-190.
27. Ando, K., Koike, S., Ohmachi, Y., Ando, Y., & Kobashi, G. (2014). Tumor induction in mice after local irradiation with single doses of either carbon-ion beams or gamma rays. *International journal of radiation biology*, *90*(12), 1119-1124.
28. Makinde, A. Y., John-Aryankalayil, M., Palayoor, S. T., Cerna, D., & Coleman, C. N. (2013). Radiation survivors: understanding and exploiting the phenotype following fractionated radiation therapy. *Molecular Cancer Research*, *11*(1), 5-12.
29. Palayoor, S. T., John-Aryankalayil, M., Makinde, A. Y., Falduto, M. T., Magnuson, S. R., & Coleman, C. N. (2014). Differential expression of stress and immune response pathway transcripts and miRNAs in normal human endothelial cells subjected to fractionated or single-dose radiation. *Molecular Cancer Research*, *12*(7), 1002-1015.
30. Le Vu, B., De Vathaire, F., Shamsaldin, A., Hawkins, M. M., Grimaud, E., Hardiman, C., ... & Panis, X. (1998). Radiation dose, chemotherapy and risk of osteosarcoma after solid

tumours during childhood. *International journal of cancer*, *77*(3), 370-377.
31. Kirova, Y. M., Vilcoq, J. R., Asselain, B., Sastre- Garau, X., & Fourquet, A. (2005). Radiation- induced sarcomas after radiotherapy for breast carcinoma. *Cancer*, *104*(4), 856-863.
32. Hawkins, M. M., Wilson, L. M. K., Burton, H. S., Potok, M. H., Winter, D. L., Marsden, H. B., & Stovall, M. A. (1996). Radiotherapy, alkylating agents, and risk of bone cancer after childhood cancer. *Journal of the National Cancer Institute*, *88*(5), 270-278.
33. Tucker, M. A., D'Angio, G. J., Boice Jr, J. D., Strong, L. C., Li, F. P., Stovall, M., ... & Hoover, R. N. (1987). Bone sarcomas linked to radiotherapy and chemotherapy in children. *New England Journal of Medicine*, *317*(10), 588-593.
34. Rubino, C., Shamsaldin, A., Lê, M. G., Labbé, M., Guinebretière, J. M., Chavaudra, J., & De Vathaire, F. (2005). Radiation dose and risk of soft tissue and bone sarcoma after breast cancer treatment. *Breast cancer research and treatment*, *89*(3), 277-288.
35. Kleinerman, R. A., Schonfeld, S. J., & Tucker, M. A. (2012). Sarcomas in hereditary retinoblastoma. *Clinical sarcoma research*, *2*(1), 1.
36. Wong, F. L., Boice, J. D., Abramson, D. H., Tarone, R. E., Kleinerman, R. A., Stovall, M., ... & Li, F. P. (1997). Cancer incidence after retinoblastoma: radiation dose and sarcoma risk. *Jama*, *278*(15), 1262-1267.
37. Buoen, L. C., & Brand, K. G. (1977). Foreign-body tumors of mice: strain and sex differences in latency and incidence. *Journal of the National Cancer Institute*, *58*(5), 1443-1447.

Chapter Six

Significance

The future of space exploration for humankind is dependent on developing an understanding of the space radiation environment and creating sound estimates of the biologic threats that are posed in such an untested environment. Carcinogenesis from exposures to galactic cosmic rays is considered one of the most significant barriers to a manned mission in deep space. NASA dictates a ceiling for cancer risk and that ceiling is defined by the upper 95% confidence interval of the risk estimate. By decreasing uncertainties surrounding cancer risk assessments in space, that 95% confidence interval can be diminished and risks can be more accurately estimated. The most significant component of uncertainty in the current estimates for cancer risk in the space radiation environment is the unclear carcinogenesis effects of HZE ions. The work presented in this dissertation attempts to address the uncertainties surrounding HZE ion exposures.

In order to provide a meaningful prediction of the carcinogenic effects of space radiation on humans, epidemiologic data from human populations exposed to ionizing radiation is utilized as a baseline. This human data is not perfect, however, most notably because the ionizing radiation in studied human populations is composed of photons, which produces sparse, isolated ionization events. The ionizing radiation in space is physically very different: it is composed of particles, or HZE ions, traveling at relativistic speeds, likely accelerated from supernova explosions. The ionization events that result from HZE ion interactions are focused and produce dense tracks through biologic material; this type of radiation is much more efficient at producing

clustered and complex damage within a cell. Because of the physical differences in the photon radiation for which there exists human epidemiologic data and the particle radiation present in space, the validity of utilizing such human data is unproven. Ground-based studies utilizing accelerator produced HZE ions and animal models provides the best strategy to test the validity of using terrestrial radiation carcinogenesis data as a surrogate for space radiation carcinogenesis. However, the animal model must be carefully chosen to avoid specific pitfalls in such validity assessments. As the majority of animal models of cancer are composed of populations of genetically identical individuals, the individuals of such a population have a narrow phenotypic window and, therefore, tend to produce the same tumor type regardless of carcinogen exposure. The genetic homogeneity obscures the variability that may exist in a genetically diverse population, such as humans. For this reason, a mouse model of population diversity was utilized in a lifetime carcinogenesis study to determine the tumor spectra that would occur following exposure to photon radiation and high-energy particle radiation. The results indicate that, although the two radiation types are differently efficient at producing specific tumor histotypes via specific mechanisms, the tumor spectra are essentially the same and both forms of ionizing radiation are capable of producing tumors via similar mechanisms.

Determining the genetics of susceptibility and resistance to radiation-induced tumors could represent a method to decrease the risks faced by individuals. It is well known that genetic susceptibility plays a significant role for human susceptibility to radiogenic tumors following exposure to low LET radiation; however, determining genetic susceptibility to high LET radiation is complicated by the lack of human exposures. If the same genetic loci that predispose an individual to tumors following low LET exposures also predispose that individual to the same tumors following high LET exposures, extrapolating the genetics of susceptibility would present

an accurate way to predict which individuals in a population will face increased cancer risk in space. This dissertation provides novel evidence for this concept in the form of genome-wide association studies in outbred mouse population exposed to HZE ions and γ-rays. A high degree of overlap in QTL are observed between exposure groups, indicating that the extrapolation of human terrestrial radiation data to space radiation cancer risk predictions represents a valid approach to cancer risk estimates.

Appendix 1

Table. Tumors arising in HS/Npt mice following exposure to HZE ions (600 MeV/n 56Fe or 240 MeV/n 28Si) or γ-ray irradiation compared to the background incidence of the same tumors in unirradiated HS/Npt mice.

	Total ♂ = 934 ♀ = 916 n = 1850	HZE ♂ = 312 ♀ = 310 n = 622	γ ♂ = 313 ♀ = 302 n = 615	Unirradiated ♂ = 309 ♀ = 304 n = 613	HZE Fe ♂ = 161 ♀ = 153 n = 314	HZE Si ♂ = 151 ♀ = 157 n = 308	M:F
Epithelial							
Thyroid							
Follicular Adenoma	43	21	13	9	12	9	21:22
Follicular Carcinoma	5	2	2	1	2	0	2:3
Parathyroid Adenoma	2	0	2	0	0	0	1:1
Ovary							
Granulosa Cell Tumor	45	3	42	0	3	0	0:45
Tubulostromal Adenoma	15	0	15	0	0	0	0:13
Tubulostromal Adenocarcinoma	2	0	2	0	0	0	0:2
Ovarian Carcinoma	2	0	0	2	0	0	0:2
Luteoma	2	1	1	0	0	1	0:2
Thecoma	1	1	0	0	0	1	0:1
Ovarian Cystadenoma	1	0	1	0	0	0	0:1
Dysgerminoma	1	1	0	0	1	0	0:1
Uterus							
Uterine Stromal Sarcoma	6	3	3	0	1	2	0:6
Endometrial Papillary Adenoma	1	0	0	1	0	0	0:1
Endometrial Stromal Polyp	16	12	2	2	4	8	0:16
Mammary Gland							
Adenocarcinoma	28	11	12	5	3	8	2:26
Adenoacanthoma	4	1	0	3	0	1	0:4
Carcinosarcoma	1	0	1	0	0	0	0:1
Pulmonary							
Pulmonary Adenoma	228	60	88	80	34	26	151:77
Pulmonary Adenocarcinoma	353	128	110	115	64	64	243:110
Hepatic							
Hepatocellular Adenoma	314	126	94	94	68	58	218:96
Hepatocellular Carcinoma	251	100	66	85	57	43	187:64
Hepatoblastoma	6	1	4	1	0	1	5:1
Biliary Cystadenoma	9	5	4	0	2	3	9:0
Cholangiocellular Carcinoma	2	0	1	1	0	1	2:0
Harderian Gland							
Adenoma	219	121	77	21	67	54	124:95
Adenocarcinoma	41	20	17	4	10	10	20:21
Unilateral Neoplasm	209	109	80	20	57	52	117:92
Bilateral Neoplasms	51	32	14	5	20	12	27:24
Gastrointestinal Tract							
Adenocarcinoma	3	1	1	1	0	1	0:3
Gastric SCC	2	2	0	0	1	1	1:1
Duodenal Polyp	12	8	3	1	6	2	8:4
Colonic Polyp	1	0	1	0	0	0	1:0
Gastric Adenocarcinoma	1	0	0	1	0	0	1:0

	Total ♂ = 934 ♀ = 916 n = 1850	HZE ♂ = 312 ♀ = 310 n = 622	γ ♂ = 313 ♀ = 302 n = 615	Unirradiated ♂ = 309 ♀ = 304 n = 613	HZE Fe ♂ = 161 ♀ = 153 n = 314	HZE Si ♂ = 151 ♀ = 157 n = 308	M:F
Gastric Polyp	1	0	1	0	0	0	0:1
Other							
Salivary Gland Carcinoma	1	0	1	0	0	0	1:0
Squamous Cell Carcinoma (lingual or laryngeal)	3	1	1	1	1	0	1:2
Squamous Cell Carcinoma (haired skin)	3	1	2	0	1	0	3:0
Adrenocortical Carcinoma	3	3	0	0	2	1	2:1
Pheochromocytoma	3	3	0	0	2	1	0:3
Renal Cell Carcinoma	3	1	1	1	0	1	3:0
Renal Adenoma	1	0	1	0	0	0	1:0
Islet Cell Carcinoma	2	2	0	0	1	1	1:1
Odontogenic Tumor	2	1	1	0	1	0	0:2
Mesothelioma	2	1	1	0	0	1	0:2
Pilomatricoma	1	0	1	0	0	0	1:0
Papillary Adenoma (gall bladder)	1	0	0	1	0	0	1:0
Sebaceous adenoma (skin)	2	1	1	0	0	1	2:0
Basal Cell Carcinoma (skin)	3	1	1	0	1	0	2:1
Nervous							
Pituitary Adenoma	40	15	22	3	10	5	9:31
Pituitary Adenocarcinoma	1	1	0	0	1	0	1:0
Meningioma	2	0	1	1	0	0	1:1
Astrocytoma	1	1	0	0	1	0	1:0
Choroid Plexus Tumor	3	1	2	0	1	0	0:3
Glial Tumor, Olfactory Lobe	1	0	1	0	0	0	1:0
Ependymoma	2	1	1	0	1	0	0:2
Messenchymal							
Hematopoietic System							
Lymphoid	570	172	195	203	84	88	274:307
Follicular B cell	209	66	59	84	34	32	101:108
Diffuse Large B cell	120	39	38	43	20	19	56:64
Lymphoblastic B cell	81	24	16	41	12	12	38:43
Histiocyte Associated B cell	13	3	3	7	1	2	3:10
Anaplasstic Plasmacytoma	4	1	2	1	0	1	2:2
Small B cell	13	6	4	3	2	4	6:7
Marginal Zone B cell	5	3	1	1	2	1	3:2
Precursor T cell	82	13	61	8	6	7	40:42
Small T cell	5	2	1	2	2	0	1:4
Anaplastic T cell	9	4	5	0	0	4	3:6
Other	29	11	5	13	5	6	14:15
Myeloid leukemia	124	18	96	10	5	13	86:38
Histiocytic Sarcoma	37	12	11	14	4	8	21:16
Osteosarcoma	19	12	6	1	8	4	4:14
Osteoma	7	1	3	3	1	0	2:6

	Total ♂ = 934 ♀ = 916 n = 1850	**HZE** ♂ = 312 ♀ = 310 n = 622	**γ** ♂ = 313 ♀ = 302 n = 615	**Unirradiated** ♂ = 309 ♀ = 304 n = 613	**HZE Fe** ♂ = 161 ♀ = 153 n = 314	**HZE Si** ♂ = 151 ♀ = 157 n = 308	M:F
Soft Tissue Sarcoma							
Rhabdomyosarcoma	14	4	4	6	2	2	4:10
Fibrosarcoma	4	2	1	1	2	0	3:1
Hemangiosarcoma	76	32	18	26	16	16	42:34
Hemangioma	22	14	4	4	7	7	31:9
Undifferentiated	29	14	4	11	5	9	5:24
Myxosarcoma	6	1	2	3	0	1	0:6
Myxoma	1	0	0	1	0	0	0:1
Leiomyosarcoma	11	6	2	3	3	3	3:8
Leiomyoma	1	1	0	0	0	1	0:1
Nerve Sheath Tumor	1	1	0	0	1	0	1:0
GIST	4	2	1	1	1	1	3:1
Liposarcoma	1	1	0	0	0	1	1:0

Appendix 2

Kaplan-Meier survival analysis for tumors arising in HS/Npt mice following exposure to HZE ions (600 MeV/n 56Fe or 240 MeV/n 28Si) or γ-ray irradiation compared to the background incidence of the same tumors in unirradiated HS/Npt mice.

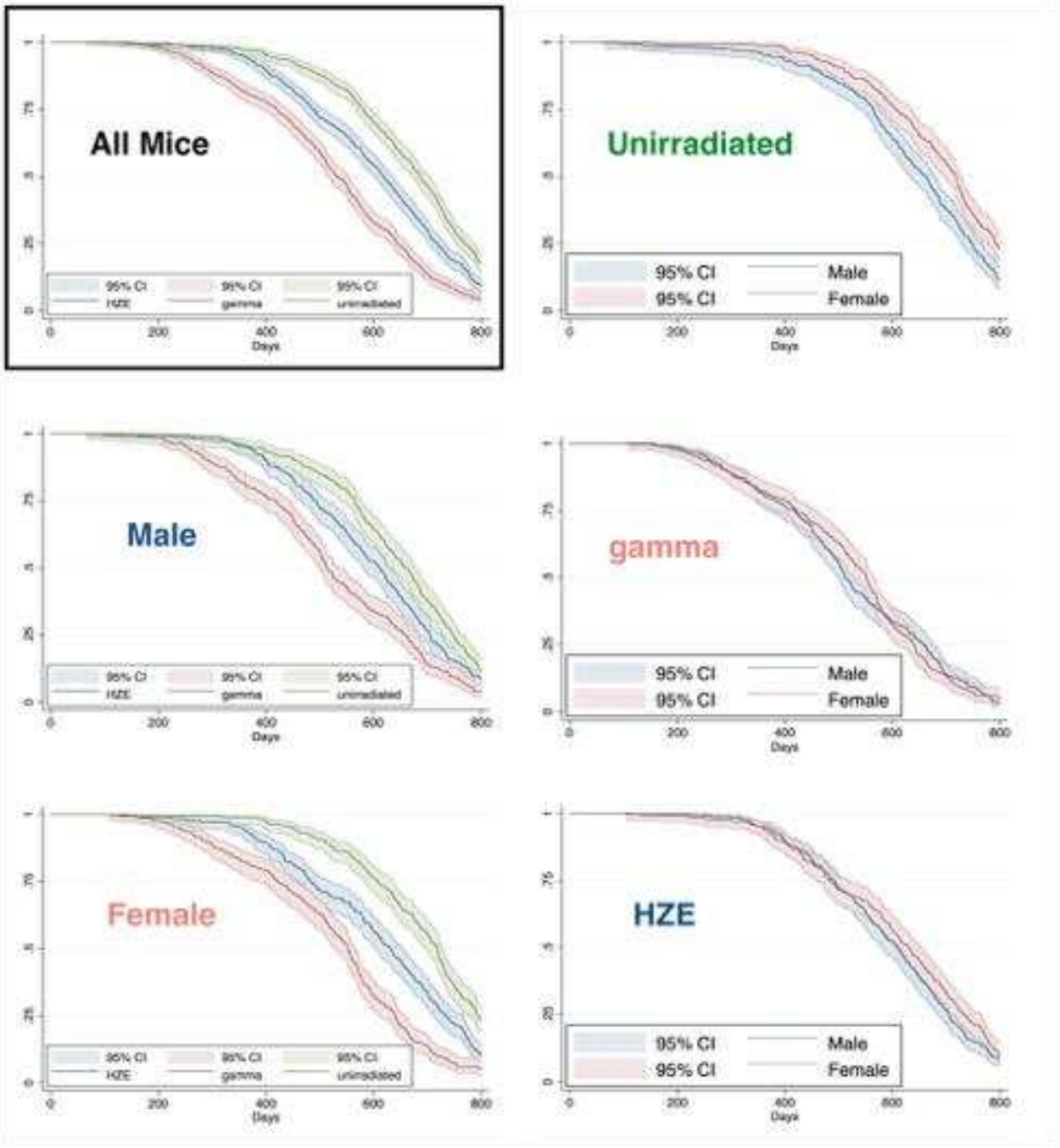
All Mice
95% CI
95% CI
95% CI
HZE
gamma
unirradiated
Days
Unirradiated
95% CI
95% CI
Male
Female
Days
Male
95% CI
95% CI
95% CI
HZE
gamma
unirradiated
Days
gamma
95% CI
95% CI
Male
Female
Days
Female
95% CI
95% CI
95% CI
HZE
gamma
unirradiated
Days
HZE
95% CI
95% CI
Male
Female
Days

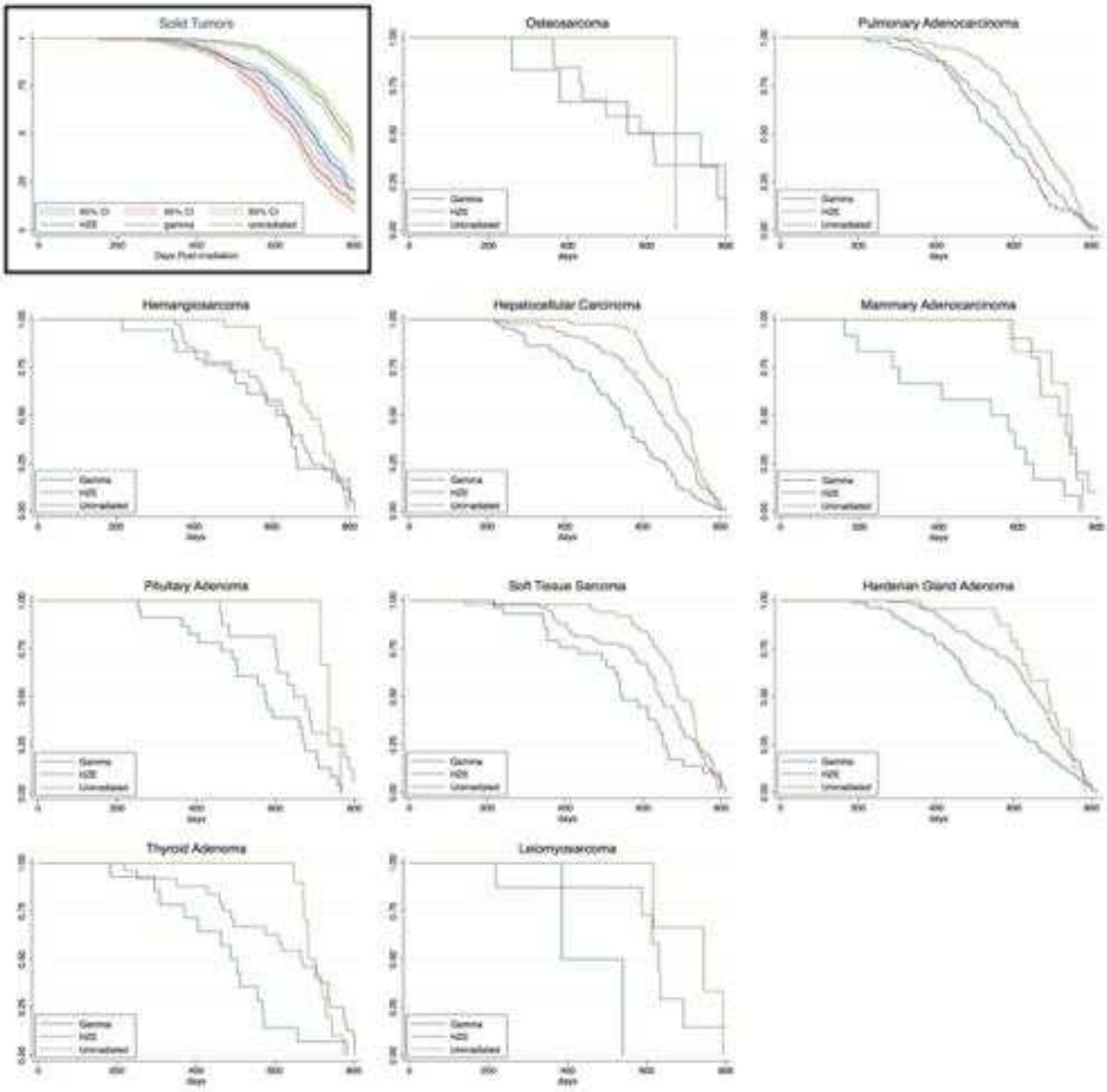
Solid Tumors
Osteosarcoma
Pulmonary Adenocarcinoma
Hemangiosarcoma
Hepatocellular Carcinoma
Mammary Adenocarcinoma
Pituitary Adenoma
Soft Tissue Sarcoma
Harderian Gland Adenoma
Thyroid Adenoma
Leiomyosarcoma

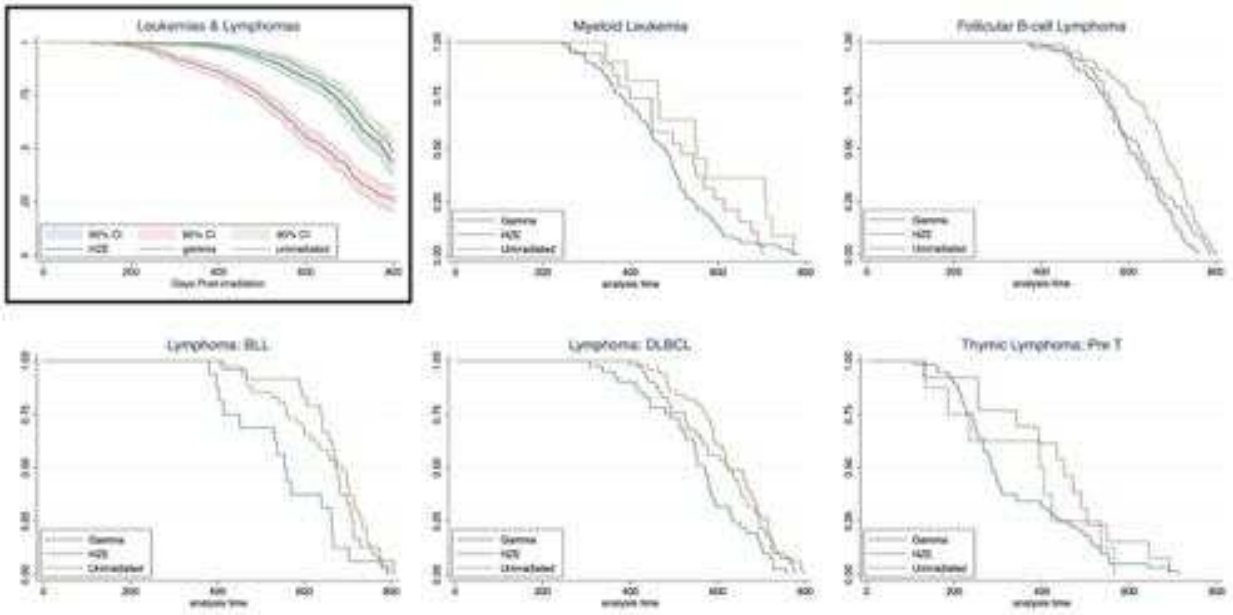
Leukemias & Lymphomas
Myeloid Leukemia
Follicular B-cell Lymphoma
Lymphoma: BLL
Lymphoma: DLBCL
Thymic Lymphoma: Pre T

Appendix 3

Genome-wide association mapping results for tumor incidence.

Phenotype	Group	Chr	Max LOD	QTL	QTL 95% Confidence Interval			Percent Variance Explained (Tjur)	Model	Covariates
					Position (BP)		Confidence Interval (Mb)			
B-cell Lymphoma	All mice	1	10.999	73732062.5	73494384	74262978.7	0.77	2.48	glm(binomial, link = "logit")	Sex
BLL Lymphoma	All mice	1	6.420	74343073	73443080	78299617	4.86	1.28	glm(binomial, link = "logit")	Sex
Thyroid adenoma	All mice	1	6.079	73078474	71335224	74931530	3.60	2.35	glm(binomial, link = "logit")	Sex
B-cell Lymphoma	Unirradiated	1	6.318	74938971	73640888.9625	77001094.4125	3.36	4.02	glm(binomial, link = "logit")	Sex
Thyroid adenoma	All Irradiated	2	10.836	122584526	120236421	124006948	3.77	4.11	glm(binomial, link = "logit")	Sex
AML	All Irradiated	2	6.995	147914389	147828068.8375	148316130	0.49	5.82	glm(binomial, link = "logit")	Sex
Hepatocellular Carcinoma	All Irradiated	2	6.386	123223410	119805949	124476777.9625	4.67	5.65	glm(binomial, link = "logit")	Sex
Thyroid adenoma	All mice	2	11.204	121483195	120236421	124006948	3.77	3.14	glm(binomial, link = "logit")	Sex
B-cell Lymphoma	All mice	2	8.300	155646718	151758335.85	159294061.825	7.54	2.06	glm(binomial, link = "logit")	Sex
Hepatocellular Carcinoma	All mice	2	6.291	117964768	115943082.975	120564786	4.62	5.37	glm(binomial, link = "logit")	Sex
Thyroid adenoma	HZE	2	7.803	123357336.5	120345725	124006948	3.66	7.00	glm(binomial, link = "logit")	Sex
B-cell Lymphoma	Unirradiated	2	6.495	152492554	152492554	155646718	3.15	4.26	glm(binomial, link = "logit")	Sex
PreT Lymphoma	All mice	3	6.095	29822410	28532178.6	33271823.8375	4.74	0.75	glm(binomial, link = "logit")	Sex
B-cell Lymphoma	Unirradiated	3	7.436	33476536	32159146	33781730.45	1.62	5.47	glm(binomial, link = "logit")	Sex
PreT Lymphoma	All Irradiated	4	7.085	82878119	82243458	86141326	3.90	3.20	glm(binomial, link = "logit")	Sex
PreT Lymphoma	All mice	4	6.814	82878119	82098201	85953208.2125	3.86	2.10	glm(binomial, link = "logit")	Sex
PreT Lymphoma	Gamma	4	8.413	89196864	85649328	90387054.5	4.74	7.46	glm(binomial, link = "logit")	Sex
PreT Lymphoma	Gamma	4	8.413	96173703	96168780	98871254	2.70	7.46	glm(binomial, link = "logit")	Sex
PreT Lymphoma	Gamma	4	8.131	82622922	82622922	85884363.4	3.26	7.46	glm(binomial, link = "logit")	Sex
BLL Lymphoma	All Irradiated	5	6.848	107760474	106744777.375	107900411	1.16	1.65	glm(binomial, link = "logit")	Sex
Thyroid adenoma	All Irradiated	5	5.850	142141592	142141592	144401281.675	2.26	1.80	glm(binomial, link = "logit")	Sex
B-cell Lymphoma	All mice	5	6.020	107350502	105230836.5	108062273.5625	2.83	1.45	glm(binomial, link = "logit")	Sex
Thyroid adenoma	All mice	5	5.986	142141592	142050181	144399143	2.35	1.25	glm(binomial, link = "logit")	Sex
B-cell Lymphoma	Unirradiated	5	5.848	7075383	5683053	8167587.775	2.48	3.97	glm(binomial, link = "logit")	Sex
BLL Lymphoma	All Irradiated	6	6.428	116924770	115490532.1	120212740	4.72	1.98	glm(binomial, link = "logit")	Sex
Pulmonary adenocarcinoma	All Irradiated	6	6.050	148261935	146889257.5	149577033	2.69	4.84	glm(binomial, link = "logit")	Sex
Amyloidosis	All mice	6	5.780	136702296	134007207	136963345	2.96	2.48	glm(binomial, link = "logit")	Sex
B-cell Lymphoma	All mice	8	6.665	72479016.5	70639782.6	74664266	4.02	1.63	glm(binomial, link = "logit")	Sex
Hepatocellular Carcinoma	All mice	8	6.546	30794428	29984337.3	33252747.4	3.27	5.28	glm(binomial, link = "logit")	Sex
Amyloidosis	All Irradiated	9	6.162	35893111	33739192.1875	36832676	3.09	3.96	glm(binomial, link = "logit")	Sex
B-cell Lymphoma	All mice	9	7.860	62452601.5	61606150.875	62993849.175	1.39	1.90	glm(binomial, link = "logit")	Sex
FBL Lymphoma	All mice	9	6.581	122891663	122867671.575	122891663	0.02	0.84	glm(binomial, link = "logit")	Sex
Thyroid adenoma	All mice	9	5.801	3455888	3455888	4254190.5	0.80	1.55	glm(binomial, link = "logit")	Sex
Harderian adenocarcinoma	HZE	9	6.018	102809143	101334669.45	105635973	4.30	2.78	glm(binomial, link = "logit")	Sex
B-cell Lymphoma	Unirradiated	9	6.903	75346491	74206387.6375	77507836	3.30	4.82	glm(binomial, link = "logit")	Sex
Thyroid adenoma	HZE	10	5.777	47711287.5	46090331.85	50595803	4.51	5.22	glm(binomial, link = "logit")	Sex
Mammary adenocarcinoma	All Irradiated	11	6.175	111549311	110639949.5	113855208	3.22	4.55	glm(binomial, link = "logit")	Sex
B-cell Lymphoma	Gamma	11	6.286	88759037	86219353	90177534	3.96	6.22	glm(binomial, link = "logit")	Sex
Pulmonary adenocarcinoma	All mice	14	6.249	97084001	94070480	99894015.5375	5.82	4.84	glm(binomial, link = "logit")	Sex
B-cell Lymphoma	All mice	15	7.901	98143056	95982213.7	98755939	2.77	1.93	glm(binomial, link = "logit")	Sex
AML	All mice	15	6.312	91425908	88406017.6	94424358.6	6.02	2.98	glm(binomial, link = "logit")	Sex
Hepatocellular Carcinoma	All mice	15	6.146	94246099	90919680.8875	97184622	6.26	5.31	glm(binomial, link = "logit")	Sex
B-cell Lymphoma	Unirradiated	15	6.814	98556922	95073624.6	98745723.575	3.67	4.84	glm(binomial, link = "logit")	Sex
Osteosarcoma	All Irradiated	17	5.962	71019344	69377022	71474706	2.10	2.49	glm(binomial, link = "logit")	Sex
FBL Lymphoma	All Irradiated	17	5.805	86662315	85568114.525	88783444	3.22	2.59	glm(binomial, link = "logit")	Sex
Osteosarcoma	All mice	17	6.013	70394500	69377022	71474706	2.10	1.68	glm(binomial, link = "logit")	Sex
DLBCL Lymphoma	Gamma	17	6.744	83589501	83534674	85336592	1.80	5.76	glm(binomial, link = "logit")	Sex
PreT Lymphoma	Gamma	17	6.154	48674981	48649945	53188104.5	4.54	5.01	glm(binomial, link = "logit")	Sex
Harderian adenoma	HZE	17	5.976	45427448	44081080.2125	45661990.15	1.58	4.43	glm(binomial, link = "logit")	Sex
DLBCL Lymphoma	Gamma	18	6.530	82809869	80244031.5	86347428.35	6.10	4.76	glm(binomial, link = "logit")	Sex

Appendix 4

Genome-wide association mapping results for tumor latency.

Phenotype	Group	Chr	Max LOD	QTL (BP)	QTL 95% Confidence Interval			Percent Variance Explained	Hazard for BB compared to AA Genotype				R^2	Model	Covariates
					Position (BP)		Size (Mb)		Hazard	Hazard Ratio	Standard Error	Pr(>|z|)			
B-cell Lymphoma	All irradiated	1	6.193	73675331	73644645.5	76156729	2.51	2.339	-0.793	0.453	0.340	0.020	0.023	coxph(surv ~ addcovar)	Sex
B-cell Lymphoma	All mice	1	11.885	73732062.5	73644645.5	75527460.5	1.88	2.911	-1.004	0.366	0.293	0.001	0.029	coxph(surv ~ addcovar)	Sex
BLL Lymphoma	All mice	1	7.036	74343073	73443080	78275804.0875	4.83	1.286	2.625	13.807	1.009	0.009	0.013	coxph(surv ~ addcovar)	Sex
B-cell Lymphoma	Gamma	1	5.940	154533061	154053089.1375	157068396	3.02	3.821	1.277	3.588	0.279	0.000	0.038	coxph(surv ~ addcovar)	Sex
B-cell Lymphoma	Unirradiated	1	7.512	73671405.5	73494384	76186572.5	2.69	5.113	-1.229	0.292	0.272	0.000	0.051	coxph(surv ~ addcovar)	Sex
AML	All irradiated	2	6.547	149081727	147808899	148316130	0.51	2.289	3.553	34.904	0.728	0.000	0.023	coxph(surv ~ addcovar)	Sex
B-cell Lymphoma	All irradiated	2	6.216	119093112	116762788	122163058	5.40	1.580	-1.350	0.259	0.710	0.057	0.016	coxph(surv ~ addcovar)	Sex
Hepatocellular Carcinoma	All irradiated	2	5.991	123096335	120896801	125682132.925	4.79	1.719	-0.841	0.431	0.456	0.065	0.017	coxph(surv ~ addcovar)	Sex
Thyroid adenoma	All irradiated	2	7.574	122584526	120235551.9875	124006948	3.77	NA	NA	NA	NA	NA	NA	coxph(surv ~ addcovar)	Sex
B-cell Lymphoma	All mice	2	8.309	155646718	151688481	159364801.15	7.68	1.877	0.729	2.073	0.142	0.000	0.019	coxph(surv ~ addcovar)	Sex
Hepatocellular Carcinoma	All mice	2	7.922	116811190	115944687	118326331	2.38	1.516	-1.437	0.238	0.582	0.013	0.015	coxph(surv ~ addcovar)	Sex
Pulmonary adenocarcinoma	All mice	2	6.150	106661333	105153951	106750991	1.60	1.243	0.721	2.056	0.169	0.000	0.012	coxph(surv ~ addcovar)	Sex
Thyroid adenoma	All mice	2	9.948	120418990.5	120236421	123716967	3.48	2.212	2.431	11.372	0.455	0.000	0.022	coxph(surv ~ addcovar)	Sex
B-cell Lymphoma	Unirradiated	2	6.419	152243135	151688481	155646718	3.96	4.418	-1.058	0.347	0.214	0.000	0.044	coxph(surv ~ addcovar)	Sex
Harderian Tumor	All mice	3	5.997	23109161	19658371	27013788	7.36	1.442	0.965	2.624	0.182	0.000	0.014	coxph(surv ~ addcovar)	Sex
Harderian adenocarcinoma	All irradiated	4	6.706	15987949	15232129	16503035.45	1.27	NA	NA	NA	NA	NA	NA	coxph(surv ~ addcovar)	Sex
PreT Lymphoma	All irradiated	4	7.339	82622922	82336059.4	85649328	3.31	2.396	1.989	7.309	0.339	0.000	0.024	coxph(surv ~ addcovar)	Sex
B-cell Lymphoma	All mice	4	7.727	149549045.5	148766129.5	152805928	4.04	1.954	-0.730	0.482	0.273	0.007	0.020	coxph(surv ~ addcovar)	Sex
Harderian adenocarcinoma	All mice	4	6.894	16498679	15232129	16672937	1.44	NA	NA	NA	NA	NA	NA	coxph(surv ~ addcovar)	Sex
PreT Lymphoma	All mice	4	6.884	82622922	81987887.5	86145148.9	4.16	1.518	1.863	6.446	0.321	0.000	0.015	coxph(surv ~ addcovar)	Sex
PreT Lymphoma	Gamma	4	8.413	89196864	85649328	90387054.5	4.74	5.453	2.243	9.423	0.357	0.000	0.055	coxph(surv ~ addcovar)	Sex
PreT Lymphoma	Gamma	4	8.413	96173703	95289711	98770176	3.48	5.453	2.243	9.423	0.357	0.000	0.055	coxph(surv ~ addcovar)	Sex
PreT Lymphoma	Gamma	4	8.131	82622922	82622922	85949860	3.33	5.453	2.243	9.423	0.357	0.000	0.055	coxph(surv ~ addcovar)	Sex
Harderian adenocarcinoma	HZE	4	6.026	16498679	15232129	16896271	1.66	NA	NA	NA	NA	NA	NA	coxph(surv ~ addcovar)	Sex
B-cell Lymphoma	All mice	5	8.653	31249669.5	30911677	31286278	0.37	2.148	-0.919	0.399	0.149	0.000	0.021	coxph(surv ~ addcovar)	Sex
Harderian Tumor	All mice	5	6.383	39081520	37450602.3875	41615415	4.16	1.366	0.932	2.539	0.183	0.000	0.014	coxph(surv ~ addcovar)	Sex
Pulmonary adenocarcinoma	All mice	5	6.219	38483317	37535263	40555253	3.02	1.216	1.029	2.798	0.226	0.000	0.012	coxph(surv ~ addcovar)	Sex
PreT Lymphoma	Gamma	5	5.819	139776662	135811213	141609050	5.80	4.169	-17.453	0.000	2363.034	0.994	0.042	coxph(surv ~ addcovar)	Sex
B-cell Lymphoma	Unirradiated	5	6.499	31286278	30527389.1375	31331455.5875	0.80	4.328	-1.156	0.315	0.235	0.000	0.043	coxph(surv ~ addcovar)	Sex
BLL Lymphoma	All irradiated	6	6.316	116425643	115696271.6	119462570	3.77	1.995	-18.749	0.000	4031.944	0.996	0.020	coxph(surv ~ addcovar)	Sex
Hepatocellular Carcinoma	All irradiated	6	7.055	92859721	92631195.5	94131082	1.50	2.232	-2.294	0.101	1.004	0.022	0.022	coxph(surv ~ addcovar)	Sex
Harderian Tumor	All irradiated	7	6.241	112491829	109861463	115478241	5.62	2.232	-0.808	0.446	0.208	0.000	0.022	coxph(surv ~ addcovar)	Sex
Hepatocellular Carcinoma	All irradiated	7	7.482	112130962	111094882	113740999	2.65	2.304	1.243	3.464	0.269	0.000	0.023	coxph(surv ~ addcovar)	Sex
B-cell Lymphoma	All mice	7	7.623	140480630	137126507	143776516.6375	6.65	1.617	-0.990	0.372	0.273	0.000	0.016	coxph(surv ~ addcovar)	Sex
Harderian adenoma	All mice	7	5.833	113864569	110698131	116131134.7875	5.43	1.152	-0.698	0.498	0.203	0.001	0.012	coxph(surv ~ addcovar)	Sex
Hepatocellular Carcinoma	All mice	7	6.079	113659296	109979745	113740999	3.76	1.317	0.828	2.289	0.198	0.000	0.013	coxph(surv ~ addcovar)	Sex
B-cell Lymphoma	Gamma	7	7.211	40246302	40078510	40371104	0.29	5.793	2.165	8.715	0.343	0.000	0.058	coxph(surv ~ addcovar)	Sex
B-cell Lymphoma	All irradiated	8	6.081	71333049	71030886.825	73078950	2.05	1.963	0.858	2.359	0.189	0.000	0.020	coxph(surv ~ addcovar)	Sex
B-cell Lymphoma	All mice	8	7.601	72326900	70783484.5	74167817.1375	3.38	1.719	0.732	2.079	0.140	0.000	0.017	coxph(surv ~ addcovar)	Sex
B-cell Lymphoma	All irradiated	9	7.452	77651694	74262311.5	80174106	5.91	2.714	-0.993	0.371	0.185	0.000	0.027	coxph(surv ~ addcovar)	Sex
DLBCL Lymphoma	All irradiated	9	5.896	61740072	60199542	64717662	4.52	2.048	-2.144	0.117	0.722	0.003	0.020	coxph(surv ~ addcovar)	Sex
Pulmonary adenocarcinoma	All irradiated	9	6.188	42454683	42218208	43296200.4875	1.08	2.140	0.486	1.626	0.583	0.405	0.021	coxph(surv ~ addcovar)	Sex
B-cell Lymphoma	All mice	9	13.490	77651694	74261739.7375	80174106	5.91	3.157	-1.042	0.353	0.139	0.000	0.032	coxph(surv ~ addcovar)	Sex
DLBCL Lymphoma	All mice	9	6.954	61740072	60264034	64268841.9375	4.00	1.764	-2.161	0.115	0.589	0.000	0.018	coxph(surv ~ addcovar)	Sex
B-cell Lymphoma	Gamma	9	7.143	77651694	74217435.0125	81322535	7.11	4.804	-1.444	0.236	0.286	0.000	0.048	coxph(surv ~ addcovar)	Sex
Harderian adenocarcinoma	HZE	9	5.902	102548277	101340795	103625549.9375	2.28	3.589	-19.933	0.000	18378.247	0.999	0.036	coxph(surv ~ addcovar)	Sex
B-cell Lymphoma	Unirradiated	9	7.705	77507836	74239441	80778575.4625	6.54	4.933	1.174	3.235	0.212	0.000	0.049	coxph(surv ~ addcovar)	Sex
Hepatocellular Carcinoma	All irradiated	10	6.296	91864700	89674477.3375	92621230	2.95	1.521	0.924	2.519	0.216	0.000	0.015	coxph(surv ~ addcovar)	Sex
Hepatocellular Carcinoma	All mice	10	5.947	92621230	89176542.5	94876655	5.70	1.197	0.863	2.370	0.195	0.000	0.012	coxph(surv ~ addcovar)	Sex
DLBCL Lymphoma	All irradiated	11	6.701	71739994	69450261	72909553.0125	3.46	NA	NA	NA	NA	NA	NA	coxph(surv ~ addcovar)	Sex
Mammary adenocarcinoma	All irradiated	11	6.643	111549311	110681119	113667011	2.99	1.995	19.250	229103533	5865.572	0.997	0.020	coxph(surv ~ addcovar)	Sex
B-cell Lymphoma	All mice	11	7.736	52250226	48448172	56039468	7.59	1.752	0.896	2.449	0.157	0.000	0.018	coxph(surv ~ addcovar)	Sex
DLBCL Lymphoma	Gamma	11	7.512	71739994	69450261	72907737.5	3.46	NA	NA	NA	NA	NA	NA	coxph(surv ~ addcovar)	Sex
B-cell Lymphoma	Unirradiated	11	5.894	49589121	46319591	52250226	5.93	3.805	1.249	3.485	0.254	0.000	0.038	coxph(surv ~ addcovar)	Sex
B-cell Lymphoma	All mice	12	5.911	16742376.5	16521324.9125	17049168	0.53	1.224	-0.626	0.535	0.152	0.000	0.012	coxph(surv ~ addcovar)	Sex
Pulmonary adenocarcinoma	All mice	12	6.745	103255981.5	102868327.675	104913631.9875	2.05	1.351	-0.691	0.501	0.165	0.000	0.014	coxph(surv ~ addcovar)	Sex
B-cell Lymphoma	All irradiated	13	6.908	111692554	110302374	112885502	2.58	2.208	2.024	7.568	0.587	0.001	0.022	coxph(surv ~ addcovar)	Sex
B-cell Lymphoma	All irradiated	14	6.023	86043426	85612342.5	88761729	3.15	1.928	0.890	2.435	0.199	0.000	0.019	coxph(surv ~ addcovar)	Sex
Hepatocellular Carcinoma	All mice	14	5.902	119083205	119173497	123365220.35	4.19	1.043	0.722	2.059	0.168	0.000	0.010	coxph(surv ~ addcovar)	Sex
Pulmonary adenocarcinoma	All mice	14	5.913	97084001	94137982.175	99920147	5.78	1.502	-0.824	0.439	0.412	0.046	0.015	coxph(surv ~ addcovar)	Sex
B-cell Lymphoma	Gamma	14	6.750	88398605.5	85978449.5	90408596	4.43	4.215	-1.337	0.263	0.271	0.000	0.042	coxph(surv ~ addcovar)	Sex
AML	All mice	15	5.982	91001963	88406017.6	93620314	5.21	1.439	-1.458	0.233	1.004	0.147	0.014	coxph(surv ~ addcovar)	Sex
B-cell Lymphoma	All mice	15	8.926	97593420.5	94584056	98932548	4.35	2.004	0.899	2.458	0.181	0.000	0.020	coxph(surv ~ addcovar)	Sex
Pulmonary adenocarcinoma	All mice	15	5.971	40258684.5	40195208.5	41652518.5	1.46	1.388	1.942	6.969	0.386	0.000	0.014	coxph(surv ~ addcovar)	Sex
B-cell Lymphoma	Unirradiated	15	7.568	98097859	96211856.0875	98692322.5	2.48	4.948	1.131	3.098	0.224	0.000	0.049	coxph(surv ~ addcovar)	Sex
B-cell Lymphoma	All mice	16	7.046	48588285	48224219.5	49493665	1.27	1.972	0.564	1.758	0.212	0.008	0.020	coxph(surv ~ addcovar)	Sex
FBL Lymphoma	All irradiated	17	7.040	86859140	85595945	87606186	2.01	2.336	-1.976	0.139	0.424	0.000	0.023	coxph(surv ~ addcovar)	Sex
DLBCL Lymphoma	Gamma	17	6.360	83599869	83565880	85336592	1.77	3.968	2.448	11.564	0.519	0.000	0.040	coxph(surv ~ addcovar)	Sex
Hepatocellular Carcinoma	All irradiated	18	6.722	60537671	60102377.4125	64122158	4.02	1.692	1.011	2.749	0.273	0.000	0.017	coxph(surv ~ addcovar)	Sex
B-cell Lymphoma	All mice	18	6.766	70839373.5	70618816.45	72863718	2.24	1.491	-2.313	0.099	1.004	0.021	0.015	coxph(surv ~ addcovar)	Sex
Pulmonary adenocarcinoma	All mice	18	6.980	54802127.5	51817892	56397454.275	4.58	1.309	0.763	2.145	0.160	0.000	0.013	coxph(surv ~ addcovar)	Sex
FBL Lymphoma	All irradiated	19	6.256	59265936	58600768	59844770.5	1.24	NA	NA	NA	NA	NA	NA	coxph(surv ~ addcovar)	Sex
B-cell Lymphoma	All mice	19	5.899	59261441.5	55748310.3	60116307.45	4.37	1.293	3.012	20.325	0.716	0.000	0.013	coxph(surv ~ addcovar)	Sex
BLL Lymphoma	All mice	19	6.645	45120113.5	42018221	46653474	4.64	1.482	1.621	5.059	0.332	0.000	0.015	coxph(surv ~ addcovar)	Sex

Appendix 5

Genome-wide association mapping results for cataract latency.

Cataract QTL

Phenotype	Group	Chr	LOD	Peak (BP)	95% Confidence Interval			Percent Variance Explained	Hazard for BB compared to AA Genotype				R^2	Model	Covariates
					Position (BP)		Size (Mb)		Hazard	Hazard Ratio	Standard Error	Pr(>|z|)			
Cataract	All irradiated	13	9.1	64380368	64314474	67923771	3.61	3.63	NA	NA	NA	NA	NA	coxph(surv ~ addcovar)	Sex
Cataract	All mice	6	8.1	38655250	35313956	39318213	4.00	2.16	NA	NA	NA	NA	NA	coxph(surv ~ addcovar)	Sex
Cataract	Unirradiated	2	7.6	151375256	147697318	152492554	4.80	5.194	1.140	3.128	0.211	0.000	0.052	coxph(surv ~ addcovar)	Sex
Cataract	All mice	9	7.6	103042275	102530474	106571000.5	4.04	2.834	1.386	4.000	0.166	0.000	0.028	coxph(surv ~ addcovar)	Sex
Cataract	All mice	1	7.2	167940750	167896138	171059788.175	3.16	1.796	1.622	5.065	0.272	0.000	0.018	coxph(surv ~ addcovar)	Sex
Cataract	All mice	11	7.1	64563496.5	63237527.5	67083594	3.85	1.644	0.648	1.912	0.139	0.000	0.016	coxph(surv ~ addcovar)	Sex
Cataract	HZE	18	7.1	57757285	56617968	58844662.925	2.23	4.453	1.177	3.246	0.328	0.000	0.045	coxph(surv ~ addcovar)	Sex
Cataract	All mice	12	7.1	93750055	91839718.65	97565394	5.73	1.845	-1.362	0.256	0.320	0.000	0.018	coxph(surv ~ addcovar)	Sex
Cataract	All mice	5	6.9	40612677.5	40448623	42716394.1625	2.27	1.617	-0.571	0.565	0.109	0.000	0.016	coxph(surv ~ addcovar)	Sex
Cataract	All mice	19	6.8	23848872.5	21851403	27418929	5.57	1.648	0.565	1.760	0.107	0.000	0.016	coxph(surv ~ addcovar)	Sex
Cataract	Unirradiated	3	6.6	57038547	55335012.7625	57506254	2.17	4.478	1.908	6.741	0.511	0.000	0.045	coxph(surv ~ addcovar)	Sex
Cataract	All mice	15	6.6	21413551	18724714	24453148	5.73	1.298	3.889	48.853	0.722	0.000	0.013	coxph(surv ~ addcovar)	Sex
Cataract	All mice	3	6.4	143469005	143314535	143590143	0.28	1.479	-0.523	0.593	0.163	0.001	0.015	coxph(surv ~ addcovar)	Sex
Cataract	Gamma	6	6.4	38655250	35313956	40516579	5.20	5.54	NA	NA	NA	NA	NA	coxph(surv ~ addcovar)	Sex
Cataract	All mice	13	6.4	67430334	63660010	70987202	7.33	1.433	-15.073	0.000	770.415	0.984	0.014	coxph(surv ~ addcovar)	Sex
Cataract	All irradiated	4	6.3	82220025	78621218	82220025	3.60	2.172	-0.493	0.611	0.322	0.126	0.022	coxph(surv ~ addcovar)	Sex
Cataract	HZE	13	6.3	64380368	64379067.9375	67430334	3.05	2.553	-16.086	0.000	1358.433	0.000	0.026	coxph(surv ~ addcovar)	Sex
Cataract	Gamma	17	6.2	31917941	31472359	34483738	3.01	4.303	1.099	3.001	0.234	0.000	0.043	coxph(surv ~ addcovar)	Sex
Cataract	All irradiated	1	6.1	170680209	168488023.325	173329713	4.84	1.867	-1.710	0.181	0.709	0.016	0.019	coxph(surv ~ addcovar)	Sex
Cataract	Gamma	4	5.9	121207745	119251300.575	123535940.5	4.28	3.812	-2.120	0.120	0.600	0.000	0.038	coxph(surv ~ addcovar)	Sex
Cataract	Unirradiated	9	5.9	83079835.5	79613654	85245479	5.63	3.651	0.981	2.666	0.216	0.000	0.037	coxph(surv ~ addcovar)	Sex
Cataract	Unirradiated	11	5.9	101354898.5	100305323	103585515	3.28	3.967	1.021	2.776	0.221	0.000	0.040	coxph(surv ~ addcovar)	Sex

List of Abbreviations

ALARA	As Low As Reasonably Achievable
AML	Acute Myeloid Leukemia
ATM	Ataxia-Telangiectasia Mutated
CC	Collaborative Cross
DO	Diversity Outbred
DNA	Deoxyribonucleic Acid
GCR	Galactic Cosmic Rays
GEM	Genetically Engineered Mouse
GWAS	Genome Wide Association Study
HCC	Hepatocellular Carcinoma
HS	Heterogenous Stock
ICRP	International Commission on Radiological Protections
IR	Ionizing Radiation
LEO	Low Earth Orbit
LET	Linear Energy Transfer
LSS	Life Span Study of the atomic bomb survivors
MB	MegaBase
MUGA	Mouse Universal Genotyping Array
NASA	National Aeronautics and Space Administration
NCRP	National Council on Radiation Protection and Measurements
NRC	National Research Council

NSCR	NASA Space Cancer Risk model
NSRL	The NASA Space Radiation Laboratory
PSC	Posterior Subcapsular Cataract
rAML	Radiation-induced AML
REID	Risk of Exposures Induced Death
RI	Recombinant Inbred
RNA	Ribonucleic Acid
SEP	Solar Energetic Particles
SNP	Single Nucleotide Polymorphism
QTL	Quantitative Trait Loci
Z	Atomic Number